Università degli Studi di Bergamo
Department of Engineering and Applied Sciences

Static and fatigue behaviour of structural light alloys in air and aggressive environment – investigation and innovation with thin hard coatings

Francesco Villa

submitted in fulfillment of the requirements
for the degree of

Doctor of Philosophy

in Mechatronics, Information Technology, New Technologies and Mathematical Methods

XXVIII Cycle

Advisor: **Prof. Sergio Baragetti**

February, 2016

Acknowledgements

It is always the hardest part to give proper thanks to the people you meet during a long journey.

First of all, I wish to thank prof. Sergio Baragetti, for all the support and teaching during these intensive three years, and for his precious advices in the first steps of my research adventure.

I wish to thank greatly prof. Riccardo Gerosa, for his dedicated support and curiosity in the experimental work linked to the present dissertation.

I must acknowledge also Eng. Alessandro Bertè and Eng. Claudio Carini from Lafer S.p.A., for their unique collaboration and advice on PVD coatings

A special thank also to the people I have encountered and worked with: from the University Labs, Daniele Di Marco and Luca Gritti as well as my friends Ph.D. candidates; from Imperial College London: prof. Ferri Aliabadi and dr. Zahra Sharif-Kodahei for their dedicated supervising during my visiting, as well as all the friends encountered in the office.

And finally, some personal thanks to my family, for having supported me so long: sorry for all the time I spent away, and for all the time I will spend away. To my old friends in Milano and Brianza, to my new friends in Bergamo and to the beautiful people I have encountered in London goes my biggest thank: with you, anywhere I roam, where I lay my head is home.

Abstract

Today, the constant need for increased energetic efficiency and resources economy leads the research in the field of structural materials, towards the investigation of new applications of structural light alloys. Such advanced materials, widespread in the aeronautic sector, nowadays are increasingly more used for advanced applications in the automotive, maritime, oil & gas market sectors. Other, less obvious application fields are seeking the advantages of such materials, such as the biomedical field and the fuel cells design field.

To increase the efficiency in the structural design, high strength-to-mass ratio alloys are adopted in weight critical structures, such as aeronautic details in which high strength is required. Ti-6Al-4V (grade 5) Titanium alloy is certainly the most widespread metallic material for highly stressed structural components of jet fighters and of new generation jet liners. The material is employed in the fuselage, nacelles, landing gear, wing and empennage frames, and in low temperature compressor blades and disks for jet engines. Its wide usage is justified by its brilliant mechanical characteristics, reaching an Ultimate Tensile Strength (UTS) of almost 1000 MPa, together with only half of the density of the typical structural steel. These brilliant results are granted by the particular $\alpha + \beta$ microstructure of the alloy, which provides superb mechanical strength. Another successful feature of this material is its brilliant corrosion resistance, obtained by the formation of a thin, spontaneous and very resistant TiO_2 passivating layer. This feature has driven the mechanical and material designers to extend its usage also for particulars of chemical and oil & gas extraction plants. New usages have been proposed also for medical prosthetic components and implanted medical devices, as well as for new designs of lightweight fuel cells.

Although the Ti-6Al-4V alloy is typically adopted also in maritime environments, due to its spontaneous formation of protective oxide, its susceptibility to aggressive media has been proven in the scientific literature. Particularly, the alloy has

shown high Stress Corrosion Cracking (SCC) sensitivity in solutions with very high concentrations of methanol. The research on this field has taken place mainly in the 50's to 70's of the last century, side to side with the development of the United States space program. More recently, new research works investigated the effects in terms of Corrosion Fatigue (CF) of the alloy in air, salted solution and methanol solution. The main reason to support research and investigation in the behaviour of high strength Titanium alloys in this field is justified by the extension of the application spectrum of this material. Particularly, new applications in the oil & gas field and in the realization of fuel cells put the material in direct contact with aggressive methanol environments and other less investigated chemical media. Standards and prescriptions in these field are being emanated by the competent entities, showing a partial recognition of the problem. However, recent experiments, which are part of the work presented in this dissertation, produced some very interesting results on the effects of methanol aggressive environments in conjunction with heat treatments. The presence of an α-layer, following a stress-relieving treatment, resulted in an increase in SCC susceptibility. This concern raises a critical warning to the adoption of Ti-6Al-4V alloy in environments with particular chemical conditions, such as the oil & gas sector, chemical treatment plants, and fuel cells. In addition to this experimental work, numerical studies have been concluded, by means of Finite Element Method (FEM) analysis of fatigue specimens of Ti-6Al-4V in air, inert environment (paraffin oil) and NaCl environment. The numerical method has been compared with experimental literature data from previous works, resulting in a consistent reconstruction of the fatigue crack growth rate obtained directly from the FE model. The results of the numerical model provided a satisfactory method to reconstruct the crack propagation in air and in an aggressive environment, for fatigue and corrosion fatigue studies.

In seeking high performance structural materials, aluminium light alloys have to be properly investigated. In the automotive sector, the adoption of aluminum

light weight components is indeed increasing, especially regarding high performance vehicles. The general trend, however, is to extend the adoption of these alloys in the mass production of motor vehicles, by designing lightweight cars for the most popular segments with a percentage of aluminum alloys superior to 50%. Concerning high performance Al-Zn-Mg 7000 series alloys, their usage is still scarce in the automotive mass production, mainly due to their difficult weldability and their sensitivity to the high temperatures involved in the stamping processes. The industrial and the research worlds are however striving to reach satisfactory solutions to both issues. Recent developments of the Friction Stir Welding (FSW) technique for lightweight alloys welding seem to encourage a wider adoption of these materials in the industrial manufacturing processes, in light of the positive results encountered for the 7000 series.

By looking at high strength applications, the most interesting material from the 7000 series is certainly the 7075 aluminium alloy in the T6 temper, commonly referred as the 7075-T6. With an UTS approaching 600 MPa and a lower density with respect to both steel and titanium alloys, the 7075-T6 represent the best material for extremely low-weighted structural components. Developed initially in the aeronautic field, mainly to produce panels, ribs and spars for wings and fuselage airframes, the material usage was reduced in the last decades. The motivation for the withdrawal of this particular alloy from the aeronautic sector has been individuated in the reduced corrosion resistance of the alloy in aggressive environments. 7075-T6 has indeed shown susceptibility to pitting, crevice, inter-granular and exfoliation corrosion, and literature sources have shown its sensitivity to SCC in NaCl-water mixtures, and reduced fatigue strength due to surface pitting. For this reason, the alloy in this particular temper is not used anymore in the design of critical aeronautic structures, and new metallurgical treatments, namely the T7x temper classes, have been developed. Metallurgical research is continuing in this field, since the substitutes to the T6 temper solve the corrosion problem at the price of a non-negligible

reduction of the alloy mechanical characteristics. In the present thesis, literature on 7075-T6 fatigue and CF behaviour is analysed. New experimental evidence is also reported, in which the susceptibility of the T6 alloy to methanol environment is proven, and new strategies to measure the corrosion protection of the alloy are indicated. Particularly, the effects on fatigue and corrosion fatigue of innovative treatments of surface modifications are investigated. Low temperature Physical Vapour Deposition (PVD) techniques have been adopted on 7075-T6 fatigue specimens, to assess the effect of thin hard coatings of Tungsten Carbide/Carbon (WC/C) and low temperature Diamond Like Carbon (DLC). The effects of such coatings on fatigue behaviour in air and aggressive methanol environment have been characterized by means of step-loading fatigue testing procedures. Scanning Electron Microscopy (SEM) has been used to identify the mechanisms involved in the fatigue behaviour of coated and uncoated specimens, in rotating bending, R = -1, fatigue tests. The experimental results have given back a precious idea of the possible application of PVD coatings on high strength aluminium surfaces. The work presented poses the basis for a future development of fatigue and corrosion fatigue studies on the subject. The final aim of the research is to produce machine components with enhanced surface and corrosion protection characteristics, without sacrificing the mechanical behaviour, and possibly enhancing it. In this way, innovative applications, which are traditionally destined to other materials, or that are not yet fully developed, may benefit for light alloys with improved fatigue, surface and corrosion resistance behaviour.

Contents

List of Figures

List of Tables

Chapter 1

Introduction

1.1 General

The world of structural materials is always in search of new solutions for innovative applications or increased efficiency for mass produced components. The recent geopolitical developments, with the introduction of a global market, accelerated the constant need for the producers and the developers of technological products to seek for innovation, to increase the efficiency of established products, and to reduce the materials and fabrication costs. Moreover, new studies and concerns regarding the environmental impact of greenhouse gases, and economic and political concerns on the provision of raw materials, fuel and energy sources in general, are moving producers and mechanical designers towards the adoption of innovative solutions. In order to increase the efficiency of machines and technological products, light-weight solutions are now imperative. In the automotive field, for example, political decisions are backing up the development plans of mass producers worldwide, imposing a reduction of fuel consumption. Weight saving is one of the mandatory requirements of each new design, since even a slight increase in the fuel economy and a reduction of greenhouse gases emission can lead to a dramatic decrease of the global request of fuels and of the CO_2 emissions [1]. Direct weight reduction has a secondary benefi-

cial effect, namely the ripple effect. By reducing the weight of the car structure, the requirements over installed power are downsized. Reduced power needs, with the same performances, results indeed in a decreased size of the engine. A lesser engine leads to reduced transmission and fuel tank dimensions, hence triggering further weight reduction and improved fuel economy [1]. Following these considerations, the sector is striving in the substitution of highly resistant steel components with other materials.

While high strength titanium components appear too expensive for mass produced components, the development of innovative techniques in the field of light aluminium alloys, such as the Friction Stir Welding (FSW) [2–6] and new wrought and forging procedures [7–9] is pushing the automotive production towards the introduction of alluminium alloys into body-in-white components [1]. The FSW technique development, proposed in 1991 by The Welding Institute [2] to overcome welding difficulties on high strength light alloys, is based on the thermomechanical agitation of the material to be welded by means of a rotating and advancing pin tool. The pin tool is forced in the material, pressing it with a flat shoulder. The material is extruded around the pin, and forged by the pressure on the flat tool shoulder, thus forming a weld bead. The bead is subdivided in three regions: i.e. the Heat Affected Zone (HAZ), the Thermomecanically Affected Zone (TMAZ) and the stirred zone [10]. The advantages of the FSW method include the capability to weld low-conducting, hardly weldable light Aluminum and Titanium alloys at temperatures inferior to the material melting point, with reduced distortions and residual stresses [10]. In a recent work by *Hirsch* [11], the actual state of the art of high class automotive examples is analysed, along with recent projects which export the idea of aluminium or multi-material concepts for powertrain, chassis and suspensions, and body and white concepts for standard cars production. Massive weight savings between 30 and 40 % can be granted by following this method, especially when applied to the heaviest part of the car, namely the body-in-white. Considering

aluminium alloys with high strenght-to-mass ratios, i.e. the 6000 AlMgSi and the 7000 AlZnMg series, the first ones are the most adopted in the car structure design, along with the 5000 AlMg(Mn) series. The main reason lies within the reduced welding capability of the 7000 series, although recent advances in the FSW may soon lead to a suitable industrialization of this problem [12, 13]. The 7000 series indeed present the best high strength performances, and their application to mass produced structural components will likely generate most desirable effects in weight saving for high strength components.

As will be deeply described in Chapter 4, 7000 series, and in particular the 7075-T6 aluminium alloy, present however critical aspects which must be dealt with care when approaching their application on mass-produced structural details. Apart from production, machining and industrialization concerns, indeed, this particular alloy suffer from sensitivity to corrosion [14–16] and reduced surface properties, including reduced hardness, which may reduce its suitability to several structural applications for mechanical components. In particular, 7075-T6 titanium alloy is susceptible to Stress Corrosion Cracking (SCC) and pitting corrosion in NaCl solution, fog or spray [15, 16], with dramatic effects on its mechanical performances. Tensile strength [14] and corrosion fatigue [15] are dramatically reduced when considering the effect of pitting due to aggressive environments. For this reason, 7075-T6 alloy is not used any more in critical high-strength applications, replaced with lower strength tempers, i.e. the T7x processes, which are less prone to SCC [14].

In order to develop new components for the aeronautic, automotive and other market sectors in which the application of high strength-to-mass materials will surely lead to outstanding performance and environmental improvements, 7075-T6 alloy is however a precious material. In order to overcome its limitations in terms of surface properties, particularly considering fatigue and corrosion fatigue, a significant research effort has been conducted towards the application of surface coating or targeted oxidizing strategies, which could overcome the intrinsic limitations of

the substrate [17–19]. In particular, protective coatings are searched to increase the resistance of aluminium light alloys against corrosion, wear, fretting wear and fretting fatigue [19, 20]. However, as will be extensively clarified in Chapter 4, the presence of a substrate-layer or substrate-multilayer system presents a complex contribution on fatigue and corrosion fatigue properties of light alloys [19, 20]. In fact, several aspects come into play in defining the fatigue strength of these complex systems, including the microstructural modification of the alloy due to the high temperatures experienced under the thermal loads of coating processes, as well as the mechanical interactions which occur at the interface between the coating and the substrate [21–27]. The development of new strategies and the evaluation of new coatings is hence mandatory to overcome the limits of the actual state of the art in terms of fatigue and corrosion fatigue performances for PVD coated components.

Considering titanium alloys, their application in terms of weight saving, high-performance applications is very well known in the aerospace sector, which for long years has been the master field in which the balances of these high strength, low density materials have been appreciated against their high manufacturing costs [28, 29]. Titanium alloys in the aerospace sector are preferred to steel and aluminium materials for several reasons. Due to its reduced density, roughly 50 to 60% compared to steel counterparts, titanium alloys are mainly adopted for weight savings in competition with steel alloys. When space is also a constraint, titanium alloys are preferable also to most of the high-strength aluminium alloys, and this is the main reason they are often adopted as substitutes also for high strength aluminium alloys, especially concerning landing gears and other volume critical high strength components, such as aeronautic springs [28, 29]. Another exclusive aspect of this metallic alloy, if compared to its steel and aluminium counterparts, is its suitability to high temperature components, such as compressor and turbine blades and disks [28–30].

The overall behaviour of titanium light alloys, in terms of mechanical characterization and resistance to aggressive environments, is directly linked to their metal-

lurgical structure. As will be explained more properly in Section 1.2, titanium alloys are divided into different classes depending on their content of α or β phases [28]. The α and near-α titanium alloys include commercially pure grades of titanium, typically alloyed with oxygen and iron, as well as alloys containing Al and Sn α stabilizers. The commercially pure grades (ASTM Grade 2) can be obtained with yield strengths below 500 MPa, and Ultimate Tensile Strength (UTS) not superior to 600 MPa [31]. α and near-α alloys, along with an increase in their mechanical characteristics, exhibit high ductility, good weldability and good creep resistance behaviour, being preferred for this reason in high temperature applications. They are also adopted for their excellent corrosion resistances. On the other hand, β alloys are highly hardenable, hence they can reach very high strengths, of up to 1400 MPa of UTS [28]. However, the advantages of β alloys come at the price of very difficult weldability in some cases, and in general in a complex metallurgy, so that the final properties depend strongly from the heat treatment. The most common titanium alloy on the market indeed, with its 80 to 90% share in terms of usage in aeronautic construction, is the Ti-6Al-4V [28, 29]. It belongs to the α/β titanium alloys class. Alloys from α/β class are capable of higher strengths with respect to near-α alloys, with good combinations of properties, and a wide processing window. Ti-6Al-4V alloys typically start from a minimum UTS of about 900 MPa. These kind of alloys are usually treated with a Solution Treatment and Over Aging heat treatment (STOA or STA), to increase fracture toughness. They are commonly welded in vacuum chambers, in order to reduce the oxidation and the formation of α layers during the welding procedure. These alloys, and in particular the Ti-6Al-4V alloy, are adopted in aerospace structure for their high strenght-to-mass ratio if compared to steels, and their relevant strength-to-volume ratio with respect to aluminium alloys.

Concerning the behaviour of titanium alloys in aggressive environment, their usage is appreciated due to their proven corrosion resistance. Although titanium is a

highly reactive metal, its ability to form a spontaneous, protective TiO_2 oxide surface film provides titanium and its alloys with corrosion resistance to most natural environments and chemicals [16, 32, 33]. For this reason, commercial Ti-6Al-4V exhibits proven immunity to corrosion attacks in a variety of environments, including salty water, acids, alkalis, and industrial chemical processes [32–34]. Proven corrosion resistance, along with high strength-to-mass ratio has indeed elected Ti-6Al-4V as one of the ideal candidates for advanced applications in new fields with respect to the classic aeronautic usage. Ti-6Al-4V is becoming popular in the oil&gas and in the chemical sector, for the production of risers, heat exchangers, underwater taper stress joints and well-head components [29, 34–36], as well as in the biomedical sector, including dental implants and surgical prosthesis for knee and hip joints, in which tribocorrosion phenomena are also present [31, 37]. Although this brilliant characteristics, Ti-6Al-4V alloy is still susceptible of corrosive effects when the protective oxide is removed via pre-cracking, mechanical or abrasive interactions [16, 33, 38]. Moreover, the TiO_2 oxide has proven to be not protective for certain environments, depending on the different titanium alloys. In particular, as will be analysed extensively in Chapter 2, Ti-6Al-4V is very susceptible to methanol containing environments [16, 39–41]. Despite the fact that such environments are not easily encountered in the typical usage field of the Ti-6Al-4V alloy, new applications in the oil&gas sector, in geothermal implants and in fuel cell technology can trigger potentially risky situations.

The aim of the present thesis is hence to provide a complete overview on the effects of an aggressive environment on high strength structural light alloys, and to increase the knowledge of potential dangerous effects on current and future applications of high strength-to-mass ratio alloys. Moreover, the effects of new surface treatments, specifically PVD thin hard coatings, on light alloys structural performances in aggressive environments will be analysed. The entire work is focused on the effects of the environment and of the surface treatments on the mechanical beha-

viour of the substrate materials, including Stress Corrosion Cracking (SCC) testing and effects on the fatigue strength in air and aggressive environments. In order to provide a complete work, a satisfactory literature review has been performed over the known effects on SCC and corrosion fatigue for the Ti-6Al-4V titanium and 7075-T6 aluminium alloy. Each of the arguments analysed are integrated with experimental and numerical work, which has been produced by the research group of which the author is afferent during the elaboration of the present work. The experiences and numerical simulations are presented in each section with material and methods, and a remark on each experimental or numerical work is provided at the end of each chapter. Details of some of the applied methods are provided in the appendices of the work. Sections 1.2, 1.3 will present in more detail the innovative applications for Ti-6Al-4V and 7075-T6 alloys. The discussion on Ti-6Al-4V SCC and corrosion fatigue will occupy chapters from 2 to 3, while fatigue effects on uncoated and PVD coated 7075-T6 specimens in aggressive environment will be discussed in 4.

1.2 Ti-6Al-4V use in innovative applications and aggressive environments

In the present section, recent applications of Ti-6Al-4V aluminium alloys are discussed in more detail, focusing on its usage in aggressive environments. A successful adoption of the alloy has been carried out in the biomedical field, due to the ability of the material to form a spontaneous TiO_2 oxide protective film in typical biologic environments, such as the conditions typically found in the human body [37]. The TiO_2 film is indeed resistant and easily healed in aqueous media, if traces of oxygen and water are present [16]. Another reason for the extensive usage of titanium alloys is in the reduced elastic modulus, with respect to steel, and their density more similar to human bones [31]. Knee and hip prosthesis, where high strength is required along with excellent tribo-corrosion resistance, is a typical application field of Ti-

6Al-4V. Another successful application concerns dental implants and other dental usages [37]. Despite the brilliant wear and corrosion resistance properties of the Ti-6Al-4V alloy in aqueous environments, the dissolution of vanadium and aluminium in the human body is reason of concern for several authors, due to toxicity and potential loosening of the implant [37, 42]. Tribo-corrosion of prosthetic surgery implants is indeed considered responsible of increased concentration of aluminium and vanadium in animal tissues, although the effective toxicity of these substance is still debated [42]. Moreover, recent results [37] show that the tribo-corrosion behaviour of Ti-6Al-4V is excellent even in biologic environment conditions. In order to improve the Ti-6Al-4V biocompatibility under corrosion and wear conditions, several authors have proposed Titanium Nitride (TiN) PVD or other kinds of surface coating techniques, with alternating results [42]. Another deeply investigated coating for the medical sector is the Diamond Like Carbon (DLC) PVD process. Tribo-corrosion results on DLC PVD coated titanium implants are however inconclusive, with some authors defending its biocompatibility while other authors express negative opinions [43]. In addition to surgical prosthetic implants, another common biomedical field is related to dental implants, where corrosion fatigue resistance and wear resistance are also important. Results from [31] show that, albeit corrosion fatigue can happen in Ti-6Al-4V in Ringer's solution with low oxygen content, and that crack propagation rates are accelerated in NaCl solution, the fracture toughness and surface hardness of the alloy are not modified after in vivo implanting. Experiments concerning fatigue testing of Ti-6Al-4V in artificial saliva and artificial saliva with fluorine have demonstrated that reduced fatigue life has to be expected [44]. The second aspect is directly linked to the susceptibility of titanium alloys to fluorine environments, although fluorine is typically responsible of general corrosion behaviour of Ti alloys, and not directly involved in SCC behaviour [45]. However, considering the results of [44], its contribution is not negligible considering when corrosion fatigue is involved. Other significant usages of PVD coated titanium com-

ponents are found in Implanted Medical Devices (IMD), such as heart stimulators and retinal implants [46].

Although the application of PVD coatings on Ti-6Al-4V has been mainly proposed for medical applications, other uses consider PVD and other coating strategies to develop a TiN layer over rotating disks for aeronautic turbines, where high temperatures and ingestion of debris and corrosive chemicals are present. Moreover, considering compressor stage blades, impact erosion is present as a worsening condition [46]. In the work by *Baragetti* et al. [47,48], numerical and experimental models are developed concerning fatigue and rolling contact fatigue of CrN coated steel spur gears. The model is hence extended to TiN coated, Ti-6Al-4V spur gears, showing a positive effect on the fatigue behaviour at the root of the teeth. The results show a behaviour of the titanium spur gears which is comparable to the standard, case-hardened steel spur gears. In this way, the adoption of titanium for high speed motorbike gears is considered possible, thus resulting in relevant performance advantages for the gearbox, in terms of weight savings and reduced inertia. Other patents involving PVD coatings and titanium consider the usage of Ti alloys for new generation fuel cells [46, 49]. The influence of PVD coatings on the corrosion performances of the alloy could be critical, when reportedly aggressive chemicals are used in the fuel cell process. Some fuel cells projects involve indeed methanol as an active medium, which, as already considered in the previous section, is a critical SCC promoter in high strength Ti-6Al-4V alloys [49].

Concerning the mechanical effects of PVD depositions on Ti-6Al-4V alloy, a few research works exist [50–52]. PVD on titanium alloys are typically limited to medical or other advanced applications, since the TiO_2 oxide layer is often considered sufficient for generic corrosion protection. Other applications concerning PVD coating on Ti-6Al-4V substrate involve components in which the reduction of the sliding friction and the surface hardness are sought for the surface properties. When designing dynamically stressed, PVD coated components, it is mandatory

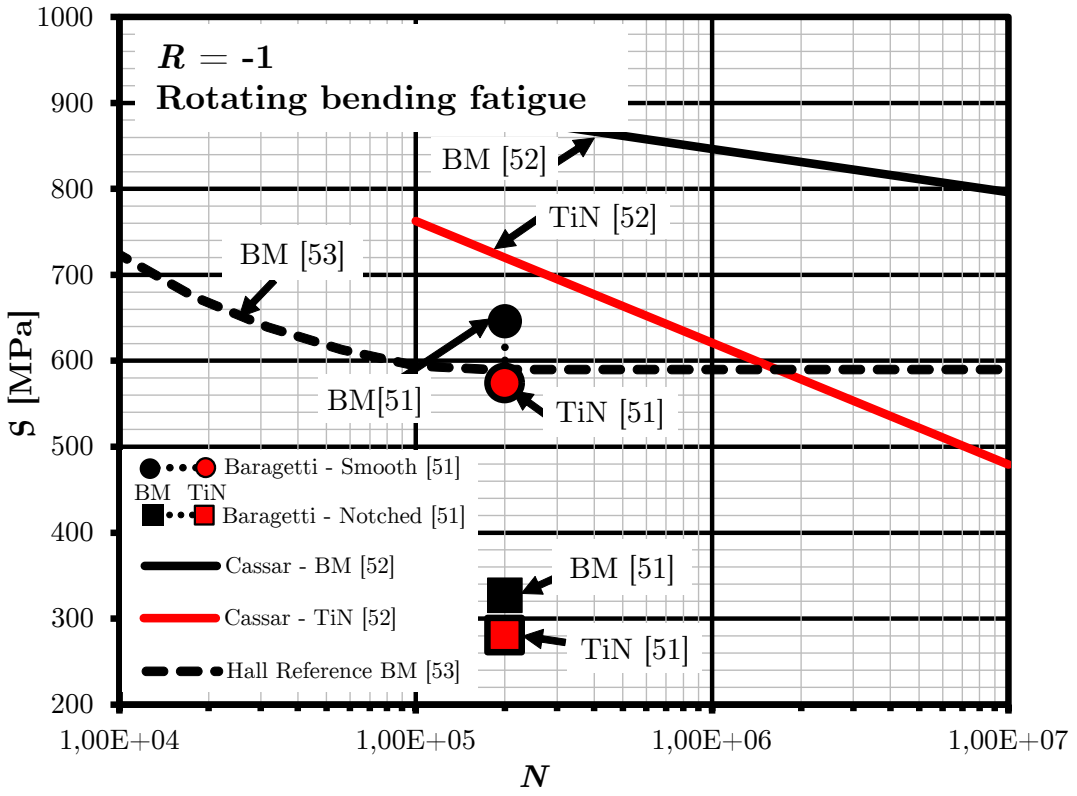

Figure 1.1: Fatigue strength of Base Material uncoated and TiN PVD coated Ti-6Al-4V specimens from rotating bending fatigue test, R = -1, N = *2e5*, adapted from [26, 51].

to assess the fatigue behaviour of the coated substrate, due to the effects of the mechanical interface between the thin hard coating and the substrate, as well as the effects of the deposition process on the substrate microstructure. In Figure 1.1, results from *Baragetti* et al. [51], obtained at *2e5* cycles for Titanium Nitride (TiN) coated Ti6Al4V ELI rotating bending ($R = -1$) specimens, for smooth and notched geometries, are displayed. To obtain a comparison, results are plotted against a reference material *S-N* curve, obtained from *Hall* [53]. By looking at Figure 1.1, it can be seen that a modest reduction in fatigue strength at *2e5* cycles is obtained from smooth specimens. The loss in fatigue strength is even inferior when considering notched specimens. Experimental data, extrapolated in [26] from the statistical analysis of *Cassar* [52] show however a reduction of fatigue strength at higher cycles. The curve is presented in Figure 1.1 as well. Other data, obtained by *Wilson* et al. [50], present a negligible effect of TiN PVD deposition on Ti-6Al-4V alloy.

Another field in which Ti-6Al-4V is gaining precious market share is the energy industry, with relevant applications in highly stressed components in the oil&gas offshore and in the geothermal plants [34, 35]. The inherent corrosion resistance of the Ti-6Al-4V alloy is preciously exploited in contexts in which stainless steels have limited applicability due to the particular environmental conditions and the high applied stresses. Moreover, even if titanium alloys may show increased Fatigue Crack Growth Rates (FCGR), with respect to stainless steels, above ΔK values of $12 \div 15\ MPa\sqrt{m}$, their higher threshold ΔK_{th} in air and seawater environments often results in longer fatigue lives [36]. Titanium alloys are precious in application which include increasing well depth, increasing reservoir fluid temperatures and pressures, increasing sourness (i.e. H_2S pressures), or higher brine acidity and chloride levels. Typical applications include geothermal brine wells, where hot chloride corrosion resistance is critical [35]. For the same reason, Ti-6Al-4V is frequently adopted in heat exchangers for the energy sector, where the combination of seawater with high temperatures is often found. In these cases, Ruthenium addition to the alloy serves to stabilize the corrosion fatigue crack growth rate in chloride crevice and the stress corrosion behaviour in seawater and sweet or sour brines up to temperatures of 330°C, and pH as low as 2.3 [35,36]. Another fundamental application of the Ti-6Al-4V in the oil&gas sector include the realization of Taper Stress Joints (TSJs) and riser applications [35, 36]. The higher flexibility of the Titanium alloy, with respect to its steel counterpart, is extremely desirable in complex, dynamic riser systems. Moreover, its high resistance and flexibility is fundamental in the TSJ design. TSJs are indeed highly deformable components, mounted in the proximity of the well-head connection on the ocean seabed, with the aim to provide large deflections to off-shore risers systems, while relieving the well-heads of the applied stress [35]. The amount of corrosion issues connected with static and fatigue loading of these components is hence significant, so *NACE International* has provided several recommendations for the adoption of titanium alloy components in sub-sea production systems [36].

In particular, concerning the Ti-6Al-4V alloy, critical SCC and corrosion fatigue occurs when the alloy is exposed to anhydrous methanol, a situation which can be found near the well-head, where the injection of methanol for de-hydrating purposes is often found [36]. As will be extensively exposed in chapters 2 and 3, the Ti-6Al-4V alloy is extremely susceptible to SCC [16, 25, 33, 54, 55] and corrosion-fatigue [56–60] in anhydrous methanol. For this reason, [36] recommends that a minimum water content of 3% is needed to passivate methanol for Ti-6Al-4V, while a 10% is recommended for Ti-6Al-4V-Ru, with Ruthenium addition. Moreover, recent studies [55, 59] have underlined that the presence of an external alpha layer can increase these percentages up to 7.5%, in case of SCC in methanol. This result is coherent with the indication of [36], which suggests the complete removal of oxide scales and alpha layers after any relevant metallurgical or technological process over titanium alloys for sub-sea applications. For the sake of completeness, it must be remembered to the reader that Hydrofluoric acid (HF) contamination is not permitted for Titanium components, and Hydrochloric acid (HCl) must be kept below 12 wt.%, and used only in conjunction with oxidizing inhibitors [36]. The SCC sensitivity in methanol may be considered a critical aspect not commonly found in the application of the Ti-6Al-4V alloy, but it must be remembered that this aggressive environment can be encountered in typical applications in the oil&gas sector, especially as dehydration agents in the extraction process [36], and in the aeronautic sector, where injection of methanol with water is performed in the engines where low air density regions are encountered during the flight [30]. Moreover, new applications include methanol as a chemical reactant, such as in fuel cells, as indicated by *Park* et al. [49].

Apart from consideration on the corrosion behaviour of Ti-6Al-4V, another reason of the increased usage of titanium components, and especially risers systems, is the recent innovation concerning radial friction welding process. This new application of the FSW procedure to offshore riser components results in welding

times reduced to the order of 1 min, providing a notable increase in the efficiency and a reduction of costs for the deployment of titanium risers [36]. Concerning the mechanical performances of the Ti-6Al-4V alloy, recent research investigations have proven that this technique is extremely effective on the selected alloy. Investigations by *Zhang* et al. [61] have shown that limited decrease is found with respect to the base material in terms of UTS and YS, with worse effects for higher tool rotational speeds [9, 26]. Shorter specimens, wholly occupied by the FSW region, showed however an overall increase in terms of UTS and YS of the zone mechanically interested by the FSW process [9, 26]. Work by *Sanders* et al. [62] emphasized that an acceptable behaviour of the FSW process on the Ti-6Al-4V was found if stress relieving, post treatment machining of the FSW surface, and low plasticity burning processes were adopted in conjunction. Finally, two papers from Edwards and Ramulu [63, 64], show that a correct FSW process produces fatigue strength values comparable between the base and the welded materials. In particular, [63] concerns the axial properties of straight specimens, showing comparable UTS and YS values, and fatigue behaviour similar to the base material for $R = 0.1$, 3 mm thickness. For other load ratios and increasing thicknesses, a small reduction in fatigue behaviour has been found. Concerning 6 mm, L-shaped Ti-6Al-4V structural details, [64] showed that comparable, if not better, fatigue behaviour was found for FSW specimens. As a results, FSW technique is extremely recommendable for fatigue loaded and high strength joining of Ti-6Al-4V structural details [26, 35, 63, 64]. The overall literature data concerning tensile and fatigue behaviour of FSW on Ti-6Al-4V is reported in Tables 1.1 to 1.4.

Tensile properties	**YS [MPa]**	**UTS [MPa]**
Base material	845	940
Long 300 rpm	825	926
Long 600 rpm	792	873
Short 300 rpm	950	1050
Short 600 rpm	940	1025

Table 1.1: Tensile properties of FSW Ti-6Al-4V alloy, extrapolated from [61], adapted from [26].

Fatigue, $R = 0.1$	N	**S [MPa]**
Base Material	1e6	620
Stress Relieve + Machining and LPB	1e6	565
Stress Relieve + LPB or Machining	1e6	485
Other treatments or no treatments	1e6	207

Table 1.2: Fatigue behaviour - $R = 0.1$ - of FSW Ti-6Al-4V alloy, extrapolated from [62], adapted from [26].

Tensile	**YS [MPa]**	**UTS [MPa]**
Unwelded	880	950
FSW	975	1025

Fatigue, $R = 0.1$	N	**S [MPa]**
Base material	1e6	760
t = 3 mm	1e6	725
t = 6 mm	1e6	665

Table 1.3: Tensile properties and fatigue behaviour of FSW Ti-6Al-4V alloy, extrapolated from [63], adapted from [26].

Fatigue, R = -1, L-joints	N	**S [MPa]**
FSW Joints	1e4	751
	1e6	328
Machining from square bars	1e4	727
	1e6	343
L-shape extrusion	1e4	679
	1e6	280

Table 1.4: Tensile properties and fatigue behaviour of FSW Ti-6Al-4V alloy, extrapolated from [64], adapted from [26].

1.3 7075-T6 use in innovative applications and aggressive environments

As already said in section 1.1, the original usage of the 7075-T6 AA was intended for high-strength, low mass aerospace components. Indeed, *Brown* [16] remarks that 2000 and 7000 series are mostly used in the rocket, spacecraft, aeronautic and maritime vehicles. As reported in [28], high strength aluminium alloys are indeed preferable to titanium ones when extremely high stresses are not needed, i.e. when the component has limited volume constraints. 7075 alloy with T6 temper possess, as previously indicated, the highest mechanical strengths for aluminium alloys. Unfortunately, most of the high strength aluminium alloys present failing conditions well under the typical YS value, due to SCC or corrosion fatigue phenomena [16]. Particularly, 7075-T6 suffers dramatically from SCC in 3.5% wt. NaCl solution, coastal land atmosfere, and even concerning inland industrial atmosphere [16]. For this reason, components realized from 7075-T6 bars and plates are forbidden for new aeronautic projects since 1975, as new alloy tempers, namely T-7x temper series, were developed to reduce the SCC sensitivity of the aluminium alloy [14]. Unfortunately, the new tempers reduce significantly the high strength typical of the T6 temper. Considering corrosion fatigue, *Sankaran* et al. [15] have investigated on the effects of pitting corrosion, which leads to nucleation of fatigue cracks on dynamically stressed 7075-T6 components. The presence of an aggressive environment can lead to crack nucleation at lower stresses, and can significantly accelerate the FCGR of fatigue cracks. To protect high strength aluminium alloys, and especially 7075-T6 AA, several authors have proposed to develop functional coatings for this particular alloy. As will be deeply investigated in section 4.2, surface coatings, and especially PVD thin hard coatings, have been applied on 7075-T6 and other aluminium light alloys. The technique has been exported directly from the surface coating procedures of steels, for the advantageous results obtained in the surface treatments practice.

However, as will be pointed out in section 4.2, the effects on light alloys are highly variable, due to the complex mechanical interaction between the coating and the substrate, and to the microstructural modifications caused by the PVD or by other coating processes. The application of PVD coatings is sought for also concerning all the application in which an hard substrate or a sliding contact is requested, since the characteristic properties of 7075-T6 alloy may be not sufficient for such applications.

Concerning applications outside the typical aeronautical field, new production techniques applied to the 7075-T6 material point to extend its application to other demanding engineering applications, especially in the automotive field. As already said, the European market show an increased appetite to include high strength-to-mass ratio aluminium alloys in the design of automotive components, with an increased penetration of the Body in White (BIW), the chassis and other structural components, such as suspensions [11]. Due to their limited weldability and formability, 7000 series are usually limited to the most stressed components, typically extruded beams and crash elements. This application is also supported by the hardenability of 7000 series, with the quenching occurring during the extrusion phase [11]. Apart from the corrosion issues, which still affect the automotive field, mainly regarding the effect of aqueous chloride environment on the high strength aluminium components [1, 7], the main limitation of the 7075-T6 alloy is linked to difficulties in the manufacturing process, were 6000 alloys are preferred, mainly due to their increased weldability, while 5000 series are used when high formability is required [1]. Despite the limitations of 7075-T6 in the production process, its adoption has been proposed as a substitute to high strength steels, for critical A and B pillars structures, since recent procedures granting sufficient formability have been carried out, as identified by *Kumar* et al. [8].

However, in order to extend the applicability of the 7075-T6 alloy to other industrial applications, an improvement in the weldability processes is mandatory. Several results are available for 6000 series alloys, including efficiencies for tensile

and fatigue data, as depicted in Figure 1.2. Figure 1.2 has been adapted from the review presented in [26], which summarizes the results in the works of [2, 5, 6]. Numerical values, reported or extrapolated from [2,5,6]. are found in Table 1.5. As can be seen from Figure 1.2, very high efficiencies on 6000 series AA, in comparison with the base material, are obtained. For the tensile strength, values between 59% and 71% were obtained in different works, while fatigue performances ranged between 58% and 62% regarding FSW obtained with unthreaded tools. The experimental use of threaded tools for the FSW technique has produced more detrimental results, especially concerning fatigue behaviour, where efficiencies between 54 and 38 % were found. Another remark concerns comparison between base materials and FSW materials for smooth specimens or in the presence of a notch. In the latter case, the efficiency of the FSW reaches a 89% efficiency, according to [6].

Unfortunately, only a few results, concerning tensile and fatigue behavior of the 7075-T6 alloy under FSW welding procedures exist in literature [13,65]. Fatigue efficiencies have been integrated in Figure 1.3, remembering that the 7075-T6 tensile FSW efficiency found in [65] was of 90%. Numerical data on tensile and fatigue strength, collected or extrapolated from [13, 65], are presented in Table 1.6. The results from [13], regarding axial tests with $R = 0.1$, showed a limited fatigue strength of 79 MPa at 2e6 cycles. The poor fatigue performance found in [13] has however been attributed to the presence of sensible welding defects, generated by the process. On the other hand, fully reversed ($R = -1$) axial fatigue loading tests, conducted by *Uematsu* et al. [65] on 7075-T6 specimens in air and 3% NaCl solution, decisively showed the remarkable efficiency of the FSW techniques on this particular material. Indeed, a UTS efficiency of 90% was obtained during preliminary tensile testing. The results concerning axial fatigue behaviour, for $R = -1$, indicate that the FSW samples show a comparable behaviour with respect to the unwelded 7075-T6 specimens in air environment, between the whole life spectrum from *1e4* to *1e7* cycles. Considering fatigue tests in 3% NaCl, the FSW specimens experienced a

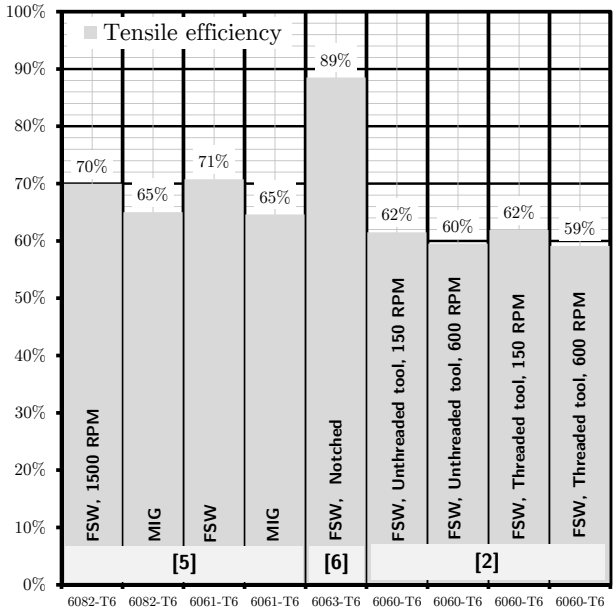

a)

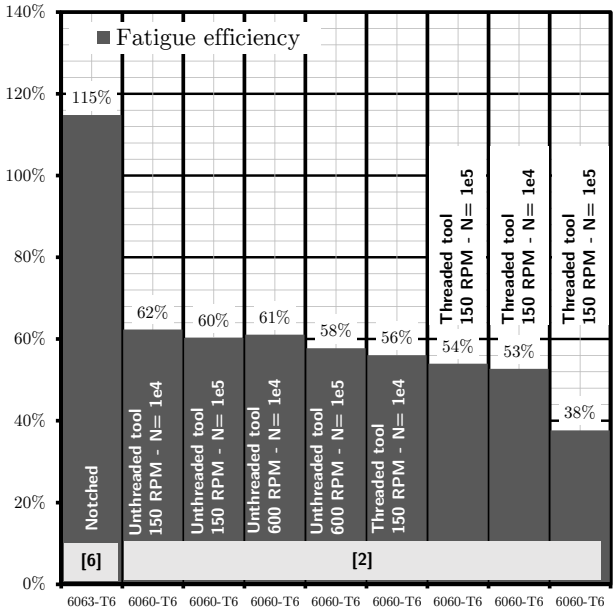

b)

Figure 1.2: Mechanical efficiencies of 6000 series AA joined with FSW, from [2,5,6]: (a) Tensile efficiency; (b) Fatigue Efficiency. Adapted from [26].

Material	Ref.	Test conditions	Tensile		Fatigue	
			YS [MPa]	**UTS [MPa]**	S_{lim} **[MPa]**	N **cycles**
6082-T6	[5]	Not welded	276	323	-	-
		FS welded	141	226	115	2e5
		Mig welded	177	210	80	2e5
6061-T6	[5]	Not welded	306	342	-	-
		FS welded	159	242	100	2e5
		Mig welded	156	221	90	2e5
6063-T6	[6]	Not welded	192	218	108*	2e5
		FS welded	112	193	124*	2e5
6060-T6	[2]	Not welded	223	252	239	1e4
					202	1e5
		FSW, unthreaded @ 150 mm/min	-	155	149	1e4
					144	1e5
		FSW, unthreaded @ 600 mm/min		150	146	1e4
					138	1e5
		FSW, threaded @ 150 mm/min	-	156	134	1e4
					129	1e5
		FSW, threaded @ 600 mm/min		149	126	1e4
					90	1e5

*Notched samples

Table 1.5: FSW tensile and fatigue strengths obtained for 6000 series AA from [2, 5, 6], adapted from [26].

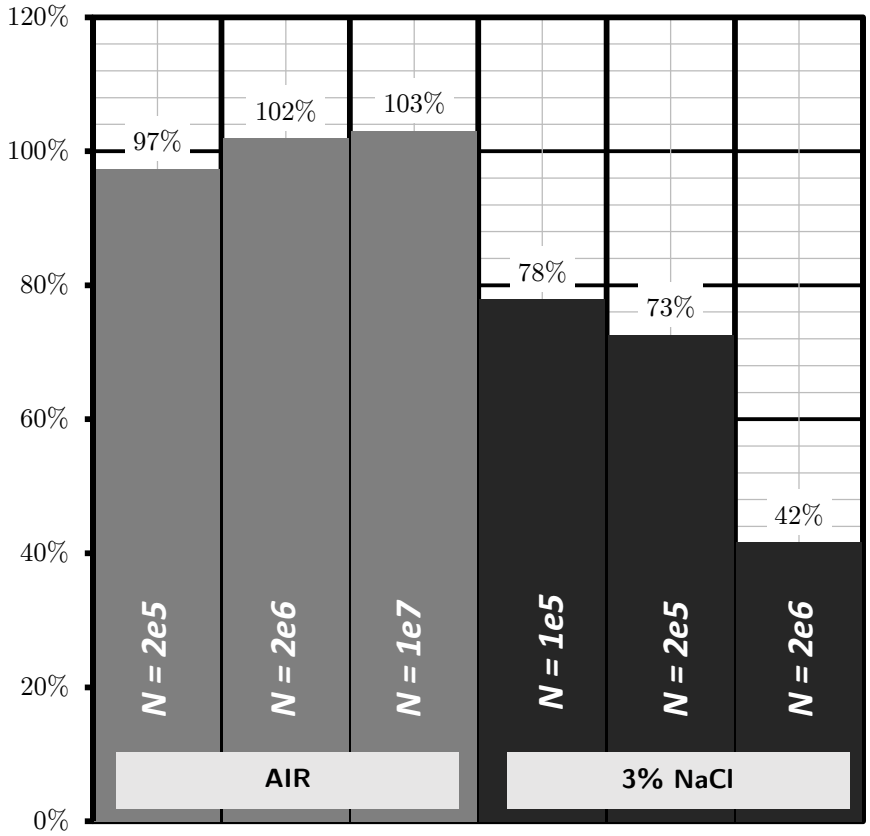

Figure 1.3: Fatigue efficiencies of 7075-T6 joined with FSW, obtained from [65] in air and 3% NaCl environment.

decay of its fatigue behaviour similar to the unwelded alloy, albeit with a slighter decrease in fatigue strength, caused by the accumulation of corrosion pits at the discontinuity between the TMAZ and the HAZ generated by the FSW process. Even if further research is mandatory on the subject, the obtained data seem to show a promising development of the FSW for the 7075-T6 alloy. With the adoption of such technique, a broad range of applications in the automotive field and in other sectors could be successfully tackled, pushing the alloy towards new, unexplored commercial applications.

Material	**Ref.**	**Test conditions**	**Tensile**		**Fatigue**	
			YS [MPa]	**UTS [MPa]**	S_{lim} **[MPa]**	N **cycles**
7075-T6	[13]	FS welded	-	-	79	2e6
7075-T6	[65]	Not welded*	474	547	115	2e5
					102	2e6
					99	2e7
		FS welded*	364	490	112	2e5
					104	2e6
					102	2e7
7075-T6	[65]	Not welded, 3% Nacl*	-	-	77	1e5
					62	2e5
					24	2e6
		FS welded, 3% Nacl*	-	-	60	1e5
					45	2e5
					10	2e6

* Fatigue values are obtained from numerical interpolation of S-N data

Table 1.6: FSW tensile and fatigue strength for 7075-T6 AA, from [13, 65].

Chapter 2

SCC on Ti-6Al-4V titanium alloys

2.1 Literature review

As briefly described in sections 1.1 and 1.2, Titanium light alloys are often chosen not only for their exceptional strenght-to-mass ratio, but also for their remarkable corrosion resistance, which puts them in direct competition with stainless steels for high strength applications in aggressive environments [16, 34–36]. However, when certain environmental, mechanical and metallurgical condition are met, titanium alloys can show dramatic vulnerability to SCC and corrosion fatigue. In the present Chapter, the mechanisms which lead to Stress Corrosion Cracking of Ti-6Al-4V in methanol environment at different concentrations are extensively explained. The work is supported by experimental methods, which were object of several published works [25, 55, 59, 60, 66]. Concerning the corrosion fatigue behaviour of Ti-6Al-4V, Chapter 3 will deal with the subject.

As anticipated in section 1.1, corrosion resistance of Ti alloys is granted by the formation of a resistant, thin layer of titanium dioxide TiO_2 . According to the work of *Aladjem* [33], titanium is a very reactive metal, and for its position on the periodic table and its electrochemical behaviour, is classified as a "film-former", i.e. a metal which is naturally capable to form a natural oxide film when

exposed to air, water or other oxygen containing media. The natural thickness and morphology of the layer depend on the oxidation condition, but according to [33], the thickness of the natural layer ranges between 5 and 70 Å. A very wide variety of layers can be realized over titanium substrates, with very different structural and electrochemical properties, as resumed in [33]. Either if the film has been formed in an artificial or natural way, however, the corrosion resistance is completely attributable to its presence [33, 37], and particularly to the inert behaviour of the TiO_2 layer with respect to most of the natural environments and chemicals. By the work of *Sanderson, Powell and Scully* [67], SCC resistance of Ti alloys is caused by the prevention of pit initiation due to the TiO_2 layer, which as a consequence prevents also crack initiation. According to [16, 33], corrosion occurs through "weak spots" in the oxide, such as surface defects, sharp notches or cracks. Although artificial strengthening is recommended by [33], natural reformation of the oxide is possible in most environments, according to [37]. Another significant parameter concerning the fatigue behaviour of the alloy is the presence of applied stresses, as found by *Brown* [16] and *Trasatti and Sivieri* [32]. The TiO_2 layer can be also removed by external mechanical stress or abrasive actions, thus leading to corrosion sensitivity of titanium alloys. Indeed, the presence of stress corrosion cracking (SCC) effects in water mixtures and other media for certain titanium alloys under surface defects and mechanical actions has been already pointed out in several research studies [16, 32, 40, 41, 45, 54, 67].

According to [16], the SCC for titanium alloys is caused by three different agents, i.e. the mechanical effects, the environmental effects and the metallurgical effects. Considering the metallurgical aspect, in $\alpha + \beta$ alloys such as Ti-6Al-4V, the α phase has demonstrated SCC susceptibility, given also the high aluminium presence in this particular phase [16]. As previously indicated, the particular environment is fundamental in Ti-6Al-4V SCC, since the TiO_2 oxide is inert to most aggressive combinations. According to [16, 45], titanium is susceptible of SCC in nitric

acid, various molten salts, nitrogen tetroxide, several organic solvents and methanol. Considering SCC in presence of chlorides, i.e. in NaCl solution in water, SCC on Ti-6Al-4V occurs only if the base material is precracked, i.e. by previous fatigue load [16], although its resistance in absence of cracks is proven in salt water environments [32, 35, 36]. [67] has indeed found SCC susceptibility of Ti-5Al-2.5Sn in acidified 3% NaCl solution, but reported that no similar effects were found for Ti-6Al-4V. Aqueous chloride environment on Ti-6Al-4V indeed accelerates crack propagation rates, but it is not responsible of crack nucleation under stresses [16,67]. However, as will be deepened in Chapter 3, the effects of prolonged exposure to salt spray environment or immersion in NaCl solution can lead to pitting corrosion, with a direct influence with respect to the heat treatments employed [38]. Considering non-aqueous media, *Trasatti and Sivieri* [32] analysed the SCC behaviour of commercially pure Ti in non-aqueous solvents, such as ethyl ether, acetic anhydride and acetic acid. The results show Ti susceptibility to SCC in acetic anhydride at 60°C.

As a well known history in literature, the most dramatic SCC behaviour concerning Ti-6Al-4V was found during the experimental testing of the fuel tanks for the Apollo mission, as reported in the technical reports by *Johnson* [40] and *Johnston, Johnson, Glenn and Castner* [41]. Pure methanol was adopted as a reference corrosive fluid during these tests, leading to a dramatic reduction of the time to failure for static pressurization and for fatigue in repeated pressurization. Considering SCC results, pressure vessels statically loaded at 827 MPa failed in less than 17 min in a methanol environment, while the same load conditions in air showed no results [41]. Fatigue results showed the same dramatic evidence, as will be exposed in Chapter 3. The SCC susceptibility in methanol was confirmed by similar results in the work of *Chen, Kirkpatrick, and Gegel* [39], involving the SCC behaviour of Ti-6Al-4V alloy in acidified methanol solution, with 0.166 wt% HCl, at different methanol concentrations. From these results, it was found that an amount of water higher than 0.05% was necessary to initiate SCC, with the maximum SCC effect in

terms of dramatic decrease of time to failure being found at 0.3–0.6% water concentration, with minimum fracture times of < 5 h. Water concentrations above 1% led to a progressive passivation of the SCC behavior, approaching the same results obtained in air, where no failure was observed. According to the authors of [39], the formation of passive oxide films was again possible, due to the increased water content, thus interfering with crack initiation and propagation.

Sanderson and Scully [54] analysed the SCC behaviour on Ti-6Al-4V U-bend specimens, immersed in reagent-grade methanol and acidified methanol, with 1.13 wt.% HCl. Both experiments presented an overall water content of 0.083 vol%. Fracture times of 30 h for reagent-grade methanol and less of 1 hour for acidified methanol were found. The $\alpha + \beta$ microstructure showed transgranular cracking across the α-phase, in accordance to the α susceptibility proposed by [16]. Detachment of the protective oxide was found on the specimens tested in the acidified methanol mixture. The oxide removal was initially detected near the stress-loaded SCC cracks, increasing to a wider region before fracture. Authors of [54] reported that SCC passivation was reached, for the acidified solution, considering an amount of water near 1.5%. The SCC sensitivity in methanol may be considered a critical aspect not commonly found in the application of the Ti-6Al-4V alloy, but it must be remembered that this aggressive environment can be encountered in typical applications in the oil&gas sector, in the aeronautic sector, and in new applications include methanol as a chemical reactant, such as in fuel cells, as indicated in section 1.2.

Apart from methanol environments, generic corrosion and corrosion fatigue can be found in fluoride rich envrionments [37, 44], and in artificial saliva environments as well, considering dental implants [44]. Another remarkable work concerning Ti-6Al-4V SCC is the analysis conducted by *Tsai, Lin and Pan* [68], where the SCC behaviour in a Lewis neutral $AlCl_3 - EMIC$ ionic liquid was investigated. Apart from the very specific environment, the work is very interesting mainly for the

Test campaign	Ref.	Specimens	Environment (wt.%)	Time to fail
Johnston et al.	[41]	Straight	Air	Not failed (>4463 h)
			Methanol (> 99.8%)	17 min
Chen et al.	[39]	U-bend	Methanol (< 98.8%)	Not failed (>200h)
			Methanol (98.8%÷99%)	180 ÷ 80 h
			Methanol (99%÷99.5%)	80 ÷ <5 h
			Methanol (> 99.8%)	Not failed (>200h)
Sanderson et al.	[54]	U-bend	3% NaCl	Not failed (>200h)
			3% NaCl + HCl	Not failed (>200h)
			Methanol	30 h
			Methanol + HCl	<1 h

Table 2.1: SCC results on Ti-6Al-4V alloy, from [39, 41, 54].

Scanning Electron Microscopy (SEM) investigation, which shows an intergranular behaviour of the crack near the initiation site, where cracking between the α/β phase boundary is found. Transition to transgranular fracture occurs at sufficient crack length, showing clear SEM examples of these two fracture modes on a Ti-6Al-4V alloy.

2.2 Materials and methods

In order to increase the knowledge of Ti-6Al-4V SCC behaviour, quasi-static SCC tests were performed on flat, slightly notched ($K_t = 1.18$) Ti-6Al-4V specimens, immersed in methanol at different concentrations [55, 59, 66]. The notch on the flat dogbone specimens, machined according to the geometry presented in [55, 59], and reported in Figure 2.1, has been realized in order to obtain failure in the test section with inferior loads, resulting in a test section area of 45 mm^2. The local stress concentration factor K_t was obtained by a linear elastic FE simulation with plane-stress elements, as reported in Figure 2.1, resulting in a value of 1.18. The specimens were then machined from the treated Ti-6Al-4V plate, resulting in a load axis transversal with respect to the rolling direction of the laminate. The samples were then vacuum heat treated following a Solution Treatment and Overaging (STOA) procedure. The STOA cycle consisted in a 1-h solution treatment at 925°C, followed by a 2-h over-

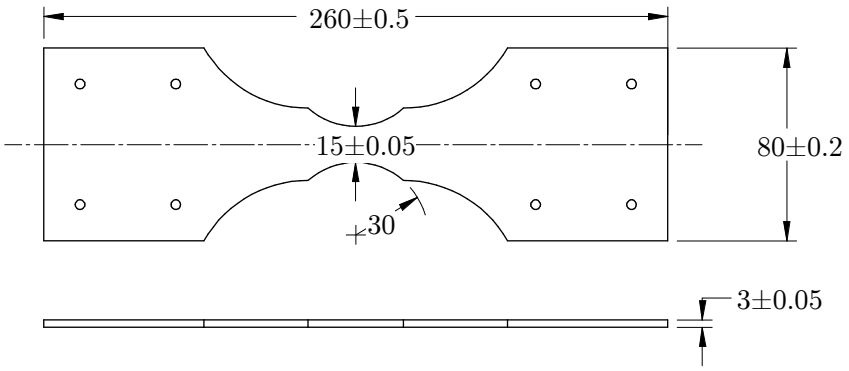

Figure 2.1: Ti-6Al-4V flat dogbone specimens, $K_t = 1.18$, adopted for the quasi-static SCC load campaign, from [59].

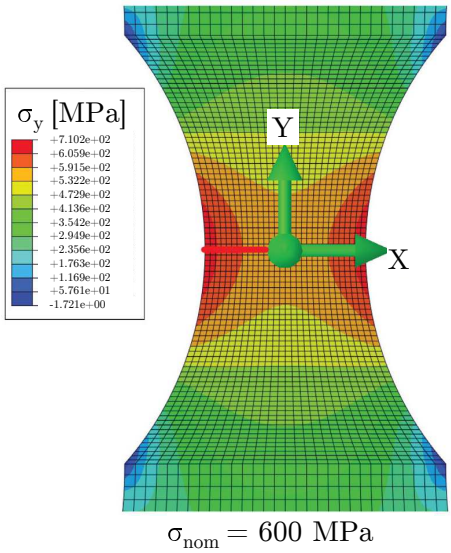

Figure 2.2: FE model for the determination of K_t at $\sigma_{nom} = 600$ MPa applied load on linear elastic model, from [55].

aging at 700°C. Tensile properties have been determined both for the raw material and after the STOA treatment. The chemical composition and tensile properties are reported in Tables 2.2 and 2.3 respectively. Vickers hardness test resulted in a material hardness of 350 HV.

Ti-6Al-4V specimens were tested in a fixed frame, specifically designed for quasi-static SCC testing. The device consists in a threaded rod support, linked to two

Al [%]	**V [%]**	**Fe [%]**	**O [%]**	**C [%]**	**Ti [%]**
5.97	4.07	0.20	0.1885	0.03	Bal.

Table 2.2: Chemical composition of Ti-6Al-4V for quasi static SCC tests [55, 59].

Condition	**YS [MPa]**	**UTS [MPa]**
Before STA	1050	1100
After STA	945	990

Table 2.3: Ti-6Al-4V tensile properties before and after STOA treatments, according to [55, 59].

spherical hinge grips, with an in-line load cell. The hinge grips are designed to reduce parasite bending moments due to misalignments during specimen mounting. The external load is applied by imposing a torque on a nut mounted on the threaded rod, and is measured using the load cell. The specimen test area is immersed in a methanol solution, at different methanol concentrations, prepared with the help of a precision scale. In order to avoid errors due to methanol evaporation, a fresh solution was provided for the specimen immersion at the beginning of each test day. In order to avoid evaporation during the test, the methanol containing envelope was sealed, as shown in Figure 2.3. Linear strain gages were applied outside the test section in order to measure the presence of parasite bending moments, and help the correct mounting and alignment of the specimens.

A quasi-static load procedure was followed, as presented in Figure 2.4. Each hour, an increment of $\Delta\sigma = 5$ MPa, in terms of nominal stress (i.e. neglecting the K_t correction) was applied by tightening the terminal nut on the threaded rod support. The initial nominal load for each test was set up at 650 MPa. In order to avoid dynamic effects, which could have affected the SCC behaviour of the specimens, very slow load increases were carefully applied, preventing dynamic effects. The mean strain rate value, considering the mean slope of the curve presented in 2.4, was 1.2×1e-8 s^{-1}, with estimated strain rate maximum peaks during the load application of the order of 1e-6 s^{-1}. The load was increased until the specimen failed, typically during the steady load phase. The failure resulted in complete separation of the sample, along the test section. The fracture surfaces were carefully protected after the failure, to be analysed with Scanning Electron Microscopy (SEM), to characterize the environmental effect in relation to the failure mechanism as reported

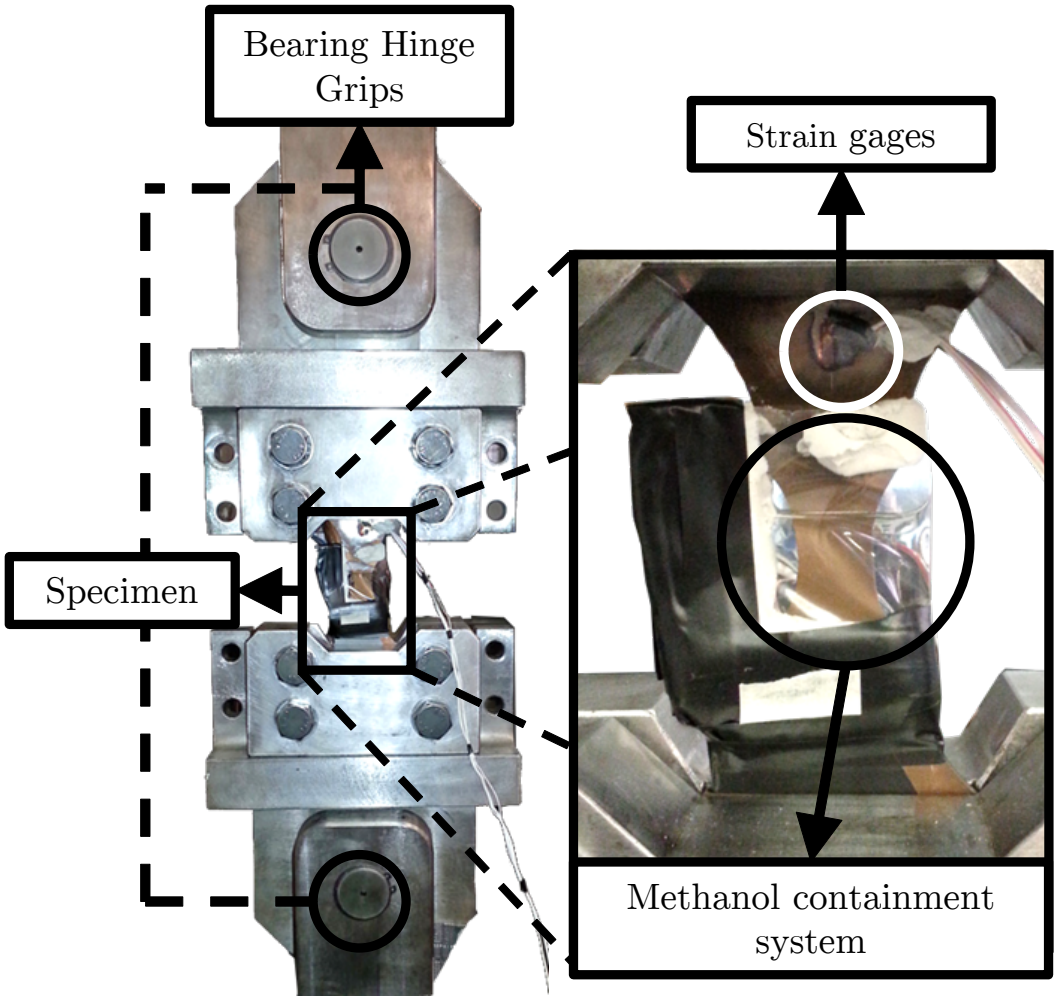

Figure 2.3: Experimental setup for the quasi static SCC tests: (a) Specimen mounted on hinge grips; (b) Methanol containment system and applied strain gages, from [55].

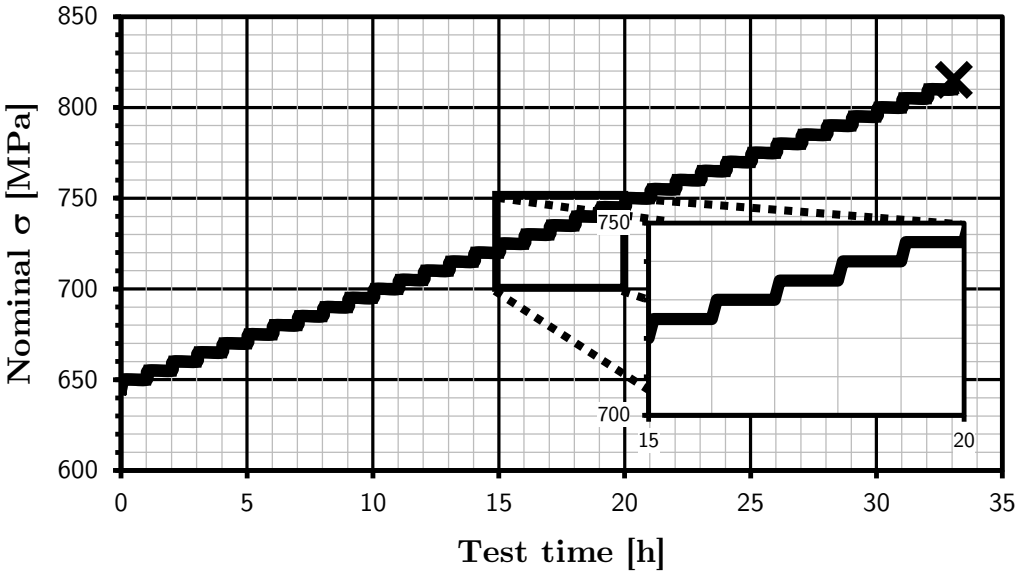

Figure 2.4: Load history for a single quasi-static SCC test procedure, adapted from [55].

in section 2.3. Metallographic sections of the tested specimens were also used for Light Optical Microscopy (LOM) analysis, in order to assess the metallurgy impact on the SCC behaviour. Microhardness tests were conducted as well, and reported with LOM analysis in section 2.3 as well.

2.3 Experimental results

The results, in terms of nominal stress σ_{nom} in the test section, are reported in Figure 2.5. σ_{nom} refers to the nominal stress, i.e. not considering the presence of the notch effect due to $K_t = 1.18$. To obtain the actual failure stress, multiplication by K_t is needed. From Figure 2.5, it can be seen that the methanol contribution becomes critical for concentrations higher than 92.5 wt%. For lower concentrations, the trend of the data points does not show a significant influence of the environment, with an average σ_{nom} value of 906 MPa. At higher concentrations, the maximum quasi-static SCC nominal strength decreases linearly, whit a steep fall leading to a maximum -25% reduction for the highest methanol concentration tested, i.e. reagent-grade,

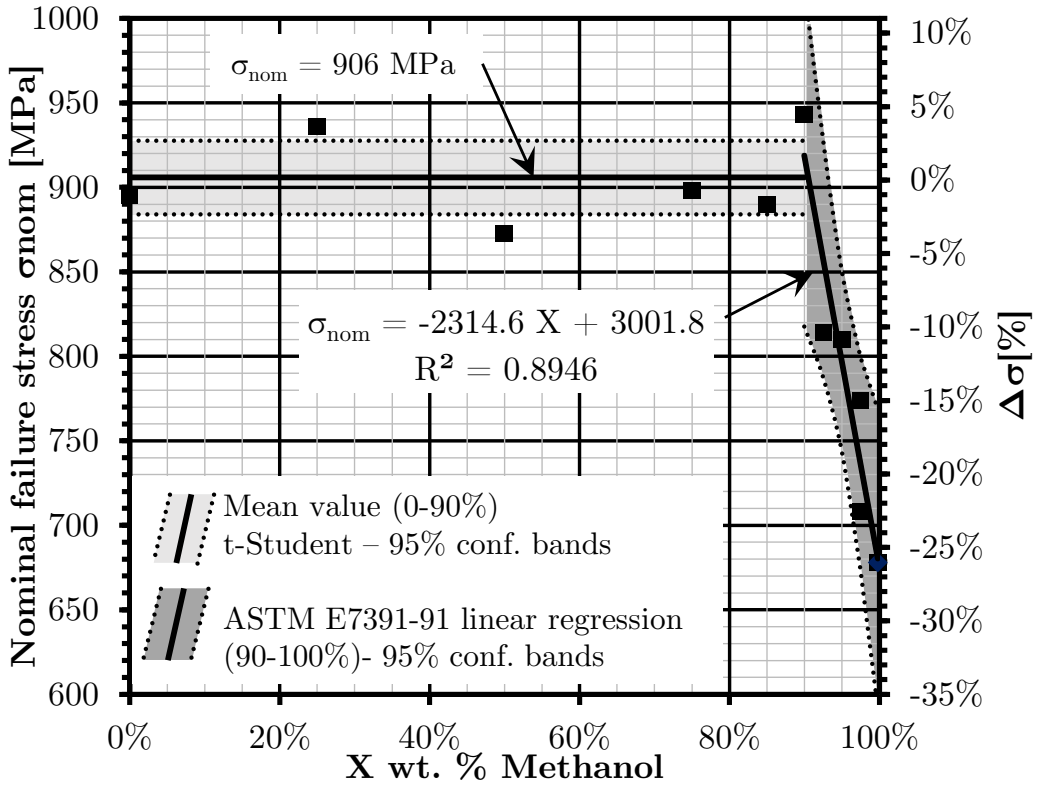

Figure 2.5: Experimental results for the different quasi-static SCC tests, in terms of nominal maximum stress σ_{max}, at different methanol wt. % concentrations, adapted from [25, 55, 59].

99.8 wt%. In Figure 2.5, *t-Student* bands with 95% confidence are reported for the region not influenced by methanol, while linear regression, 95% confidence bands have been reported considering data between 90 and 99.8%. The confidence bands have been calculated according to the ASTM E739-91 standard [69].

After failure, the fracture surfaces were analysed with SEM, to assess the morphology of the fracture surface, and the effect of the microstructure on the fracture mechanism. The SEM microscopies showed, for the specimen tested in air, a region of transgranular fracture near the external edge of the fracture surface, extending for a depth of roughly 60 to 80 μm, as seen in Figure 2.6. The fracture surface of specimens tested in high methanol concentrations showed however an extended transgranular fracture feature, covering the whole region near the crack initiation, as reported in Figure 2.7.

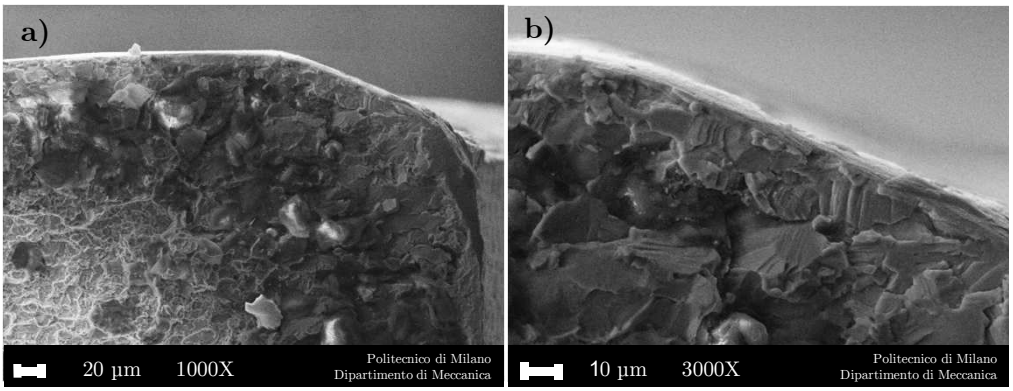

Figure 2.6: SEM observation of the sample tested in laboratory air near the crack initiation region: (a) 1000 ×; (b) 3000 ×. Adapted from [55].

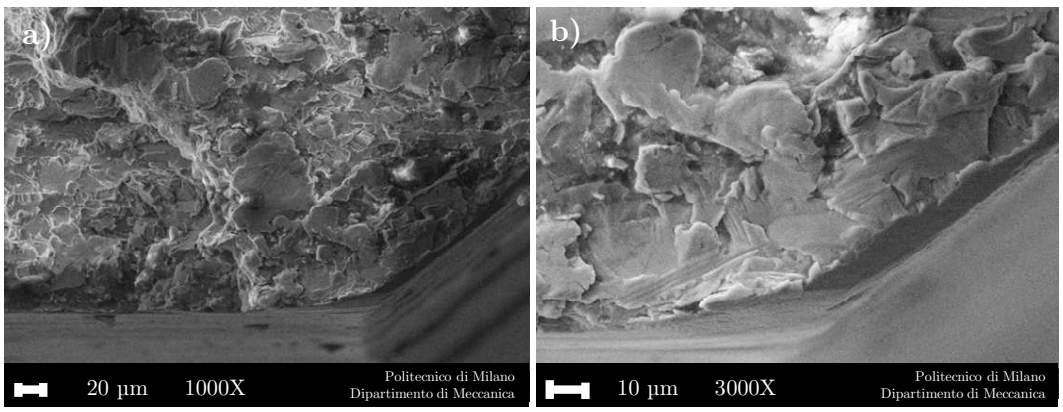

Figure 2.7: SEM observation of the sample tested in 99.8% methanol solution near the crack initiation region: (a) 1000 ×; (b) 3000 ×. Adapted from [55].

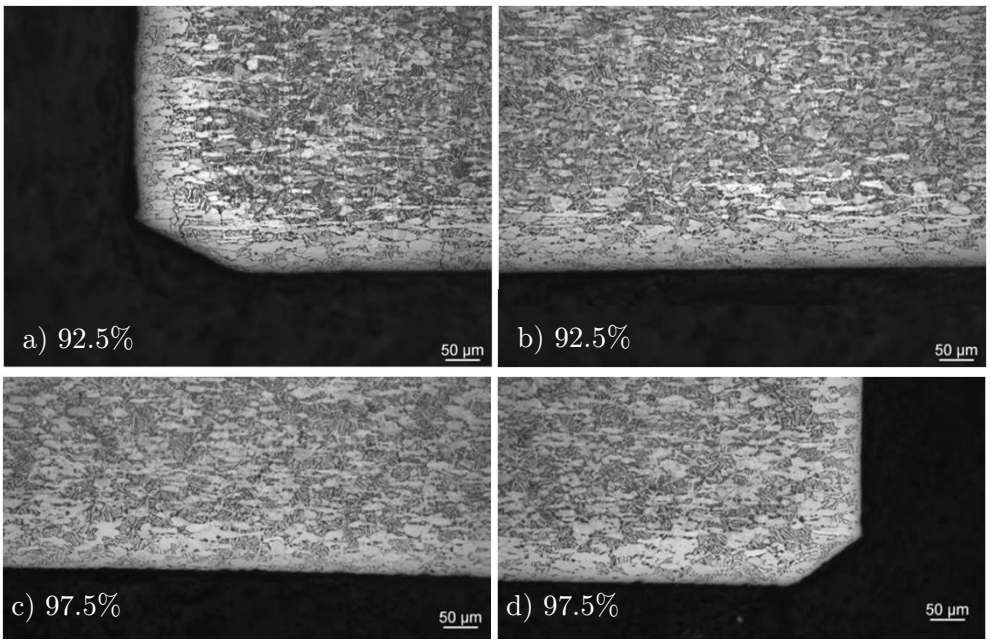

Figure 2.8: LOM of the metallographic sections parallel to the fracture surface: α-case is observed on the samples' microstructure near the surface edge. Sections were taken from samples: (a) 92.5 wt.% near fracture initiation edge; (b) 92.5 wt.% external edge; (c) 97.5 wt.% external edge; and (d) 97.5 wt.% near fracture initiation edge. Adapted from [55, 59].

In order to evaluate the origin of the transgranular features in the fracture surface of the specimen failed in air, metallographic sections were taken, and analyzed using Light Optical Microscopy (LOM). In order to assess the metallurgic morphology of the material, a first set of sections was taken parallel to the fracture surface, as in Figure 2.8, highlighting an α-enriched layer, ~60 µm thick, all around the external surface of the sample. A microhardness profile was carried out on the sample tested with 97.5 and 92.5 wt% methanol solution, resulting in very high values, especially within the 60 µm α-case, as shown in Figure 2.9. Very high $HV_{0.01}$ values, around 550, were found within the α-case, and they were reduced outside it. Consider that the values of microhardness outside the α-case, in the bimodal region of the microstructure, which reach an approximate value of 380, are taken within the α grains.

In order to clarify some dynamics related to the fracture mechanism, metallographic cross sections were cut along a plane orthogonal with respect to the fracture

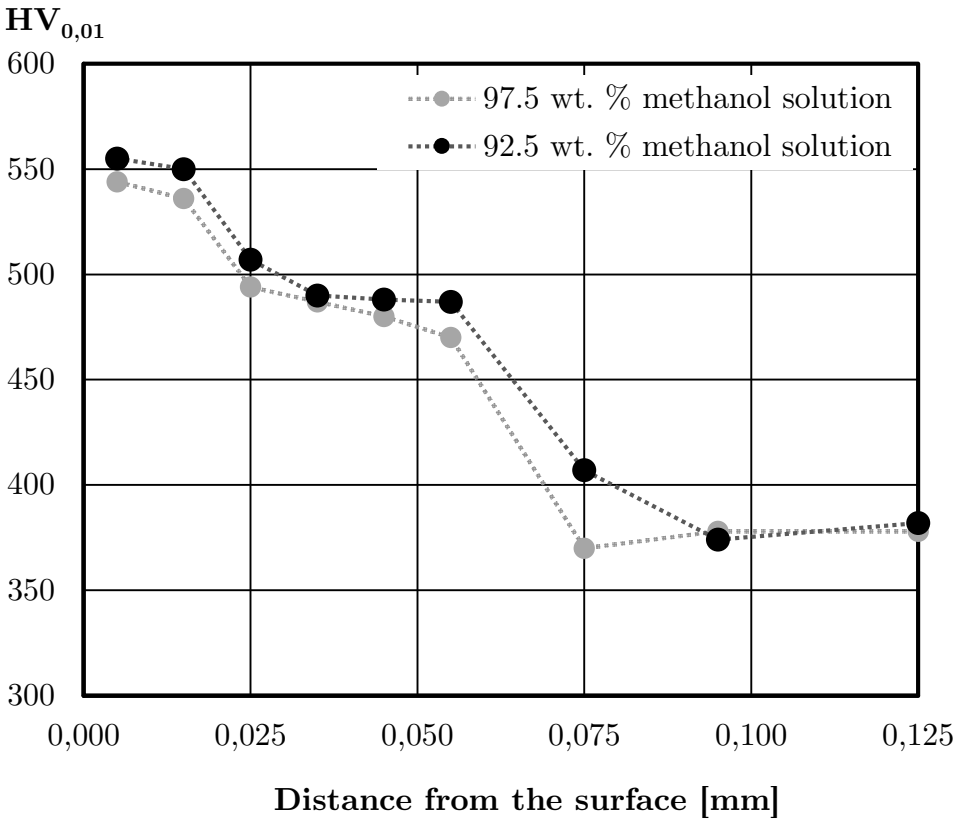

Figure 2.9: Microhardness profile focused on the α-case layer. The microhardness values within the bimodal microstructure (distance from the surface higher than ~60 μm) refer to the α-grains, adapted from [25].

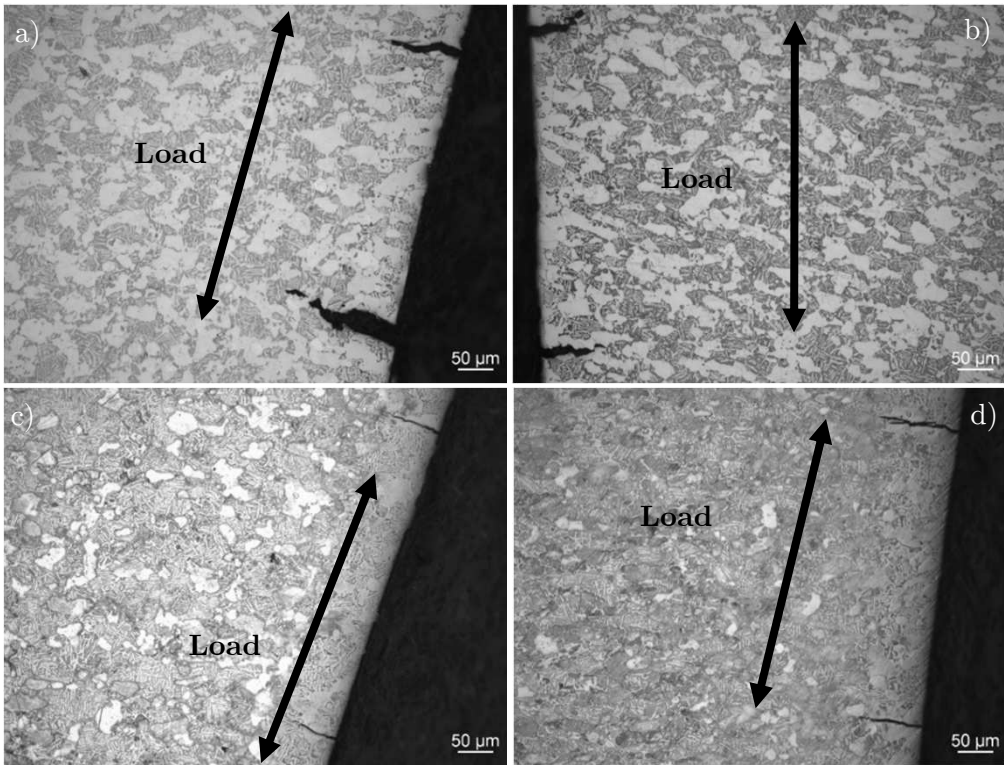

Figure 2.10: LOM of the metallographic sections perpendicular to the fracture surface, and parallel to the load application: cracks orthogonal to the load directions are visible through the α-case, for different concentrations: (a) laboratory air; (b) 50 wt.% methanol; (c) 95 wt.% methanol; and (d) 99.8 wt.%. Adapted from [25,55,59].

surface, so that the surface to be analysed was parallel to the applied load. After polishing and etching, they were observed by LOM, the results being showed in Figure 2.10. As it can be clearly seen by comparing the LOM micrographics at different concentrations, the cracks show a similar penetration through the α case. Cracks with reduced methanol concentrations show a wider opening in the direction of the load, probably due to the higher stress levels reached in low methanol testing: the samples tested in the 95% and 99.8% methanol solution, e.g., failed with stresses, respectively 15% and 25% less than the laboratory air and 50% methanol concentration specimens.

2.4 Discussion

Considering literature evidence previous to the current study, it has been found that the presence of methanol inhibits the formation of the passive film because it reacts with titanium, resulting in a non-protective titanium methoxide, according to the reactions identified in [54]. A practical and effective way to interfere with this phenomenon, as described in several literature works [36, 39, 54], is to add water to the methanol solution. According to [36, 39, 54], the presence of sufficient water in methanol, in fact, promotes full repassivation. According to the experimental tests described in the present chapter, the minimum water content found preventing SCC is ~7.5%. The minimum required value in NACE recommendations [36] is lower for Ti-6Al-4V (~3%). *Chen* et al. [39] and *Sanderson and Scully* [54] report even inferior values, for passivating the methanol mixture in their works, with progressive passivating effects starting from 1-1.5 wt.% water concentration.

The reason for the higher required level of water in the present study for complete passivation, i.e. $> 7.5\%$, lies in the individuation of an α-case on the external surface of the specimen. Theα-case, commonly generated by oxygen absorption at high temperatures, for example, during a heat treatment. is generally hard and brittle, as reported by *Dong* et al. [70]. SCC can be increased by the presence of small cracks, as widely reported in [16, 32, 37], which are promoted by the presence of the α-case. The transversal LOM images, presented in Figure 2.10, clearly depict the presence of these cracks, even in specimens tested outside the methanol environment. Moreover, from the work of *Polmear* [71], it is found that the simple presence of an α-enriched layer results in a SCC resistance decrease. The crack depth is consistent with the α-case presented in the parallel metallography showed in Figure 2.8, and with the transgranular fracture region, of approx. 60 - 80 μm, found in the specimens tested in air, as presented in Figure 2.6. Moreover, microhardness testing highlighted the increased hardness associated with the α-layer, leaving little doubt regarding the presence of the α-layer, and the increase in SCC sensitivity it granted during the

presented tests.

Another possible responsible for the high amount of water, needed to passivate the SCC behaviour related to the presented test, can be found in the reduced oxygenation of the methanol water solution. As seen from the test setup in Figure 2.3, the methanol solution envelope is closed during the sample loading. The absence of oxygenation leads to detrimental effects in the mechanism responsible of the TiO_2 layer repassivation, even in the presence of sufficient amount of water, as reported by *Aladjem* [33]. In summary, the reduced water passivation effect found in the present results, with respect to literature evidence, is caused by the presence of a 60 μm α-case, resulting in enhanced SCC sensitivity, and by the reduced oxygenation of the solution, which interferes with the surface repassivation by the formation of a TiO_2 layer.

2.5 Remarks

Considering the work exposed in the present chapter, a SCC campaign was conducted over STOA Ti-6Al-4V flat dogbone specimens, with light notch geometry (K_t = 1.18). The samples were immersed in methanol-water mixture, with different concentrations. The quasi-static load tests, in which the load was raised of 5 MPa per hour, highlighted a sensible SCC influence of the methanol water mixture, starting from a 92.5 wt.% methanol concentration, and arriving to a maximum strength drop of of -25% for the reagent-grade (99.8 wt.%) methanol. For water content higher than 7.5 wt%, no SCC effects were found, the specimen tested at 90 wt.% methanol concentration resulting in failure at a stress level comparable to air tests.

In order to understand the effects involved in the failure mechanism, and especially the relatively high amount of water needed for the SCC sensitivity passivation, the specimens were characterized by microindentation tests, fracture surface SEM observation, and optical investigation of the microstructure, both on parallel and

perpendicular fracture planes. Microindendation tests and metallographic analyses revealed an α-case layer, ~60 µm thick, on the external surface of the specimen, just below the oxide layer. Metallographic analysis on planes perpendicular to the fracture surface showed extended cracking of the α-case, on specimens tested in the whole concentration range. SEM analyses corroborated the presence of an α-layer, resulting in transgranular fracture near to the outer edge, even considering specimens which failed in laboratory air. The transgranular region depth was coincident with the α-layer width, as assessed by LOM metallographic analysis on cuts parallel to the fracture surface, and microhardness analysis. On the other hand, specimens tested at high methanol concentration resulted in a wider transgranular fracture region, as expected. Moreover, a low oxygenation in the solution may increase the SCC susceptibility of the Ti-6Al-4V alloy. The results of the present work clarify the detrimental contribution of an α-case layer in Ti-6Al-4V specimens in methanol solutions, with water passivation not working even at water contents higher with respect to industrial recommendations [36]. The work presented in this chapter raises a significant warning for the quality control of heat-treated Ti-6Al-4V material employed in critical aggressive environments.

Chapter 3

Corrosion Fatigue of Ti-6Al-4V

3.1 Literature review

The presence of an aggressive environment under a fatigue dynamic loading presents a more complex scenario with respect to SCC under static loads. In particular, two different contributions of the environment must be considered. The first concerns the impact of the environment in generating pitting defects, depending on the aggressive medium, the material composition and the eventual discontinuities in the film. In the work by *Codaro* et al. [38], a detailed analysis of the pitting effects over Ti-6Al-4V in NaCl solution immersion and salt fog exposure is presented, showing an increased pit density in the annealed condition. The presence of pitting can lead to dramatic results on fatigue behaviour, anticipating nucleation of fatigue cracks due to the presence of defects. Fatigue cracks can propagate hence at lower levels of ΔK_{th}. In addition to this effect, the presence of an environment can lead to sensible changes in the Fatigue Crack Growth Rate (FCGR) during crack propagation. Considering Ti-6Al-4V, as well as similar alloys, a deep investigation on corrosion fatigue in aqueous media has been conducted by and *Dawson and Pelloux* [56] and *Dawson* [57]. Several parameters were analysed, under the perspective of fracture mechanics, considering in particular the effects on corrosion fatigue of the specific environment, frequency

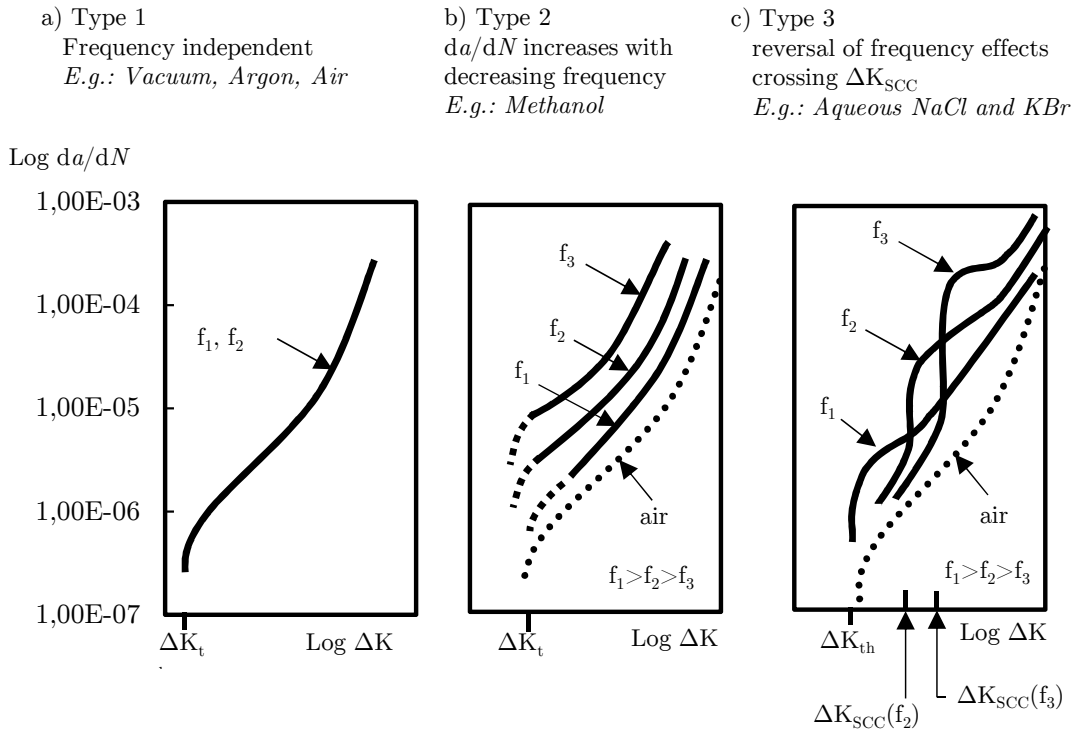

Figure 3.1: Schematic illustration of the effects of frequency on corrosion fatigue of titanium alloys, adapted from [57].

and cyclic load wave shape, thus resulting in a parametrized collection of $\mathrm{d}a/\mathrm{d}N$ vs. ΔK curves for different test conditions.

The work of *Dawson and Pelloux* [56], which analyses the crack growth behaviour of titanium alloys in aqueous solutions, presents a detailed investigation on the frequency effects on the corrosion fatigue of such alloys. In particular, according to [57], three possible frequency dependencies are found in titanium alloys in different environments, as reported in Figure 3.1.

The first possible corrosion-fatigue behaviour is frequency independent, and it is typical of air, vacuum, and water containing corrosion inhibitors (e.g., Na_2So_4), even if the fatigue crack growth rate (FCGR) absolute values may change between these environments, as presented in Figure 3.1a. A second typical case is presented in 3.1b, and is commonly found in presence of methanol. In this second case, the frequency plays a positive role. Higher frequencies reduce the FCGR in the whole ΔK range,

since lower frequencies grant more time to the environment to successfully attack the crack tip during the fatigue loading. The third possible scenario, presented in Figure 3.1c, presents a more complex behaviour, typical of aqueous NaCl and KBr solutions. At low ΔK values, below the ΔK_{SCC} threshold, low frequencies play a positive role, since a partial repassivation of the crack tip is possible, due to the sufficient time granted by the slow dynamic loads. Above ΔK_{SCC} however, repassivation is not possible anymore, and cyclic SCC sets on. In this region, the behaviour is again similar to the FCGR found for methanol solutions, i.e. lower frequencies are more detrimental, since they grant more time for the corrosion to take place during the dynamic load. In [56], the effect of the waveform is also investigated, by comparing the FCGR curves of Ti-6Al- 6V-2Sn in an aqueous KBr solution. The worst FCGR effects, found for ΔK values above ΔK_{SCC}, are related to square load cycles, if compared to haversine waves, due to the increased time granted by the square wave for the onset of the cyclic SCC behavior. A brilliant example of this double behaviour, reported in [56], is found in testing of Ti-6Al-4V in 0.6 M NaCl solutions, at frequencies of 1, 5 and 10 Hz. The reported FCGR curves, presented in Figure 3.2, show a definite inversion of the frequency dependence trend above ΔK_{SCC}, especially evident for the 1 Hz experimental results. In Figure 3.2, it is also evident the dependency of the ΔK_{SCC} value from the load frequency, the highest value of ΔK_{SCC} being found for the lowest frequency (1 Hz).

In the work by Dawson [57], the effects of a methanol-containing environment on a Ti-6Al-6V-2Sn titanium alloy have been analysed. In particular, the effects of a rising methanol concentration in an halide LiCl water solution is considered, beside pure methanol and pure water environments. The study confirmed that no repassivation mechanism are active below ΔK_{SCC} for this environment. A significant

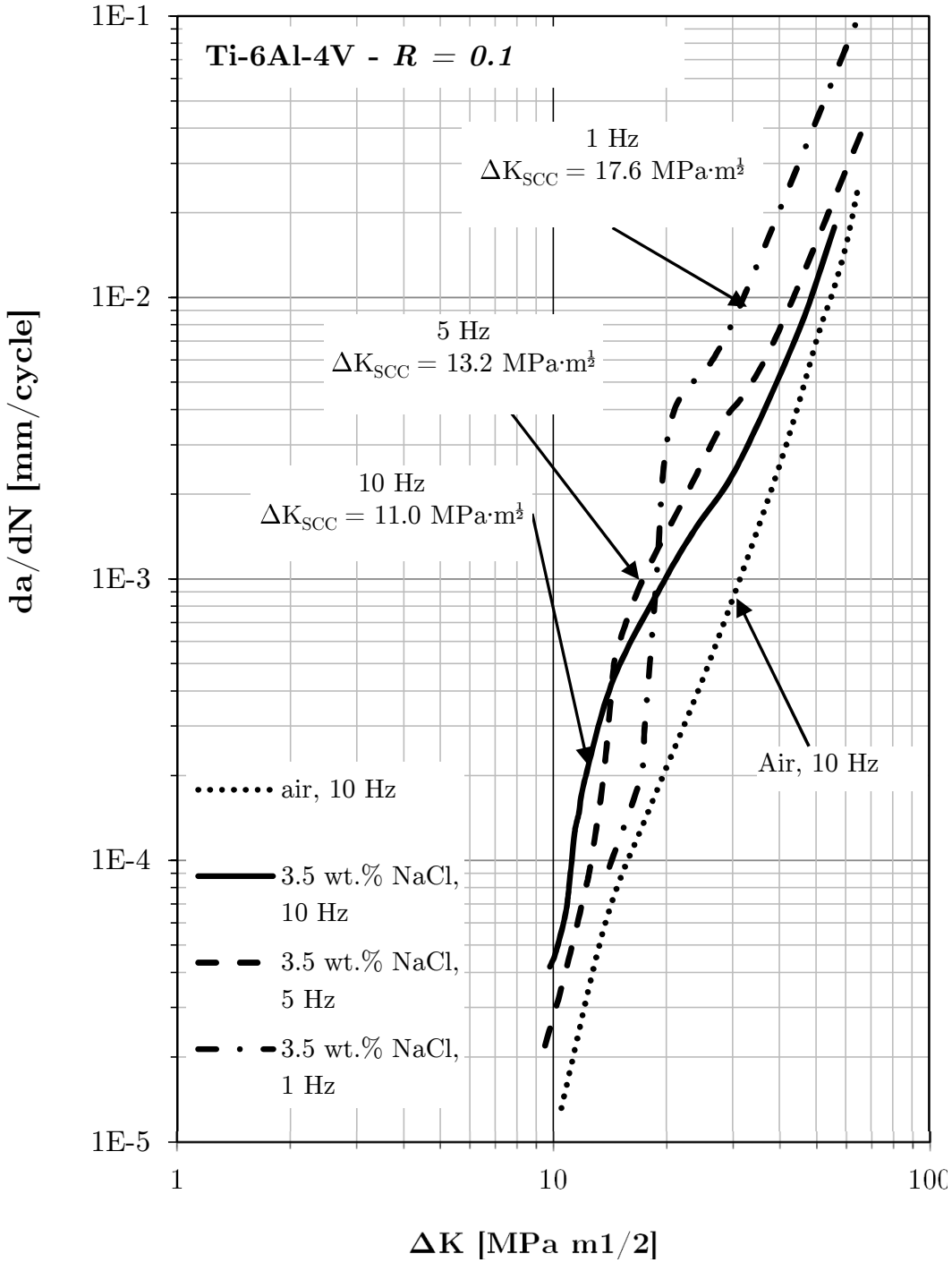

Figure 3.2: da/dN vs. ΔK curves with frequency effect on FCGR of Ti-6Al-4V in aqueous 3.5 wt.% NaCl, $R = 0.1$, haversine wave form, adapted from [56].

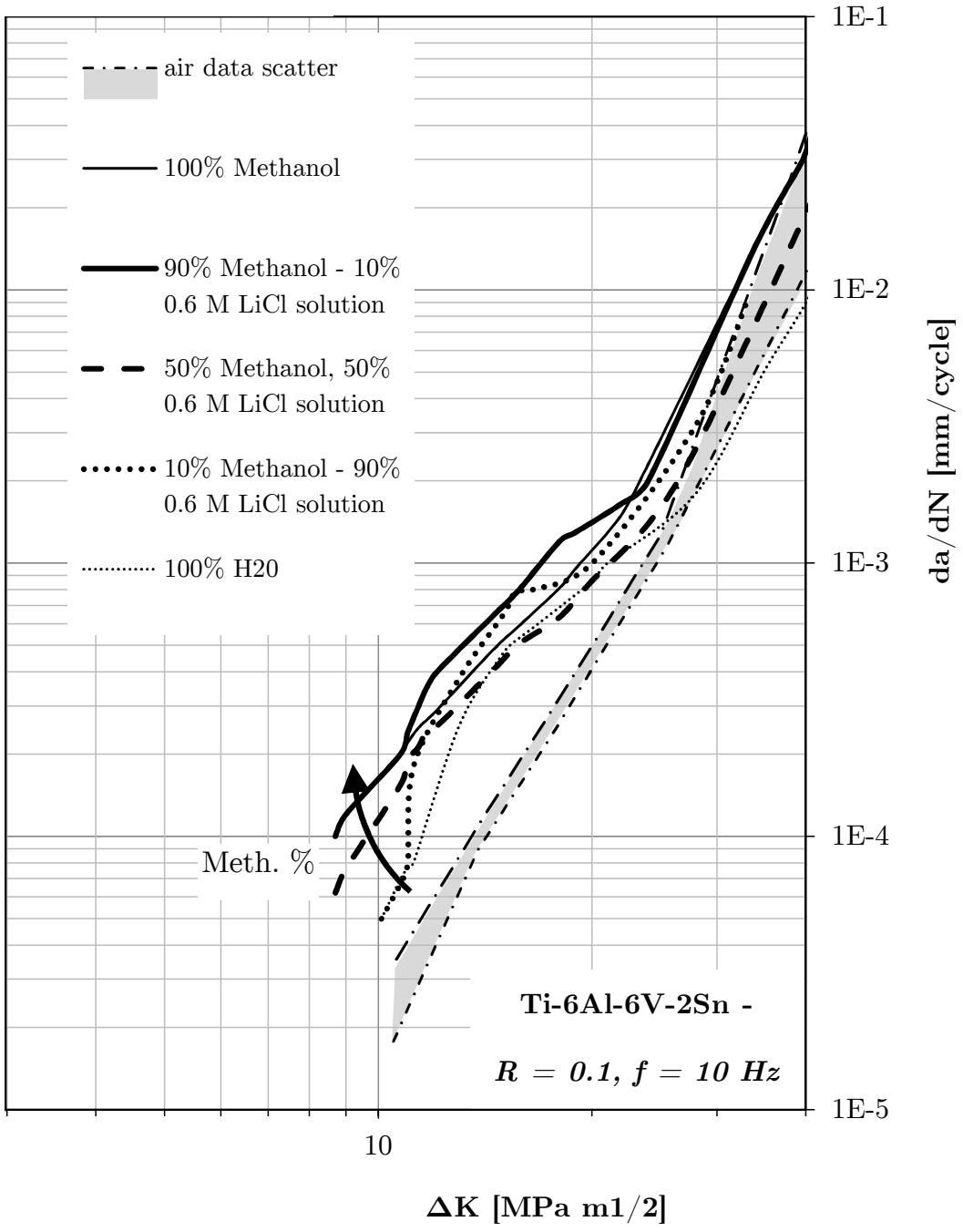

Figure 3.3: Methanol concentration effect on FCGR of Ti-6Al-6V-2Sn in aqueous 3.5 wt. % LiCl, compared with pure methanol and distilled water, $R = 0.1$, $f = 10\ Hz$, haversine wave form, adapted from [57].

increase in FCGR is found also for the lowest methanol concentrations, i.e. 10%, and even if a certain repassivation can be seen below ΔK_{SCC}, it is not dominant even for very low ΔK values. Moreover, the arrangement of the curves suggests that even the ΔK_{th} is moved towards inferior values by the increasing methanol concentration, as shown in Figure 3.3. From the results of [57], it can be clearly seen that water passivation phenomenon, which typically prevents fracture in static SCC methanol tests [36,39,54] is hence not effective under fatigue loads, because the formation of a stable film is not granted for dynamic mechanical actions. Indeed, even at 10% methanol concentration, significant effects on FCGR are present, and from the curves trend it seems that also nucleation is deeply affected, with possibility of crack propagation in low methanol concentrations even from smaller defects.

Considering initiation threshold ΔK_{th}, and load ratio R effects, an interesting work is presented by *Lee* et al. in [72]. In the study, axial fatigue testing of Ti-6Al-4V ingot moulded specimens at different R values is investigated. Tests are performed in air, inert environment and 3.5 wt.% NaCl mixture. FCGR rates vs. $\mathrm{d}a/\mathrm{d}N$ are presented for very low $\mathrm{d}a/\mathrm{d}N$ values, near the threshold zone, for a testing frequency of 10 *Hz*. Specimens tested at higher load ratios, i.e. $R = 0.9$, show a very reduced ΔK_{th} value, roughly around 2.1 $MPa\sqrt{m}$, while specimens tested at lower load ratio, i.e. $R = 0.1$ show a slightly higher value, i.e. ΔK_{th} roughly 3.1 $MPa\sqrt{m}$, as can be assessed in Figure 3.4. In particular, from results in air and methanol solution, it can be assessed that the two environments present a similar ΔK_{th}, regardless of the load ratio R. Concerning FCGR behaviour, specimens tested in NaCl showed a noticeable FCGR acceleration between $\Delta K = 4$ and $\Delta K = 9$ $MPa\sqrt{m}$, in agreement with the third corrosion fatigue behaviour found by *Dawson and Pelloux* [56], as presented in Figure 3.1c. The acceleration is limited due to the high testing frequency, i.e. 10 *Hz*. It is likely that reduced test frequencies could increase the FCGR acceleration bubble found in Figure 3.4. A different kind of behaviour is found for $R = 0.9$, where the acceleration of FCGR persists even up to very high $\mathrm{d}a/\mathrm{d}N$ values. It is possible

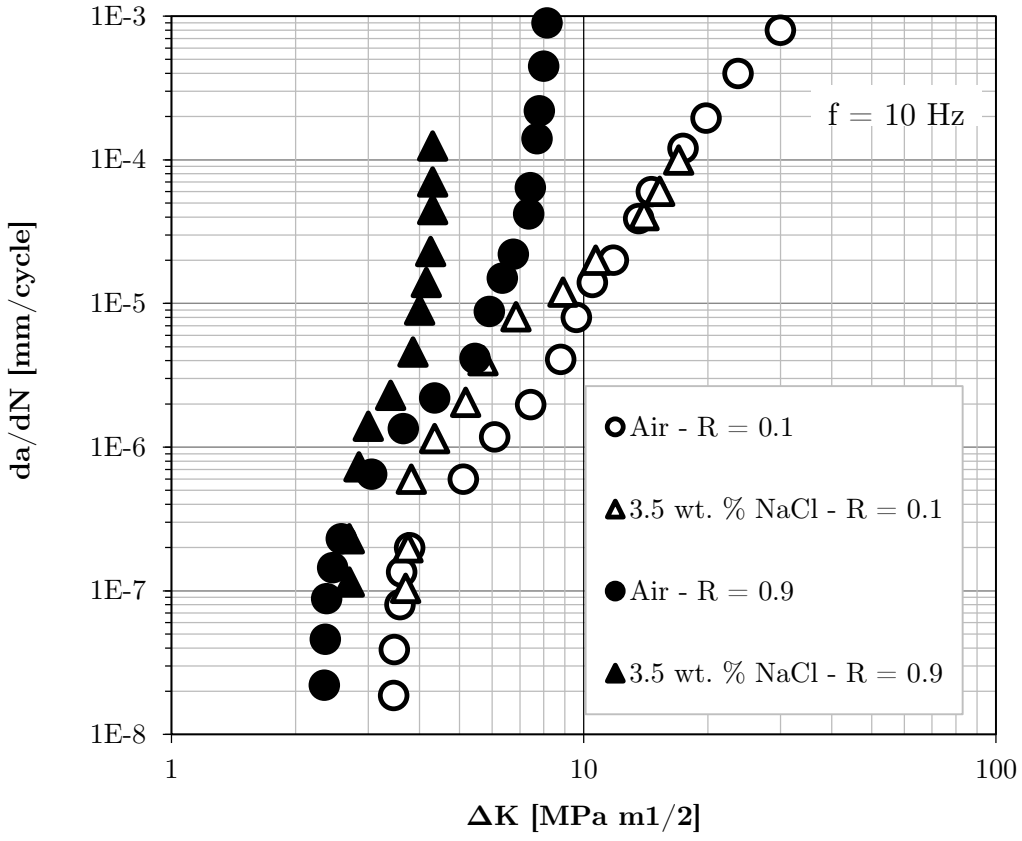

Figure 3.4: da/dN vs. ΔK FCGR curves, for ingot moulded Ti-6Al-4V specimens, at $R = 0.1,\ 0.9$, in air and 3.5 wt.% NaCl mixture. Adapted from [72].

that, for $R = 0.9$, the behaviour could be similar to the second trend identified by *Dawson and Pelloux* [56] in Figure 3.1b, although the graph presented by *Lee* et al. ends at a da/dN too low, i.e. 1e-3, to assess if the FCGR does not return to air values for high ΔK, as in in Figure 3.1c. The main reason for this behaviour could lie in the increased opening of the crack tip during the whole load cycle, assured by a load ratio $R = 0.9$. In [72], effects related to different manufacturing processes of the Ti-6Al-4V specimens, including laser formed material, are considered. Considering FCGR curves and deviation from the pure fatigue line in a ΔK vs. K_{max} curve, it has been assessed that the laser formed material is less sensitive to the environment, mainly due to the larger β - phase grains of the laser formed material.

Apart from considerations of the FCGR effects on initiation and crack growth, the raw effects of corrosion fatigue on Ti-6Al-4V strength are absent in earlier literat-

ure. Recently, experimental results were performed by *Baragetti* et al. [58,60,73,74], considering smooth $K_t = 1.18$ specimens in methanol [73], and notched specimens in air, paraffin oil (inert) environment and 3.5 wt.% NaCl solution [58, 74]. In the following sections, the experimental campaigns related to the test are presented in detail, and the results are properly discussed. Moreover, a numerical method, based on the experimental results of [58] is reported, as presented in [59]. Based on this model, predicting numerical tools can be developed for environmental fatigue testing. In order to present more clearly the material, the experimental campaigns and the numerical model are discussed separately, in sections 3.2 and 3.3 respectively.

3.2 Experimental campaigns

3.2.1 Materials and methods

The experimental testing corrosion fatigue campaigns were conducted on the same raw laminated plates adopted for the quasi-static SCC campaign. Considering chemical composition, and tensile properties the reader can refer to Tables 2.2 and 2.3 in section 2.2. The specimens were machined with the rolling direction of the plate orthogonal to the load direction. Regarding the thermal treatments, the fatigue specimens were subjected, after mechanical machining, to a STOA treatment, consisting of a 1 h solution treatment at 925C, followed by a 2 h overaging at 700C. The final microstructure of the specimens, obtained after the STOA treatment, is reported in Figure 3.5.

Two types of flat fatigue specimen geometries were adopted in the testing campaign: a smooth geometry with $K_t = 1.18$ was realized for smooth fatigue testing, presenting the same notch geometry of the specimens used in the SCC campaign, presented in Figure 2.1, section 2.2. The smooth fatigue specimens presented however a different width of the terminal grips, which was of 60 mm instead of 80 mm, to be compatible with the testing machine grips. Notched specimens followed the

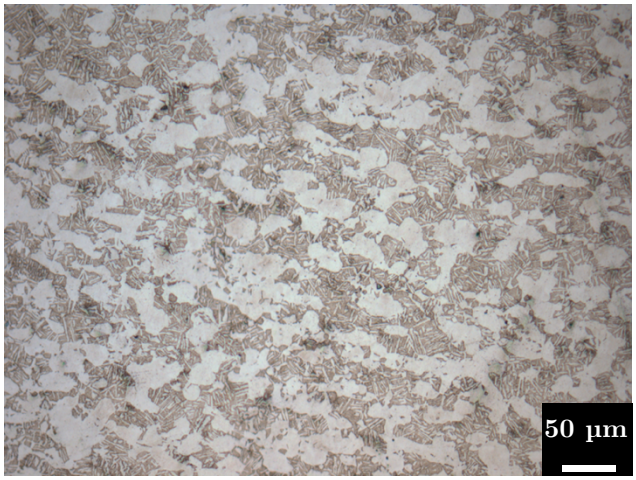

Figure 3.5: Bimodal microstructure ($\alpha + \beta$) of Ti-6Al-4V alloy after the STOA treatment - 200x magnification, from [58].

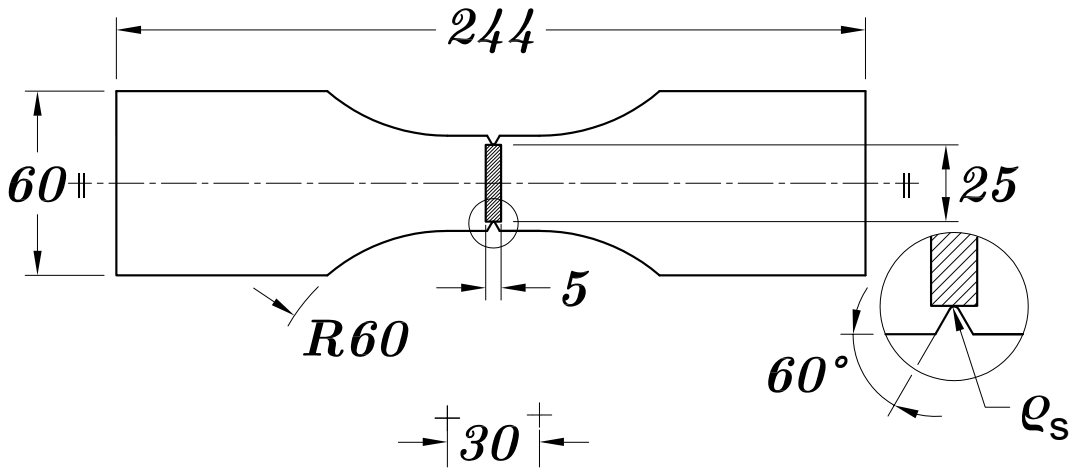

Figure 3.6: Notched specimens geometry, for the fatigue tests in air, paraffin and NaCl performed in [58]. Radius ρ_s variable according to Table 3.1.

geometry presented in Figure 3.6. The different notches radii ρ_s and correspondent K_t values, obtained by a numerical finite-element analysis as reported in [58,60], are presented in Table 3.1. Concerning the different environments tested, the correlation between geometries and analysed media is found in Table 3.1.

Both experimental campaigns consisted in axial fatigue testing at $R = 0.1$ and $f = 10\ Hz$, conducted on dynamic, universal hydraulic BRT T1000 testing machine with allowance up to 1000 kN in tension/compression, and on Instron 1273, with max allowance 250 kN in tension/compression. The specimens were mounted on hinge grips to reduce misalignment and parasite bending moments during the fatigue

Parameter	ρ_s - K_t correlation by FE analysis								
ρ_s	30	30	2.5	1.5	0.45	0.26	0.06	0.05	0.025
K_t	1.16	1.18	2.55	3.10	5.17	6.63	13.34	14.34	18.65

Table 3.1: Notched specimen radii ρ_s and associated numerical K_t, adapted from [58, 60].

Specimen geometry	Testing Environment	Concentrations [wt.%]			
K_t = *1.18*	*Air*			-	
	Methanol	5	25	50	95
Ref. [73]	*NaCl*			3.5	
	Air			-	
K_t= *1.16÷18.65*	*Paraffin (inert)*			-	
Ref. [58]	*NaCl*			3.5	

Table 3.2: Different specimen geometries related to the testing environment, concerning experimental tests performed in [58, 73].

testing, and strain gages were adopted to verify the absence of parasite contributions. Fatigue results were obtained by adopting the step loading technique, validated by *Bellows* et al. [75] and *Lanning* et al. [76], to obtain fatigue strength at *2e5* cycles with gradual increase of the applied load. A detailed description of the method is reported in Appendix A.

3.2.2 Results - Smooth Specimens in Air, Methanol Mixture, and 3.5% NaCl Mixture

The results related to the testing of smooth, $K_t = 1.18$ Ti-6Al-4V specimens, immersed in 3.5 wt.% NaCl and methanol at different concentrations, according to Table 3.2, are reported in Figure 3.7. The values were obtained using the step-loading procedure, and selecting load blocks of *2e5* cycles, with axial fatigue testing at $R = 0.1$ and $f = 10\ Hz$. The resulting limiting stress $\sigma_{lim,2e5}$ represents the fatigue limiting stress obtained for an expected life of *2e5* cycles. Each of the data points related to testing in methanol presented in Figure 3.7 represents an average

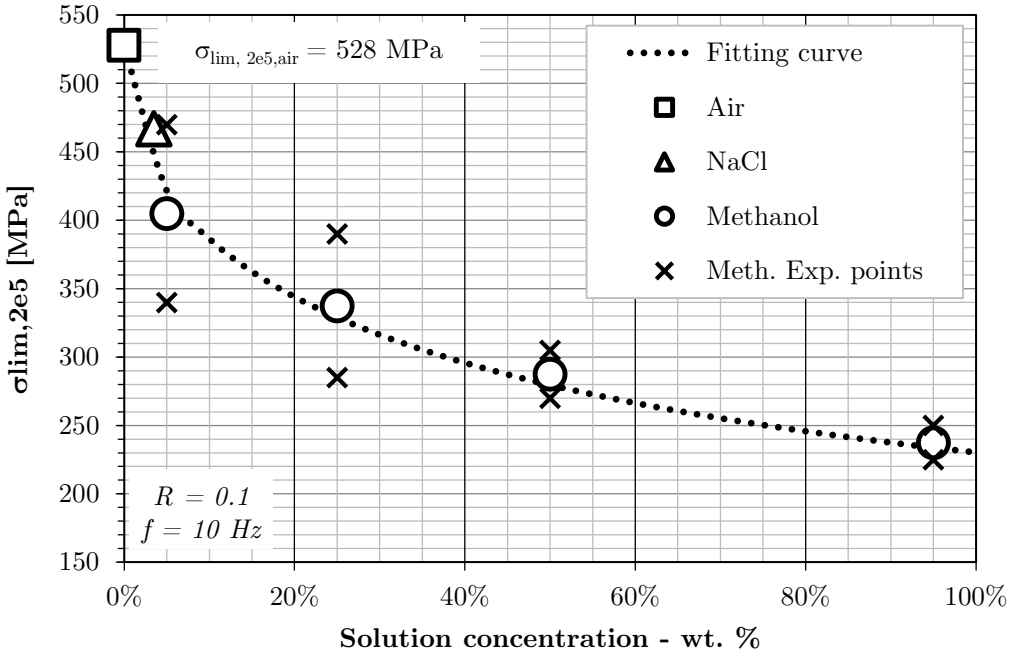

Figure 3.7: Limiting stresses for axial fatigue testing on smooth (K_t = 1.18) Ti-6Al-4V specimens in air, NaCl 3.5 wt.% solution, and methanol solution at different concentration. Adapted from [60], integrated from [73].

between the results from two different, step-loading tested specimens. The related $\sigma_{lim,2e5}$ values, obtained by repeating the step-loading procedure for each concentration, are reported as well. As it can be seen from Figure 3.7, the dispersion of the different $\sigma_{lim,2e5}$ is reduced proportionally with respect to the methanol concentration. The maximum $\sigma_{lim,2e5}$ loss has been found being -55% for the maximum concentration tested, i.e. 95 wt.% methanol.

Data obtained in air and methanol, presented in Figure 3.7, have been interpolated by an exponential fitting curve, presented in [60, 66], where X represents the methanol solution wt.% concentration. The curve is fitting methanol and air data with an R^2 index of 0.989, and seems adequate to describe also the data point related to fatigue testing in 3.5 wt.%. The equation is reported here below:

$$\sigma_{lim,2e5} = \sigma_{lim,2e5,AIR} + 395 \cdot e^{-0.14\sqrt{100 \cdot X}-1}$$

3.2.3 Results - Smooth and Notched Specimens in Air, Paraffin Oil, and 3.5% NaCl Mixture

Considering smooth and notched specimens, with $K_t = 1.16 \div 18.65$, tested in air, paraffin oil (inert environment) and 3.5 wt.% NaCl solution, limiting stresses $\sigma_{lim,2e5}$ at *2e5* cycles, obtained with step-loading procedures, are reported in Figure 3.8, as a function of the specimens' notch K_t. Results are related to axial fatigue testing at $R = 0.1$ and $f = 10\,Hz$. The nucleation values, obtained whereas a crack was recognized by means of periodic acetate replica analysis, are reported as well. Three different curves are interpolated, isolating specimens tested in air, paraffin oil and 3.5 wt.% NaCl respectively. Limiting values for smooth specimens, obtained by literature work from *Sadananda* et al. [77] and *Peters* et al. [78] are reported as well. Moreover, a $\sigma_{lim,2e5}$ vs. K_t failure curve, obtained by interpolating the experimental data obtained by *Lanning* et al [79], concerning Ti-6Al-4V $R = 0.1$ fatigue test on notched specimens in air at 1e6 cycles, is reported as well. The higher fatigue limit is recognizable by the highest placement of the curve from [79] in the logarithmic graph of Figure 3.8. Interpolation curves, and K_t intervals of validity, are reported in Table 3.3.

3.2.4 Discussion

By analysing the fatigue results obtained in methanol solution at different concentrations, obtained for $R = 0.1$, $f = 10\ Hz$ on smooth specimens ($K_t = 1.18$), presented in Figure 3.7, a clear relation between methanol concentration and limiting stress at *2e5* cycles is observed. The loss of fatigue strength ranges from a -56% for 95 wt.% concentration, to a -24% drop for 5 wt.% concentration. Concerning fatigue crack nucleation and propagation rates, although surface replicas with acetone were taken at every 5000 cycles, according to [73], no nucleation was detected prior to the final fracture. This aspect highlights the extreme crack propagation

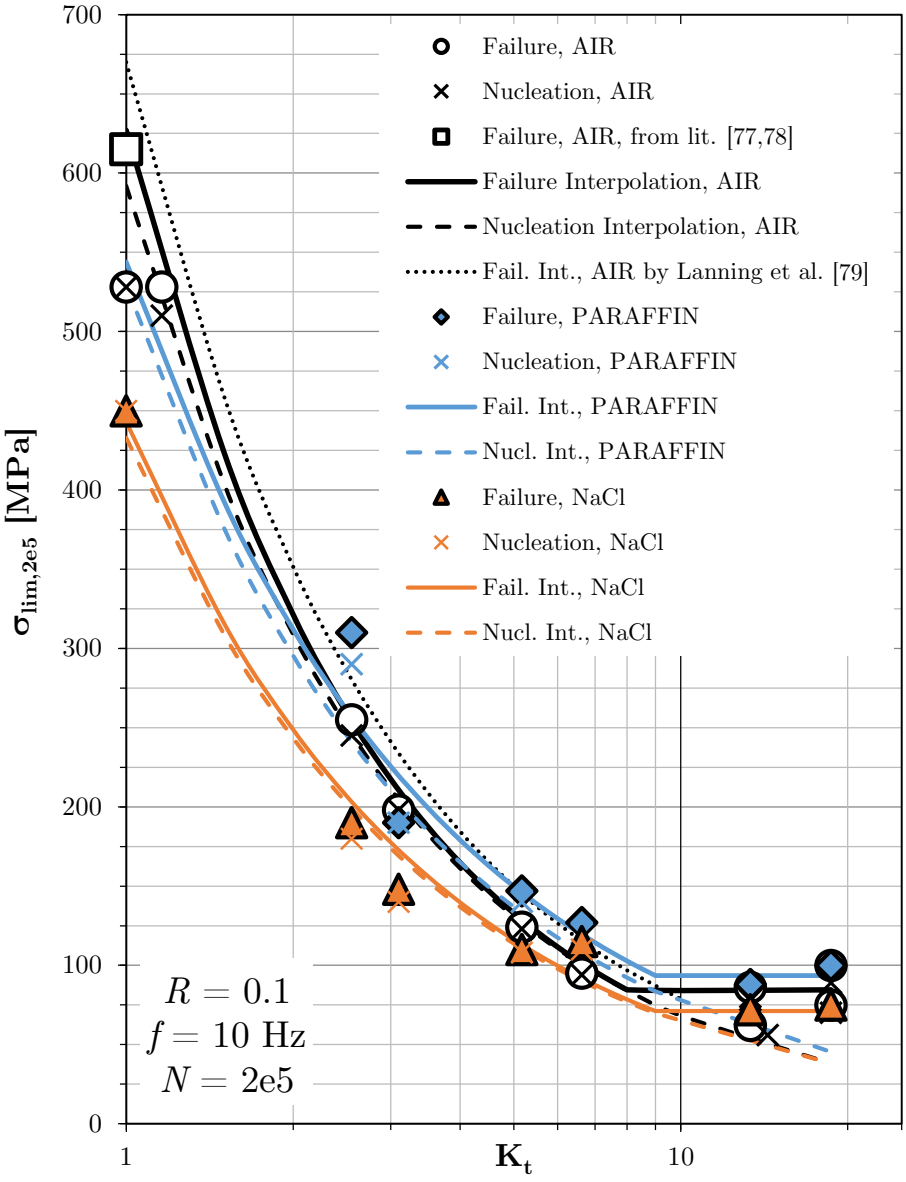

Figure 3.8: Limiting stresses for axial fatigue testing on smooth and notched Ti-6Al-4V specimens in air, paraffin oil, and 3.5 wt.% NaCl solution. Data from [58, 77–79] , adapted image from [60].

Curve	K_t interval	$\sigma_{lim,2e5}$ [MPa]	R^2
Air			
Failure	$1 \leq K_t \leq 8$	$627\ K_t^{-0.964}$	0.946
	$K_t > 8$	84	-
Failure *Lanning et al.* [79]	$1 \leq K_t \leq 8$	$670\ K_t^{-0.930}$	-
Nucleation	-	$592\ K_t^{-0.938}$	0.876
Paraffin Oil			
Failure	$1 \leq K_t \leq 9$	$544\ K_t^{-0.801}$	0.814
	$K_t > 9$	94	-
Nucleation	-	$529\ K_t^{-0.84}$	0.706
3.5 wt. % NaCl			
Failure	$1 \leq K_t \leq 9$	$443\ K_t^{-0.832}$	0.983
	$K_t > 9$	76	
Nucleation		$433\ K_t^{-0.833}$	0.983

Table 3.3: Interpolating curves related to Figure 3.8, adapted from [60].

rate increment obtained due to the aggressive environment. In order to correctly assess the environmental contribution on the anticipation of crack nucleation, and on the FCGR during propagation, more advanced crack detection and propagation techniques are needed, i.e. with environment protected crack gages. Concerning nucleation and propagation, in the work of *Sanderson and Scully* [54], it is clearly demonstrated that TiO_2 layer dissolution is present under applied stress, and that repassivation is prevented. By considering the work of *Dawson and Pelloux* [56], it is clearly seen a that a Type 2 corrosion fatigue behaviour is present on titanium alloys in methanol solution, see Figure 3.1. In this Type 2 case, repassivation of the fresh cracked surfaces is not effective against cyclic SCC phenomenon, with dynamics similar to the sustained load SCC mechanisms presented in Chapter 2. The specimen tested in NaCl presented a limited loss in fatigue strength, with respect to the specimen tested in air. As reported in [16,56,67], NaCl solution seems to not affect nucleation in Ti-6Al-4V alloys, although an acceleration of FCGR above ΔK_{scc} is found, according to type 3 corrosion fatigue mechanism highlighted in [56]. The mechanism seems coherent with the limited, but sensible reduction of the fatigue strenght found in Figure 3.7.

By looking at Figure 3.7, another aspect which must be considered is the high dispersion found on the fatigue data in methanol for low concentrations. The data dispersion reduces significantly with the increase in methanol concentration. This phenomenon is an indicator of the effect of the methanol environment concentration on the crack nucleation. Indeed, by looking at data from *Dawson* [57], it can be seen that higher methanol concentrations are likely to lead to a reduction of expected ΔK_{th}, thus resulting in a crack nucleation for smaller defect size, at the same level of applied stress. The reduction of data dispersion could be indeed an indication of a reduction of ΔK_{th} at higher concentrations, sufficient to initiate a crack from a defect size with high probability to be found on the specimen surface. On the other hand, higher ΔK_{th} at lower methanol concentrations could limit the crack initiation to defects of a certain size, which can either be found or not near the test section of the specimens, at the considered stress level, thus motivating the data dispersion of Figure 3.7.

Considering the effects of notched specimens, fatigue tested in air, paraffin oil and 3.5 wt.% NaCl solution, presented in Figure 3.8, it can be noticed that the environmental effects are clearly recognizable for low values of stress concentration, i.e. low notched specimens. For K_t tending to unity indeed, the inert (paraffin oil) environment shows a clear higher fatigue limit, the specimens tested in air show a limited reduction, highlighting the fact that also laboratory air has a corrosion fatigue effect, as discussed also in [72], whilst test in NaCl solution show a clear decrease of fatigue strength. As K_t increases, air, paraffin and NaCl limiting strengths become more similar, highlighting a reduced environmental effect. Moreover, while the strength values found for nucleation continue to diminish with increasing K_t, the limiting failure stresses reach a plateau for $K_t > 8 \div 9$ in the three environments. The results are in agreement with the results found by *Frost and Dugdale*, as presented in Figure 7.19, Pag. 387 of [80], or in [58], as reported in Figure 3.9.

From Figure 3.9, related to mild steel notched specimens, it can be seen that,

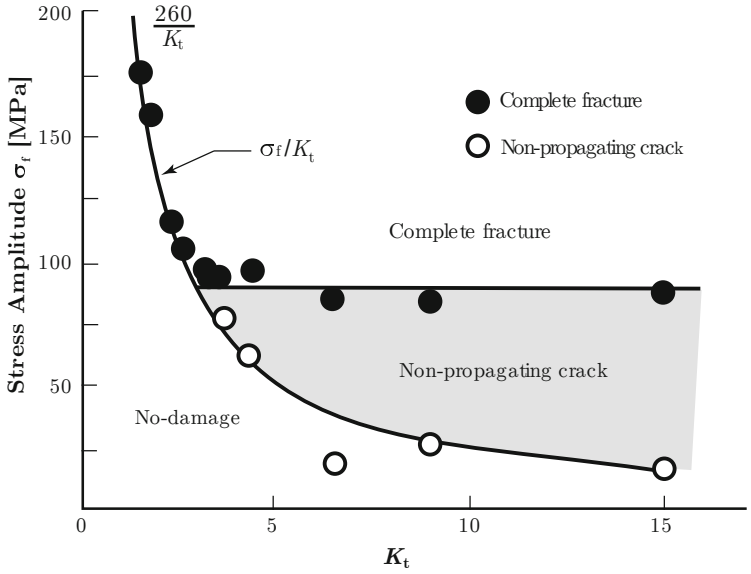

Figure 3.9: Trend of the fatigue limit σ_{lim} vs. the theoretical stress concentration factor K_t in mild steel specimens containing a 1.3 mm depth V shaped notch. Adapted from [80].

above a certain value of K_t, the applied stress was sufficient to nucleate fatigue crack, but the cracks were found to be not propagating in the material. The reason of this phenomenon is caused by the stress gradient generated by the presence of the notch. In the proximity of a sharp notch indeed, a high value of tip stress σ_{tip} can be found, driving the nucleation of the crack in the first grains of the microstructure. Once the crack is generated, it propagates away from the notch tip, where the applied stress decreases abruptly, and the stress driving the propagation region, σ_{prop}, is not sufficient for the crack to propagate. The same σ_{tip}, necessary to nucleate a crack, can be found in smoother specimens. In this second case however, the gradient is lower, and the nucleated crack encounters a higher applied stress σ_{prop} in the propagation region. In this latter case, the crack propagates towards final fracture. The mechanism is clearly exposed by *Baragetti* et al. [58, 60], and presented in Figure 3.10. Considering the trend of the NaCl solution, presented in Figure 3.8, it can be seen that the environmental effect is maximum at low K_t values, with a drop of -29 % with respect to the σ_{lim} in air. At higher K_t indeed, where cracks are nucleated, but the non propagating crack plateau is found, the

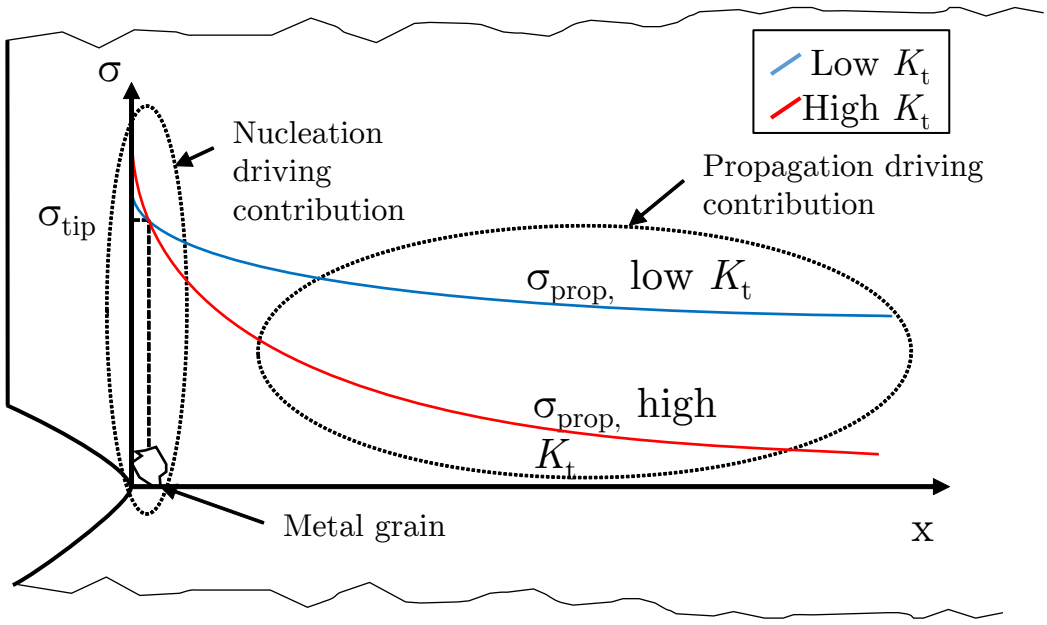

Figure 3.10: Different stress gradient trends for high and low K_t geometries for the same mean tip stress σ_{tip}, adapted from [60].

effect is limited, with a drop of -9.5 %. Remembering Figure 3.2, it can be seen that NaCl solutions have significant effects on Ti-6Al only in the propagation stage, by increasing FCGR, while the nucleation stage seems not affected at all, as confirmed also by static experiences [16,67]. In light of this, from the results of [58,60], it seems that mechanical fatigue propagation is necessary for the NaCl environment to exert noticeable effects on FCGR. When nucleation occurs at low applied stresses, but propagation is not present due to the notch effect discussed here, the environmental effect plays hence a limited role.

3.3 Numerical model

3.3.1 Model realization

In order to characterize the results obtained from [58] including FCGR data consideration, a numerical model based on elastic linear theory for fracture mechanics has been developed, to calculate the values of ΔK vs. $\mathrm{d}a/\mathrm{d}N$. The model was based on unpublished experimental data related to the experimental work on notched spe-

cimens fatigue tested in air, paraffine oil and NaCl solution environment [58]. In particular, the specimens tested in [58] were subjected to crack profile detection by means of acetate replica technique, performed at every 1e4 or 2e4 cycles, during step-loading load blocks of *2e5* cycles. The data obtained by the corrosion fatigue testing of the specimens with notch radius ρ_s = 2.5, 0.26 and 0.06 mm (see Table 3.1) were considered for the present study. For each test, a complete recording of the applied stress, number of cycles and crack length was available. From such measurements, it was possible to reconstruct the approximated value of $\mathrm{d}a/\mathrm{d}N$ by means of the finite differences method. For the first and last data point, forward and backward 1st order finite differences were adopted, while for the central points, centered 1st order differences were adopted. In order to obtain the values of ΔK, a separate FEM model was elaborated for each entry of the measured crack length a, with a precise replication of the maximum applied stress σ_{max} for each data point, with the intent to obtain K_{max}. Each FEM model was realised by adopting CPS4 linear plane stress elements, with a maximum mesh size of 10 μm in the proximity of the crack tip, obtaining a stress-strain map as reported in Figure 3.11. The material was modelled as linear, with a Young's modulus E = 110000 MPa, and a Poisson ratio ν = 0.31. The choice is coherent with the adoption of elastic fracture mechanics models. The model is plausible in the hypothesis of Small Scale Yielding Condition, as defined in [80], i.e. when the plastic zone is inferior to 1 mm. This condition is likely to be met in Ti-6Al-4V STOA treated specimens, in which the YS is extremely near to the UTS, as reported in Table 2.3.

The value of K_{max} was obtained by means of linear elastic stress relations, based on the equations presented in [81], and adopted in the work of *Baragetti et al.* [82, 83], concerning the analysis of the fatigue life for crack propagation steel case-hardened and titanium PVD-coated spur gears for motorbike transmission. The elastic relations adopted are, in the formulation presented in [59]:

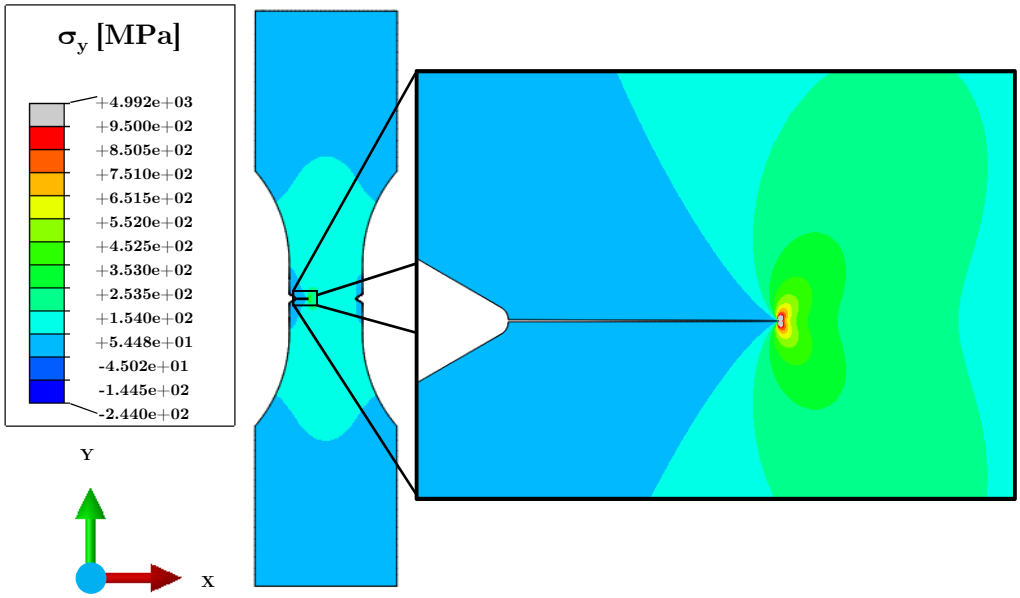

Figure 3.11: Stress-strain map (σ_y axial component) for a $K_t = 6.63$, $\rho_s = 0.26\ mm$ fatigue specimen tested at σ_{lim}= 107 MPa.

$$K_I(\rho, \theta) = \frac{E}{1+\nu}\sqrt{\frac{2\pi}{\rho}}\frac{u}{f(\theta)}$$

$$f(\theta) = sin\left(\frac{\theta}{2}\right)\left[\kappa + 1 - 2cos^2\left(\frac{\theta}{2}\right)\right]$$

$$\kappa = \begin{cases} 3 - 4\nu & \text{plane strain} \\ (3-\nu)\ /\ (1+\nu) & \text{plane stress} \end{cases}$$

The parameters to obtain the value of K_I are u - half of the Crack Tip Opening Displacement (CTOD), θ - crack tip angle and ρ, i.e. the distance of the measuring point with respect to the crack tip. In order to calculate K_{max}, the three parameters were obtained for each FEM simulation, according to the methodology illustrated in Figure 3.12. The applied stress intensity factor ΔK was then reconstructed, due to the linearity of the problem, by considering the load ratio, i.e. imposing $\Delta K = (1 - R)K_{max}$, in agreement with *Lee et al.* [72].

Prior to the application to the experimental crack growth data obtained from

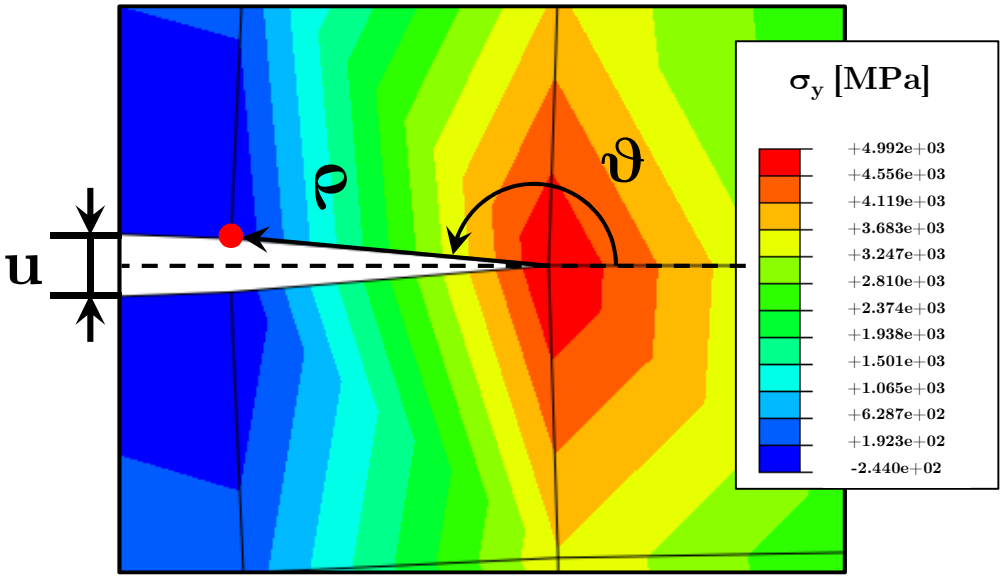

Figure 3.12: Input parameters for the linear K_I calculations from the FE model, adapted from [59].

[58], a test of the numerical method was performed on the FCGR data obtained by the work of *Lee et al.* [72], as presented in Figure 3.4, in order to validate the method. Since in this case crack growth data was not available, three theoretical models were adopted to reconstruct the da/dN value from the applied stress intensity factor ΔK, namely the models of *Paris* [81], *Walker* [84] and *Kato* et al. [85]. The first model by *Paris*, commonly adopted for the crack propagation growth rate in metallic alloys [81], simply assumes a power-law dependence of the growth rate from the stress intensity factor, thus describing only the stable propagation rate. *Paris*' law takes the form:

$$\frac{\mathrm{d}a}{\mathrm{d}N} = C\,(\Delta K)^n$$

where C is the *Paris'* constant of the material, which for a Ti-6Al-4V alloy can be considered as $C = 3.8 \cdot 10^{-8}$ $\left[(mm/cycle)\,(MPa\sqrt{m})^n\right]$, and $n = 3.11$, as of [86]. The *Walker* model takes into account the load ratio of the test as a parameter, and adds a further parameter γ, which according to *Beden* et al. [84] is a curve fitting parameter. The *Walker* model formulation is:

$$\frac{\mathrm{d}a}{\mathrm{d}N} = \frac{C}{(1-R)^{n(1-\gamma)}} (\Delta K)^n$$

According to [84], γ is obtained by trial and error, and its value is the one that best consolidates the data along a single straight line on the log-log plot of da/dN versus ΔK. According to *Pitt et al.* [87], the value of γ for the Ti-6Al-4V alloy is 2.5. The models by *Paris* and *Walker* are however limited to the description of the linear region in the log-log diagram of $\mathrm{d}a/\mathrm{d}N$ vs. ΔK. In order to describe also the near threshold region, a more accurate model is presented by *Kato* et al., originally developed for case carburized steel gears [85]. The model consists in two crack propagation rate laws, one for the initial and the other for the stable growth region:

$$\begin{cases} \frac{\mathrm{d}a}{\mathrm{d}N} = \frac{C}{(1-\lambda)^n} (\Delta K^n - \Delta K_{th}^n) & \text{for } \Delta K_{th} < \Delta K < K_C \\ \frac{\mathrm{d}a}{\mathrm{d}N} = \frac{C}{(1-\lambda)^n} \left(\frac{\Delta K^n K_{IC}^n}{K_{IC}^n - \Delta K^n} \right) & \text{for } K_C < \Delta K < K_{IC} \end{cases}$$

K_{IC} is the fracture toughness of the material, while ΔK_{th} is the usual propagation threshold value. K_C is an intermediate threshold value, introducted by *Kato* et al., separating the slow FCGR region described by the first equation from the faster propagation region, identified by the second relation. λ is defined as the ratio between the threshold value ΔK_{th} and the fracture toughness of the material, identified by K_{IC}:

$$\lambda = \frac{\Delta K_{th}}{K_{IC}}$$

The value of the intermediate threshold is obtained by another relation between ΔK_{th} and K_{IC}:

$$K_C = \sqrt{\Delta K_{th} K_{IC}}$$

The three models were adopted as a base to validate the extrapolation of ΔK from linear elastic fracture relations and linear FEM models of the Ti-6Al-4V specimens. The results of the model validation are reported in the next section, related to the results, in Figure 3.13. The aim of the validation is to assess if correct data can be obtained from FEM simulation of thin fatigue specimens, as the ones presented in Figure 3.6.

3.3.2 Results and comparison with experiments

The validation of the model against the data from *Lee* et al., obtained by using $\mathrm{d}a/\mathrm{d}N$ values derived from the *Paris*, *Walker* and *Kato* models presented in the previous section, is reported in Figure 3.13. From Figure 3.13, it is evident that the *Paris* and *Walker* model provide excellent approximations of the da/dN vs. ΔK curve especially in the stable propagation region, i.e. above $\Delta K = 10$. For lower propagation speed regions, i.e. in the range $\Delta K_{th} < \Delta K < 10$, a major correlation of the experimental data points from [72] is found with the *Kato* model. A transition between the two models is present for values of ΔK between roughly 9 and 11.

After the successful validation, the numerical formulation was applied to the experimental data from the campaign on notched Ti-6Al-4V specimens tested in air, paraffin oil and NaCl mixture by *Baragetti* et al. [58]. As previously said, the $\mathrm{d}a/\mathrm{d}N$ values are obtained no more from the theoretical models presented in section 3.3.1, but directly from the discrete derivation of actual crack length data. The results, extrapolated from notched specimens with $\rho_s = 2.5$, 0.26 and 0.06 mm, are reported in Figure 3.14, where the comparison with corrosion fatigue data from *Dawson and Pelloux*, concerning similar fatigue tests on Ti-6Al-4V in air and 3.5 wt.% NaCl, with the same load ratio $R = 0.1$. Since at high K_t values the effects of laboratory air and paraffin oil in [58] were superimposable, see Figure 3.8, the curve in air presented in 3.14 is obtained from data point by both environments. The results show a satisfactory agreement of the data, especially concerning air and paraffin data for

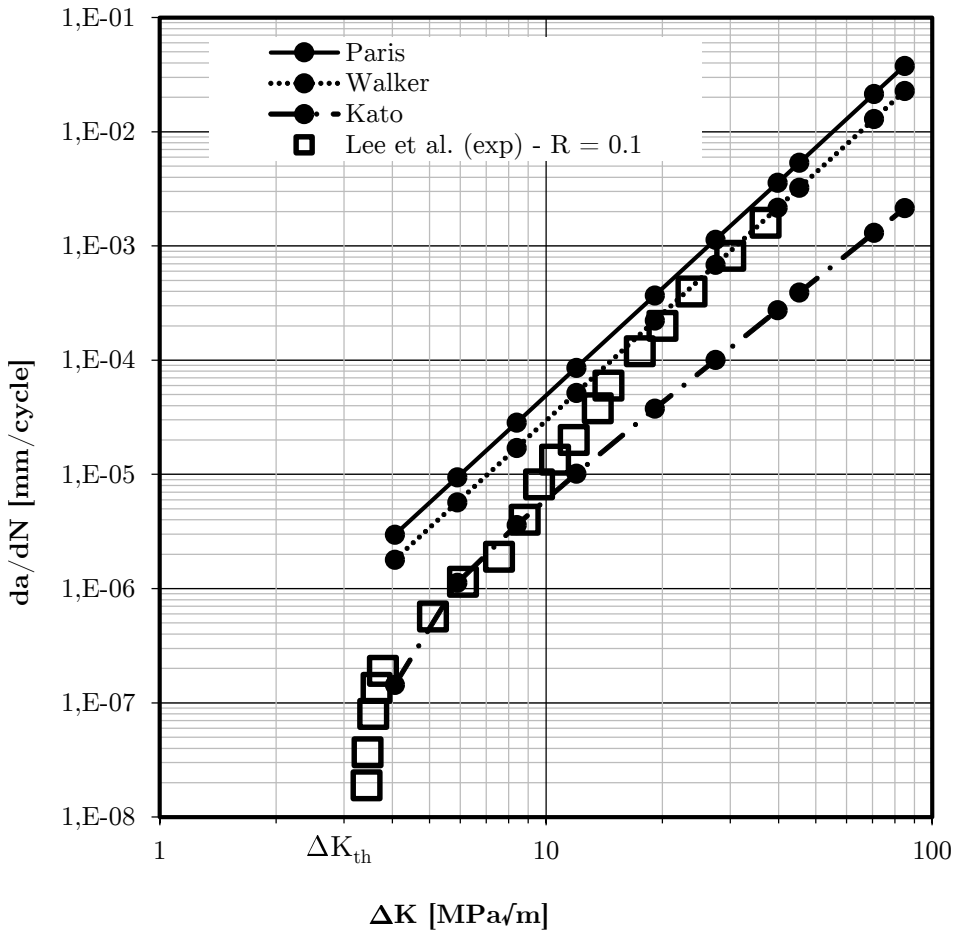

Figure 3.13: Comparison between the proposed propagation models of Paris, Walker, Kato, based on actual FE results, and the experimental data from *Lee* et al. [72]. Each solid point represents the da/dN value obtained by a single FE simulation. Adapted from [59].

$\Delta K < 12$. At higher values of ΔK, the curve tends to distance itself from the data by *Dawson*. A possible reason of this fact could be searched in the very thin geometry of the Ti-6Al-4V specimens adopted for the fatigue investigation in [58], compatible with a plane stress condition, in contrast with the typical thick geometry of FCGR specimens, as the Single Edge Notched (SEN) specimens adopted by *Dawson and Pelloux* [56]. Considering the values in NaCl solution, good agreement is reached for intermediate values of ΔK, namely between 10 and 12. FCGR near the threshold value are overestimated, possibly due to the difficulty of measurement of the crack growth near the crack initiation. Another reason could be found by considering the step-loading procedure, which could have led to anticipated cracking in previous stages, leading to biased values due to unnoticed crack propagation in combination with finite differences approximations.

3.3.3 Fatigue life prediction

The FCGR rates obtained in Figure 3.14 have been adopted to reconstruct failure predictions, in terms of number of cycles to failure. The aim of the work is to reconstruct a method to predict environmental assisted failure of Ti-6Al-4V components under applied fatigue stresses. The number of cycles is obtained, once the relationship $\mathrm{d}a/\mathrm{d}N$ is known, by integrating between the FE models for a certain fatigue test at different crack lengths. Curve in air from Figure 3.14 is used for specimens tested in air and paraffin, due to the considered similarity between air and paraffin data at K_t higher than unity highlighted in Figure 3.8. Curve in 3.5 wt.% NaCl is used for specimens tested in this environment. If N_s simulations are run between nucleation and final fracture, the number of cycles between the first and the last are calculated according to the formulation:

$$N_{i+1} = N_i + \frac{a_{i+1} - a_i}{\langle da/dN \rangle_i}$$

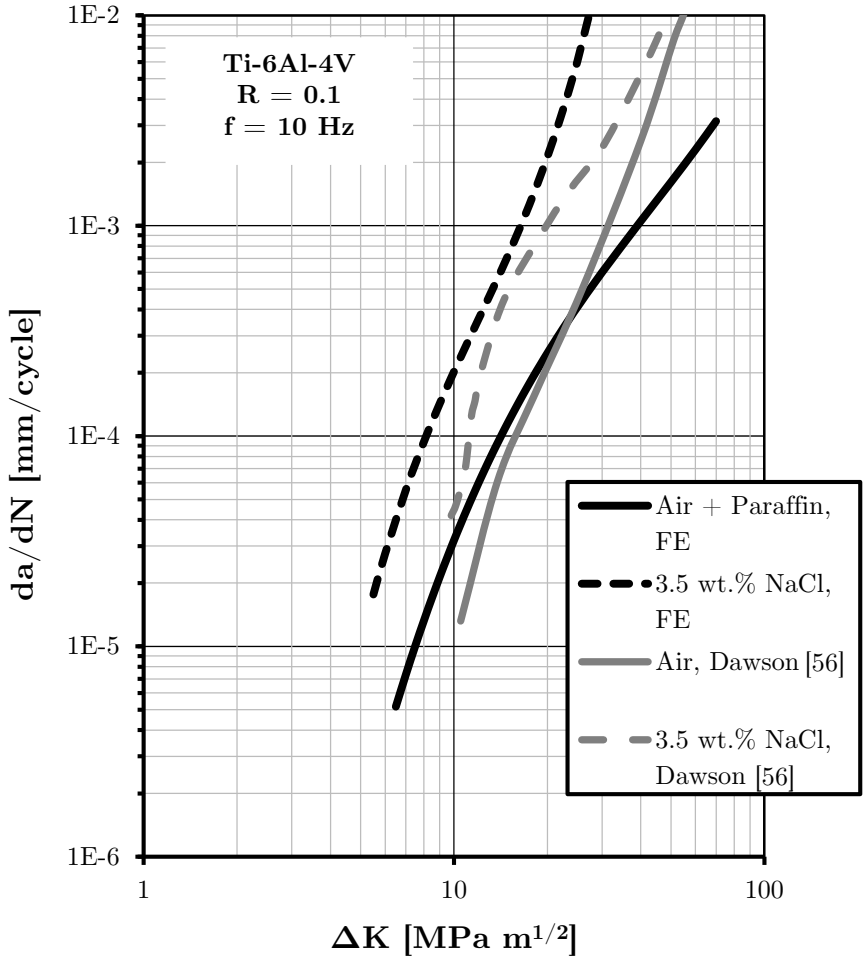

Figure 3.14: Air and 3.5 wt.% da/dN vs. ΔK FCGR experimental data, reconstructed from crack length measurements and FE linear elastic models related to $R = 0.1$ fatigue specimens tested in [58], compared to the FCGR data by *Dawson and Pelloux* [56]. Adapted from [88].

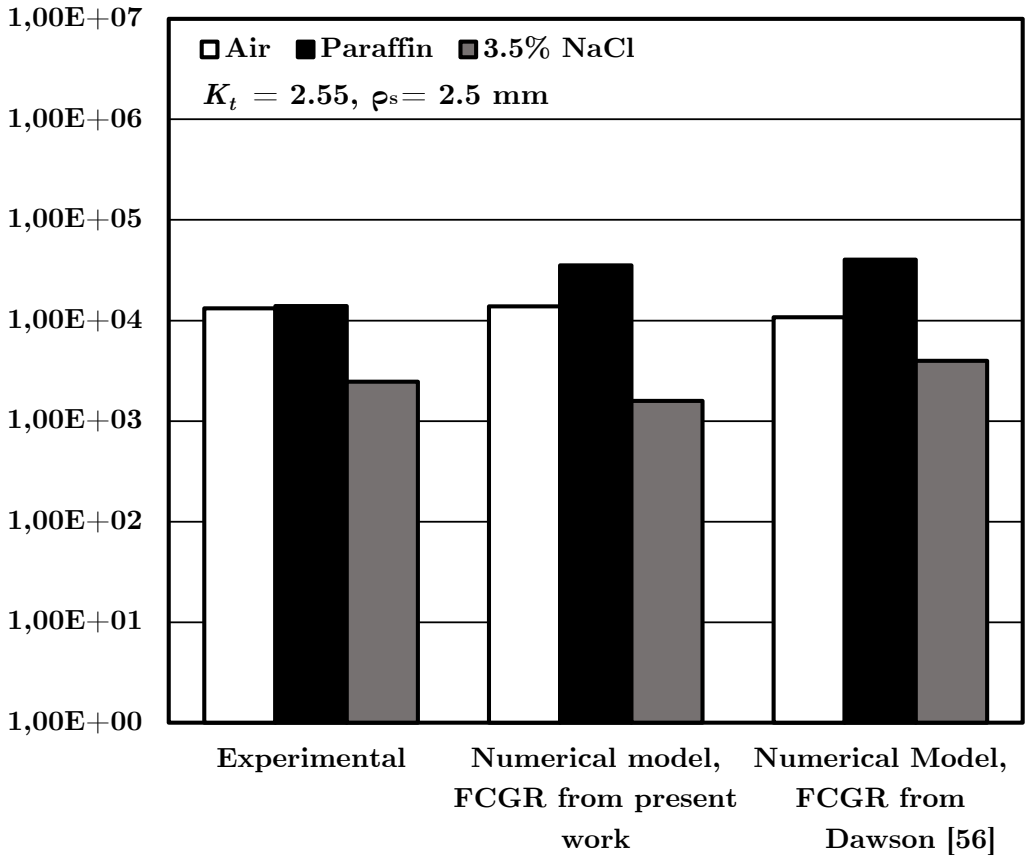

Figure 3.15: Prediction of number of cycles obtained by simulating the test conditions for the $\rho = 2.5$, $K_t = 2.55$ specimen. Comparison between experimental number of cycles [58], predicted number of cycles using FCGR curves obtained in Figure 3.14, predicted number of cycles obtained using FCGR from *Dawson and Pelloux* [56]. Adapted from [88].

$\langle da/dN \rangle_i$ is calculated as the mean da/dN value, with respect to the values of da/dN at the simulation points, i.e.:

$$\langle da/dN \rangle = \frac{(da/dN)_{i+1} - (da/dN)_i}{2}$$

The results, calculated with the presented formulation by the FCGR obtained in 3.14, and by the data from *Dawson and Pelloux* [56], are presented in Figure 3.15, related to an experimental test in air, paraffin and NaCl of different specimens with $K_t = 2.55$. In Figure 3.16, the same results for notched specimens with $K_t = 13.34$ are reported as well.

From the obtained data, it can be seen that the presented numerical method

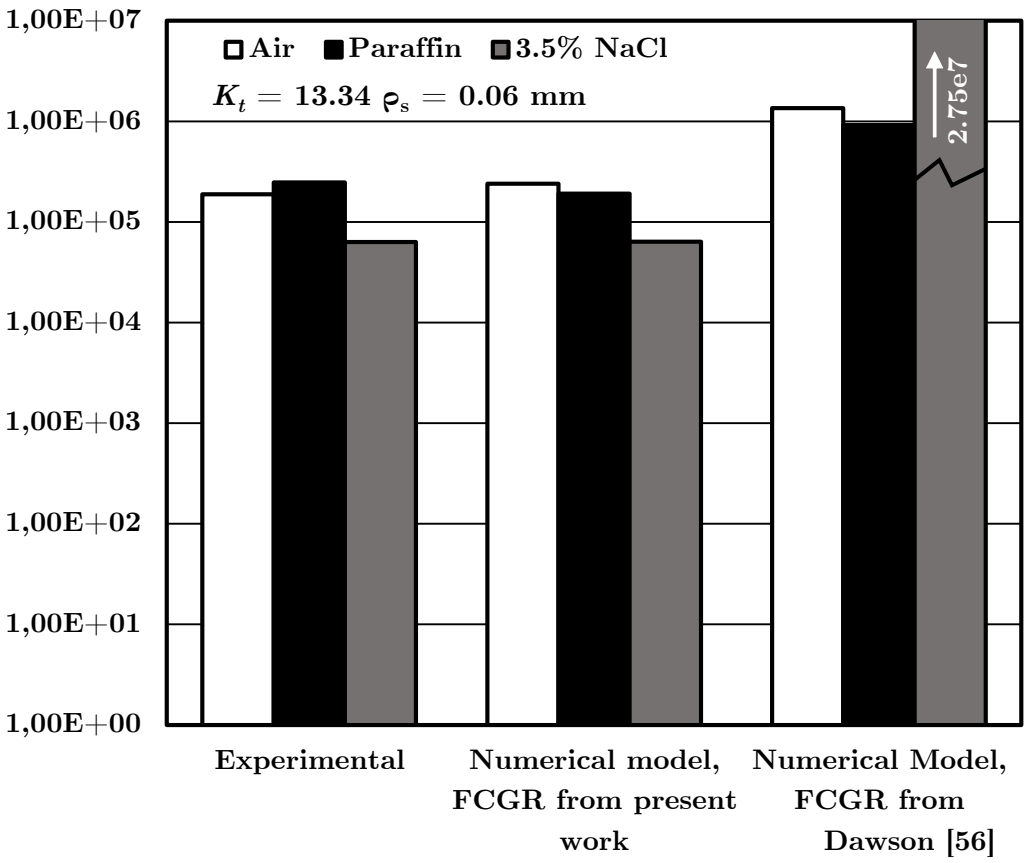

Figure 3.16: Prediction of number of cycles obtained by simulating the test conditions for the $\rho = 0.06$, $K_t = 13.34$ specimen. Comparison between experimental number of cycles [58], predicted number of cycles using FCGR curves obtained in Figure 3.14, predicted number of cycles obtained using FCGR from *Dawson and Pelloux* [56]. Adapted from [88].

is able to reconstruct a correct prediction of the number of cycles to failure, by obtaining the FCGR directly from experimental data. In particular, the prediction obtained by using the direct FCGR data, reconstructed by FE simulation from the crack growth data of [58] is more coherent to the experimental failure results. Predictions made by using the FCGR curves by *Dawson and Pelloux* [56] show indeed an excessive overprediction at high K_t values, especially concerning the specimens tested in NaCl solution. By looking at the $\mathrm{d}a/\mathrm{d}N$ curves presented in Figure 3.14, the reason of such slow propagation is found in the extrapolation of the NaCl curve taken from *Dawson and Pelloux* [56] in the low ΔK region, near to ΔK_{th}. Indeed, low FCGR rates, similar to values obtained in air, are found in this region by NaCl data from [56], in contrast with the FCGR obtained by the presented numerical procedure. Remembering the discussion in section 3.3.2, related to the discrepancies of the NaCl curve at high K_t values, it seems clear now that the difference between the curves of Figure 3.14 lays in some physical phenomenon, and it is evident also in the low ΔK threshold region. The different FCGR curves from [58] and from [56], stem from a physical difference between the two tests, and hence not from a modelling inconsistency. Remembering the possible physical differences, the geometrical discrepancy between the thin, plane stress specimens used for [58], and the thick, plane strain samples employed in [56], may account for the distinction in FCGR behaviour. Moreover, highly notched specimens are more sensitive to the behaviour at low ΔK values, hence a more correct reconstruction of the FCGR curve from actual experimental data may have contributed to an improved prediction of the exact result.

3.4 Remarks

In the present chapter, a complete analysis of the effects of several environmental effects of aggressive media found in the operative life of Ti-6Al-4V alloy, including

NaCl mixtures and methanol, has been carried out. The literature review points out the effects of pitting in aggressive NaCl environment, which can cause degradation in the fatigue properties by anticipating nucleation [38]. A more detailed analysis, which includes effects on nucleation and propagation of cracks in Ti-6Al-4V and Ti-6Al-6V-2Sn titanium alloys, in methanol and Cl and Br halide mixtures, has been presented in [56, 57]. From the results of these studies, the corrosion fatigue behaviour regarding the considered alloys in aggressive media has been reported, as a function of the different environments and the load frequency. The dependence from frequency is explained by the increased time of exposure of the crack tip to the environment, which is longer for lower frequencies. By the work of [56], three different behaviour types have been identified, as presented in Figure 3.1. Less aggressive environments, such as vacuum, noble gases and air present a FCGR crack growth rate which is independent from frequency, classified as type 1. In type 2, common to the methanol solutions, the aggressivity of the environment precludes the passivation of the crack tip. For this reason, cyclic SCC is present at any ΔK value, and lower frequencies, i.e. increased exposure time of the tip, lead to higher FCGR rates in the whole ΔK range. For the same reason, load wave shapes which maximize the exposure time, as the square wave, have been found to maximize the FCGR effects. For NaCl solutions, and other halide solutions, at $\Delta K < \Delta K_{SCC}$ a certain repassivation of the crack tip is present, and beneficial effects are found for low frequencies, due to the sufficient time allowed for repassivation. When the condition $\Delta K > \Delta K_{SCC}$ is reached, passivation is no more present, and cyclic SCC sets on, thus privileging high frequency phenomena, when the exposure time is reduced. Moreover, from results in methanol and halides solution, presented in [57], it has been clearly pointed out that the FCGR is directly dependent from the methanol content, with higher propagation rates at higher methanol concentrations, with likely anticipation of the ΔK_{th} values, as can be seen in Figure 3.3. In [72], effects of the load ratio on FCGR rate are considered: while $R = 0.1$ specimens

show an increase of the propagation rate limited to a reduced range of ΔK above ΔK_{SCC}, $R = 0.9$ test show that the increased FCGR, which sets on after ΔK_{SCC} as usual, does not return at lower values for higher ΔK values, due to the increased opening of the crack tip promoted by the high load ratio.

Despite the wide literature available on the environmental effects of aggressive media on titanium alloys, mainly regarding FCGR data and its sensitivity to environmental and loading factors, no recent direct studies on the effects on the fatigue strength of Ti-6Al-4V have been found in literature, excluding the recent works performed by *Baragetti* et al. [58–60, 73], in which the effects of corrosion fatigue on methanol at different concentrations have been analysed on smooth specimens [73], and the corrosion fatigue on smooth and notched specimens has been evaluated in air, paraffin oil (inert environment) and 3.5 wt.% NaCl solution, considering also the effects of the stress gradient at the notch tip [58, 60]. In [73], a relationship between methanol concentration and fatigue strength drop at *2e5* cycles has been found, the maximum fatigue drop of -55% being found for the highest methanol concentration, i.e. 95 wt.%. Results on repeated tests showed higher dispersion of maximum strength $\sigma_{lim,2e5}$ for lower concentrations of methanol, and very limited dispersion for the highest tested methanol concentrations. This aspect may highlight the fact that, at higher methanol concentrations, ΔK_{th} is reduced to a point in which the smallest defects, found with higher probability on all the tested specimens, can initiate the fatigue crack. At lower methanol concentrations, only bigger defects, found only on some specimens, may initiate the cracking.

The results of corrosion fatigue tests in air, paraffin oil and NaCl mixture performed on smooth and notched specimens in [58,60] highlight that the environmental effect is maximum for smooth specimens, while the difference between the various environments decreases at higher K_t values, i.e. for sharper notches. Moreover, while the strength values found for nucleation continue to diminish with increasing K_t, the limiting failure stresses reach a plateau for $K_t > 8 \div 9$ in the three environ-

ments. This result is caused by the stress gradient beyond the notch tip, which may not be sufficient to propagate the crack, until higher levels of stress in front of the propagating crack are reached, as depicted in Figure 3.10, from [60]. From crack propagation data recorded during the testing of notched specimens analysed in [58], a numerical model has been developed, in order to reconstruct the da/dN vs. ΔK curve. The model exploited linear elastic fracture mechanics relations. The value of ΔK for each crack length was reconstructed by means of a FE model, with linear material model and linear plane stress elements, to reconstruct the geometry of the thin specimens adopted in [58]. The results have been validated over the propagation data presented by *Lee* et al. [72], considering theoretical da/dN correlations with ΔK , identified as *Paris*, *Walker* and *Kato* relations, presented in [81], [84] and [85] respectively, showing good correspondence, although the first two models, i.e. *Paris* and *Walker*, provided better results in the stable propagation region, while the model by *Kato* was more accurate near the threshold. The numerical model was then applied to the crack data available for the fatigue tests presented in [58], and the exact test applied load and crack length were reconstructed with numerical FE models for each single crack measurement available, for tests in air and paraffin oil, compared with tests in NaCl mixture, for specimen notches radii from 2.5 *mm* to 0.6 *mm*. The results provided FCGR curves related to the experiments in NaCl and in non aggressive environment, presented in Figure 3.14. The curves were compared with data from *Dawson* [56], showing a good correspondence for low ΔK values. FCGR curves have been integrated with finite differences, to obtain the number of cycles to failure, to be compared with the exponential results. The results from the data obtained in the present work and from [56] showed very good correspondence concerning tests in air, paraffin and NaCl for mild notches, i.e. $\rho = 2.5$, $Kt = 2.55$. For sharper notches, i.e. $\rho = 0.06$, $Kt = 13.34$, only the results obtained from the present work showed good agreement with experimental data, while FCGR curves from [56] sensibly over-predicted the final result. The FCGR data extrapolated from

actual experiments showed hence major precision in the prediction of the number of cycles to failure, mainly due to the major adherence to the adopted specimens geometry, and for a better description of the near-threshold behaviour, fundamental for a correct prediction of the fatigue crack propagation for sharp notched specimens.

In conclusion, the present chapter offers a full overview of the literature work on corrosion fatigue of the Ti-6Al-4V alloy, including experimental methods on recent works on the environmental effects of aggressive environments on the fatigue strength of the alloy. Considerations on the environmental effects in presence of notches are also deeply investigated, and a numerical procedure to reconstruct FCGR data and to generate satisfactory predictions of number of cycles to failure on notched Ti-6Al-4V in different environments is presented. The overall mole of data and procedures is intended to provide a toolbox for mechanical designers involved in the use of titanium alloys for high strength engineering applications subjected to aggressive environments and dynamic loading.

Chapter 4

Fatigue of PVD coated 7075-T6 alloy in aggressive environments

4.1 7075-T6 in aggressive environments

7075-T6 aluminium alloy, developed specifically for the aeronautic sector, has been a privileged choice for designers involved in the development of high strength-to-mass ratio components. With UTS values approaching 650 MPa and a density of roughly one third of steel's value, its usage has been widely proposed for decades for high strength lightweight aeronautic applications, including ribs, spars and skins for wing and fuselage. However, concerning its behaviour in aggressive environments, a marked sensitivity to halide solutions, and particularly to NaCl aqueous solutions has been found. According to the literature data collected by *Brown* [16], SCC behaviour is found on 7075-T6 in seacost atmosphere, with failure of the material at very low applied stresses, i.e. inferior to 80 MPa, in roughly 80 days of service. Failures at applied stresses values nearing the material YS have been found in less than a dozen days of applied load. The same behaviour, although with longer failure periods and higher applied stresses, i.e. above roughly 100 MPa, have been found in applications in inland industrial atmosphere, always according to [16]. For this

reason, the adoption of the 7075-T6 alloy for brand new aeronautics projects has been discontinued from year 1975, since its rating in terms of SCC behaviour has been scored to the lowest grades in terms of military standards, according to [14]. Concerning *Al-Zn-Mg-Cu* alloys, such as the 7075-T6, it has been found that the SCC sensitivity is directly linked with the adopted heat treatment, i.e. the T6 temper, resulting in intergranular corrosion between the heterogeneous microstructure, particularly due to the coarse inclusions [14, 16, 89]. It has been found that, for thin sheets of 7075-T6, a dramatic increase in the quenching rate could results in SCC immunity, due to the finer microstructure composition [16]. Unfortunately, the effect is lost for plates and other products, and specimens obtained from 50 mm thick 7075-T6 plates have showed the same poor SCC sensitivity, with intergranular corrosion, already found on common T6 treated material, even at the highest obtainable quenching rates. The only viable solution to solve SCC sensitivity from the metallurgical point of view is to abandon the T6 temper in favour of heat treatments which reduce the sensitivity of the alloy to the SCC phenomenon, such as the T73 and the T76. On the other hand, the adoption of these treatments results in a reduction of the high strength proper of the 7075-T6 material. In order to maximize the level of strength available, while maintaining SCC resistance of the base material, studies on the heat treatments have been carried out, as been reported in [14]. The best results in terms of SCC resistance were however unfortunately always linked to the highest decreases in terms of UTS and YS.

Concerning corrosion fatigue, the contribution of the aggressive environment is linked both to the reduction of the ΔK_{th} threshold value, and to the increase of the FCGR in aggressive environments [15], as reported previously for the Ti-6Al-4V case. According to *Sankaran* et al. [15], the initiation of fatigue crack occurs either if the corrosion pit grows to a critical size, sufficient to increment the applied stress intensity factor ΔK to a level above the threshold, or when the fatigue crack growth rate exceeds the corrosion pit growing rate. The transition between corrosion and

fatigue crack growth is indeed identified by a combination of these two dynamics. A very detailed analysis on the pit to crack transition study has been conducted by *Jones* et al. in [90], where 7075-T6 axial specimens, with different origin and microstructure, have been fatigue tested at $R = 0.1$ and $f = 10\ Hz$ in air, and in continuous immersion in distilled water and 3.5 wt.% NaCl solution. The results showed that the fatigue crack transition depends on a complex combination of crack pit depth, original substrate microstructure, resulting corrosion pits layout and proximity. Particularly at low applied stresses, such as the ones of the study of [90] - i.e. 121 MPa, the fatigue crack nucleation depends over the microstructural complexity, with concomitant corrosion as a worsening factor.

In [15], fatigue tests on axially loaded, $R = 0.02$ fatigue specimens were conducted, after alternate immersion of the 7075-T6 base material in a salt acidified fog spray, with prohesion testing technique. The results showed that a significant decrease in terms of fatigue strength, of constant amplitude of about 100-150 MPa is found between 1e4 and 1e5 cycles, the worst results being obtained on the specimens machined from long-exposure material. In order to explain the mechanics of the crack nucleation, numerical predictions with linear elastic stress intensity factor relations were carried out, resulting in correspondence with experimental data when the starting elliptic crack was taken with a depth coincident with the average pit size measured for a certain exposure time. Longest exposures resulted in deeper pits, with a power law relationship between pit size and exposure time. Fracture surface analysis showed that fatigue cracks initiated at a single corrosion pit, or from two or more adjacent pits. From each pit, a fatigue crack started, eventually coalescing into a final semi-elliptical fatigue crack, which propagated toward the specimen failure. Similar results are found also in the work of *Genel* [91], where rotating bending, $R = -1$ fatigue strength on pre-corroded samples has been investigated. The specimens were immersed in areated, 3.5 wt.% NaCl solution prior to the fatigue testing, for time periods from 6 to 240 h. The results on the external surface showed pitting

and degradation proportional to the immersion time, with most detrimental effects and pit coalescence for 240 h immersion. The fatigue strength was found by the author of [91] as proportional to the pit depth, with strengths decreasing from -25 to - 50% at 1e6 cycles with increasing corrosion time. Another interesting study on fatigue crack initiation from pre-corroded 7075-T651 specimens in salt spray was performed by *Zupanc* et al. [89]. In [89], the effects of shot peening in prevention of fatigue crack from corrosion pits is investigated, by means of $R = 0.05$, high frequency resonant bending fatigue test. The shot peened specimens resulted in a significant increase of the fatigue strength of roughly 15% if compared to untreated specimens in air, for most of the S-N curve. Concerning pre-corroded specimens, shot peened and corroded specimens showed indeed a very positive behaviour, with only a -13% of fatigue strength reduction with respect to non corroded, as machined specimens in air. The as machined and precorroded specimens showed indeed a dramatic reduction of -55% in terms of fatigue strength at higher fatigue life - i.e. 1e7 cycles.

Apart from the methods cited in the present section, i.e. the selection of different tempers on the 7075 substrate, reducing the final material strength, or the application of shot peening techniques, a viable idea is the deposition of protective thin hard coating layers, in order to protect the 7075-T6 surface. In this way, the corrosion resistance under dynamic load could be increased. The topic will be exposed in section 4.2.2, where different literature on corrosion protection via PVD coatings will be presented. Prior to analyse the effects of PVD on the fatigue of the 7075-T6 substrate in aggressive environments, a description of the PVD technique and of its mechanical and microstructural effects on aluminium substrates, and in particular on the 7075-T6 substrate, is discussed in section 4.2.1.

4.2 PVD coatings on 7075-T6 in air and aggressive environments

4.2.1 Thermal and mechanical effects of PVD coatings on fatigue in air

The application of Physical Vapour Deposition (PVD) technique on a metallic substrate involves the generation of a vapour from a solid target, by means of a physical process, i.e. magnetron sputtering, thermal evaporation or laser ablation. The vapour is then transported into a vacuum environment, and deposited over the target substrate, usually exploiting electric bias and plasmas to control the process. A PVD process in the latter condition is usually referred to as a Plasma Enhanced PVD (PE-PVD) [92]. A first proposed application of PVD coatings on aluminium substrates has been proposed by *Lugscheider* et al. [93]. In [93], the effects of the presence of alumina oxide layer (Al_2O_3) are discussed, along with the temperature effects of the PVD cycle on the substrate characteristics. Concerning the oxidation of the surface, it has been found that excessive alumina layer may be detrimental for the coating adhesion, although increments in the coating bonding have been experienced for oxidized substrate, especially considering Titanium - Carbon (TiC) coatings. Substrate hardness is another crucial element in the mechanical behaviour of PVD coatings, since too soft substrates may led hard coatings in being pushed into the substrate by mechanical actions, e.g. for Titanium Nitride (TiN) coatings. The most critical aspect when adopting a PVD coating over an aluminium substrate is indeed the microstructural modification produced by the high temperatures involved. In order to avoid deterioration of the mechanical properties of the substrate, PVD processes with a deposition temperature inferior to the material ageing temperature have to be selected. Another very interesting choice is to select a PVD deposition with an heat load cycle very similar to the solution treatment of the

target alloy, followed by post deposition quenching and overaging treatment, highly recommended in [93].

Another significant study concerning PVD deposition techniques involves the analysis of axial fatigue, with $R = 0.1$, regarding TiN coated 7075-T6 specimens, in the work by *Oskouei, Ibrahim* et al. [19, 20, 94, 95]. The investigation resulted in the conclusion that TiN deposition produced a significant decrease in the fatigue strength of the aluminium substrate, with a decrease of roughly 100 MPa in the cycles range between 1e5 and 1e5. Although the extremely high compressive stresses introduced by the PVD deposition, resulting in - 4.54 GPa indeed, the microstructural modification induced by the PVD process heat load resulted in a non negligible deterioration of the fatigue strength. The adoption of a Post Heat Treatment (PHT) procedure with 530 °C solution in argon for 1 hour, followed by hot and cold water quenching at 60° and 25° C respectively, resulted however in a significant restoring of fatigue strength properties. The TiN coated and PHT treated specimens showed indeed a satisfactory recovery of the fatigue strength properties, with an S-N behaviour similar, if not superior, to the uncoated specimens behaviour. The PHT treatment also markedly increased the compressive stresses, to a value of -7.56 GPa. Excellent adhesion of the coating to the substrate was found in this latter case for low and moderate applied stresses, although at higher stresses - i.e. above 200 MPa - delamination in the proximity of the final fracture surface has been found.

The presence of delaminations found in [95] highlights another effect of the deposition of thin hard coatings on 7075-T6 surfaces. Indeed, the presence of a thin coating with very high elastic modulus, if compared to the modulus of the substrate, can generate very high shear stresses even under elastic deformations. In [95], it is stated that a difference in elastic modulus from 400 GPa for the TiN layer to the 75 GPa of the aluminium substrate generates high strain differences, resulting in elevated alternate shear stresses concentrated at the discontinuity. The same behaviour in the elastic regime has been described in the work of *Puchi-Cabrera* et

al. [18], with elastic modulus for the ZrN of 280-360 GPa is deposited on the aluminium substrate. The realization of an intermediate layer between the substrate and the coating is proposed to reduce the shear stresses. Moreover, the expectable cracking of the hard coating is found where ductile deformations are reached on the sample. On this aspect, it must be remarked that the realization of a 0.2 μm Zr-based metallic glass thin film, with high strength and good bending ductility, combined with a 0.05 μm Ti buffer layer, recently developed by *Chang* et al. [96], resulted in a marked increase in four point bending fatigue strength at $R = 0.1$. The authors of [96] attribute the positive behaviour to the excellent ductility of the coating, resulting in superior adhesion, combined with the high compressive stresses introduced in the substrate. Unfortunately, no indication on the process temperature is reported in [96], with no indication on the impact of the thermal effects of the deposition process on the substrate mechanical properties.

Concerning other aluminium alloys, a significant study on the fatigue behaviour of PVD WC/C (Tungsten Carbide/Carbon), PA-CVD DLC (Diamond-like Carbon) and PE-CVD SiOx (Silica Oxides) on 2011-T6 aluminium is presented in [97]. The coatings resulted in a slight increase in fatigue strength at 1e7 cycles, with a more marked beneficial behaviour related to the WC/C deposition of +10%, with evidence of subsurface crack growth nucleation, caused by the presence of compressive stresses. The limited beneficial effects found on CVD DLC and SiOx coatings are related to the poor adhesion, highlighted by scratch test result when compared to the WC/C samples. Another aspect to be taken into consideration is the fact that in the latter two cases, it is not a PVD process to be considered, but a Chemical Vapour Deposition (CVD), which is likely executed at higher temperatures.

4.2.2 Effects of PVD coatings on fatigue in aggressive environments

The effects of protective coating in terms of fatigue behaviour are mostly desired when considering corrosion behaviour in aggressive environment. The necessity to improve the corrosion fatigue sensitivity of the 7075-T6 alloy has driven several research works into the direction of surface protection via coating generation. In the work by *Genel* [98], the fatigue behaviour of 7075-T6 rotating bending specimens, anodic oxidation was used to generate a 23 μm protective layer on the samples surface. Results showed that the uncoated specimens underwent a significant reduction in terms of resistance in aggressive 3.5 wt.% NaCl mixture, with a 1.5 degradation factor at *1e5* cycles, logarithmically increasing to almost 3 at *1e7* cycles. The main reason of failure was found by the authors in fatigue crack nucleation from pitting corrosion. Concerning oxide coated specimens, the coating resulted in a detrimental degradation of 1.5 for the whole fatigue life interval. Within the aggressive environment however, the coated specimens experienced a more modest reduction of fatigue strength, from 1.5 degradation factor at *1e5* cycles, logarithmically increasing to a maximum of 2 at *1e7* cycles, with an overall improvement in corrosion fatigue of 42% in the higher cycles region. The S-N curves extrapolated from the actual data are presented in Figure 4.1. This behaviour suggest a protective effect of the oxide, identified by the inferior dimension of the corrosion pits found on oxide coated specimens. In another work by *Puchi-Cabrera* et al. [99], the effects of Ni-P coated 7075-T6 specimens, subjected to axial testing in air and 3 wt.% NaCl solution resulted in positive, albeit not impressive, increase in fatigue and corrosion fatigue strength of the base material for the coated substrate. Concerning aluminium substrates coated with non-PVD techniques, a remarkable result is found by the High Velocity Oxigen Fuel (HVOF) deposition technique, involving the generation of a WC–10Co–4Cr layer on a 6063-T6 substrate, in the work by *Villalobos-Gutiérrez* et al. [100]. In the proposed work, a significant increase of roughly one order of

magnitude in terms of number of cycles to failure is obtained on coated specimens in air and 3 % NaCl solution. The main reasons of this behaviour are to be found in the increased thickness of the hard coating, i.e. 250 μm, and in the generation and propagation of the crack in the external coating, for a great extent of the fatigue life. A reduced sensitivity of the substrate alloy to the aggressive environment has also to be considered when referring to corrosion fatigue behaviour. In any case, the high thickness of the external coating excludes the process from the actual discussion, restricted to thin hard coatings.

The most significant work concerning corrosion fatigue behaviour of PVD coated is proposed by *Puchi-Cabrera* et al., in [18]. Within the investigation of [18], a 3 μm thick ZrN (Zirconium Nitride) layer is deposited over 7075-T6 rotating bending fatigue specimens, on the basis of successful applications, in terms of fatigue and corrosion fatigue strength, on steel substrates. Concerning tensile properties, the application of the process resulted in a significant decrease of the YS and UTS of -43% and -28% respectively, due to the high temperatures experienced in the process. Testing of the coated specimens in air resulted in poor fatigue behaviour, with a decrease in the range of -73 to -82%, with higher detrimental effects at higher applied stresses. The S-N curves extrapolated by the authors of [18] are reported in Figure 4.2. The reason of such behaviour is identified by the authors of [18], by the combined action of the high temperatures experienced by the substrate during the PVD process, and by the diffuse cracking and delamination of the thin hard coatings at high applied stresses. A consequence of this behaviour is found in the multiple crack nucleation on the specimen external surface, leading to a complex fracture surface, with multiple crack propagation fronts divided by finite steps outside the fracture plane. Considering fatigue in aggressive 3.5 wt.% NaCl, a positive corrosion behaviour is found at lower applied stresses, i.e. at longer fatigue lives. In this latter case, better fatigue behaviour is expected for the coated specimens at lives above *1e5* cycles, with respect to the uncoated material. At lower applied stresses indeed, the

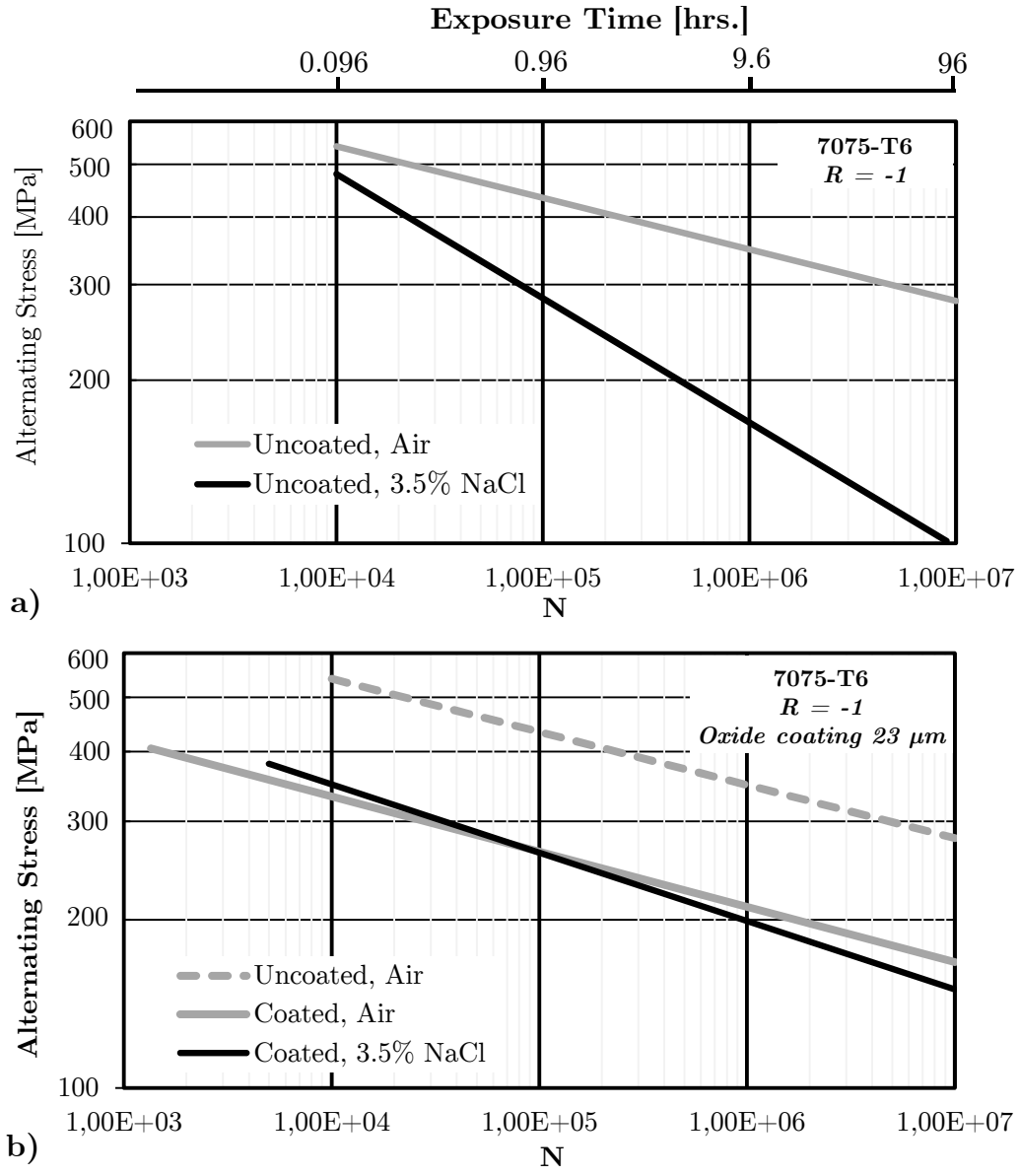

Figure 4.1: 25 μm oxide coated 7075-T6 $R = -1$ fatigue and corrosion fatigue behaviour: (a) Uncoated specimens in air and 3.5 wt.% NaCl solution; (b) Oxide coated specimens in air and 3.5 wt.% NaCl solution. Adapted from *Genel* [98].

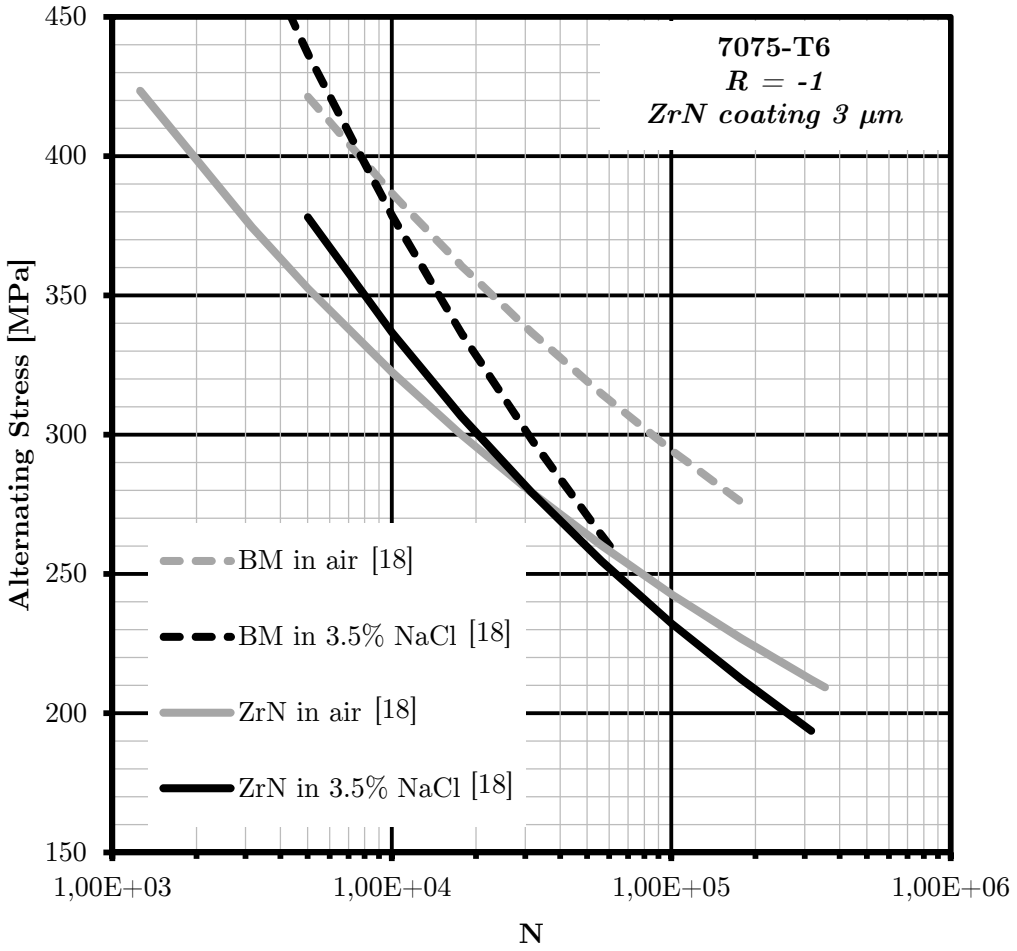

Figure 4.2: Fatigue and corrosion fatigue behaviour of uncoated and $3\mu m$ ZrN coated 7075-T6 rotating bending specimens in air and 3.5 wt.% NaCl solution, from the work of *Puchi-Cabrera* et al. [18].

adhesion of the ZrN layer is sufficient to grant a certain corrosion protection of the surface, resulting in a reduced number of crack initiations on the external surface, as noticed in the fracture surface analysis. The overall fracture surface presents indeed a more regular pattern.

Taking as a starting point the work of *Puchi-Cabrera* [18], several tests were arranged, considering the deposition of WC/C and DLC coatings on the 7075-T6 substrate. The choice of the processes was made by their low deposition temperature, granted with a maximum of 180 °C from *Lafer S.p.A.* [101], which, although superior with the T6 ageing temperature of 121 °C [18] is reduced in comparison with the high temperatures involved in PVD TiN and ZrN processes, ranging above

400 °C [18, 101]. In the following sections, several works produced in the field of the present research are presented, including rotating bending fatigue test which analyse the effects of the PVD coating deposition, of the process temperature, and on the corrosion protection effect of the proposed coatings in aggressive methanol environment.

4.3 Materials and methods

In the presented works, fatigue tests were performed on 7075-T6 specimens, both coated and uncoated, machined according to the geometry presented in Figure 4.3. The tests were object of several works which analysed the performance of 7075-T6 substrate, bare and coated with WC/C and DLC low temperature PVD coatings [21, 23, 25, 27]. The base material chemical composition is reported in Table 4.1. In order to characterize the mechanical properties of the substrate material, tensile tests and Vickers hardness tests were conducted, resulting in a UTS of 658 MPa and a YS of 597 MPa, with a substrate hardness of 194 HV. The specimens were then machined, and the test surface was prepared by means of mechanical polishing with abrasive paper up to 1200 grit. The final polishing was taken along the specimen length, resulting in an overall longitudinal roughness inferior to 0.1 μm, as obtained by an average of three measures per sample with a Form Talysurf profilometer. The specimens were then industrially coated, following the commercial process performed by *Lafer S.p.A.* [101], and tested both in air and in aggressive methanol environment. The coating process resulted in a 2.5 μm thickness for both coatings. The actual configuration of the coatings is multi-layered: both coatings were deposited on a Cr substrate, the WC/C treatment consisting in a double layer of WC/C, while the DLC process consisted in a inner layer of WC/C and an external hydrogenated amorphous carbon layer. The WC/C coating hardness is in the range of 1200-1400 HV, the DLC within 1800-2600 HV, as reported in [101]. From research work concerning the

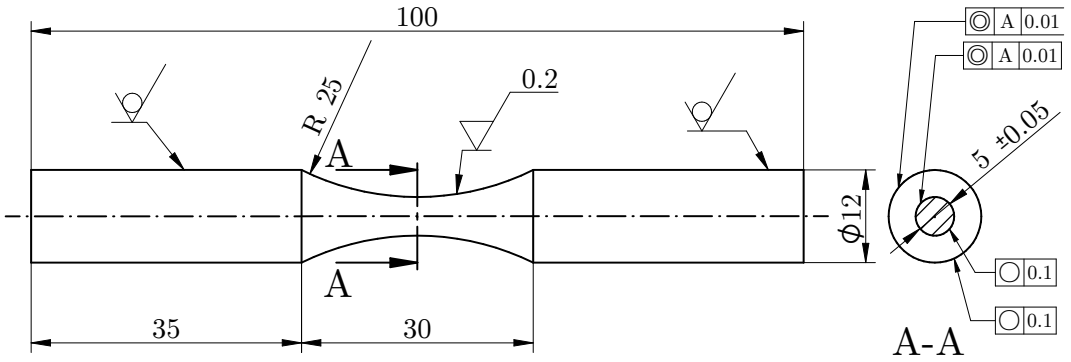

Figure 4.3: Rotating bending fatigue 7075-T6 specimen shape, used in [21,23,25,27].

deposition of analogous WC/C and DLC and layers [97], the compressive stresses were estimated around the value of 1.3-1.6 GPa, while the elastic modulus was assumed to be between 200 and 150 GPa.

The reference environment was chosen due to its proven aggressiveness showed against titanium light alloys [41], and the specimens were fully immersed in methanol for the whole duration of the step-loading procedure. The general setup for all the considered tests followed the step-loading procedure on a ItalSigma four point bending machine, with digital force and number of cycles control, which permitted the exact setup of the applied load and of the number of cycles, with a precision of less than 5 MPa on the applied stress and of less than 200 cycles on the number of cycles. The tests were executed at 2000 rpm, resulting in test runs of approximately 100 mins per load block. The step-loading procedure was performed from a starting value $\sigma_0 = 150\ MPa$, with increments of load between a load cycle and the following of $\Delta\sigma = 9\ MPa$. The load cycle block length chosen was of *2e5* cycles, to identify the fatigue limit $\sigma_{lim,2e5}$ corresponding to a fatigue life of $N = 2e5$. For each step-loading tested specimen, a confirmation run was performed, by imposing the limiting strength found with the step loading method, i.e. $\sigma_{lim,2e5}$, and measuring the number of cycles to failure. For major details on the step-loading procedure and on its validity on light alloys, the reader is encouraged to refer to Appendix A.

Al [%]	Zn [%]	Mg [%]	Cu [%]	Fe [%]	Si [%]	Cr [%]	Mn [%]	Ti [%]
Bal.	5,6	2,55	1,75	0,32	0,25	0,22	0,2	0,12

Table 4.1: 7075-T6 material chemical composition, from raw commercial bars, adapted from [21].

4.4 Experimental Results

Preliminary step-loading fatigue tests were performed on 7075-T6 specimens, to assess the effects of the PVD heat cycle on the fatigue of the material, highlighting the role of the microstructure modification of the alloy during the PVD process. Results related to uncoated specimens subjected to the same heat cycle of the two selected PVD processes are reported in Figure 4.4, as reported in [21]. The results are related to the fatigue strength $\sigma_{lim,2e5}$ at *2e5* cycles, identified by means of the step loading procedure. As can be seen from Figure 4.4, both WC/C and DLC cycles result in a deterioration of the microstructural properties, resulting in a limiting strength of 232 and 223 MPa respectively, against a fatigue limit for the specimens tested in air of 274 MPa. A drop in fatigue strength of -15% and -19% is hence found at *2e5* cycles for the microstructural modification associated with the WC/C and DLC processes respectively.

Concerning the fatigue testing of PVD coated specimens in air and methanol, the results are presented in Figure 4.5. If considering the effects on fatigue limit at *2e5* cycles of the coating process alone, a -24% is found for the WC/C coating, while a -15% is reported on specimens with a DLC layer, with respect to the uncoated specimen in air. By comparing the uncoated specimen in methanol with its counterpart coated with WC/C layer, a mere -3% reduction of the fatigue strength is found. Furthermore, The DLC coated specimen tested in methanol with the step-loading technique provides a positive contribution of +8% with respect to the uncoated specimen in aggressive environment. Against a reduction of fatigue strength due to the methanol environment of -29% related to the uncoated specimens indeed, the WC/C and DLC coated specimens demonstrate a reduction of fatigue strength in

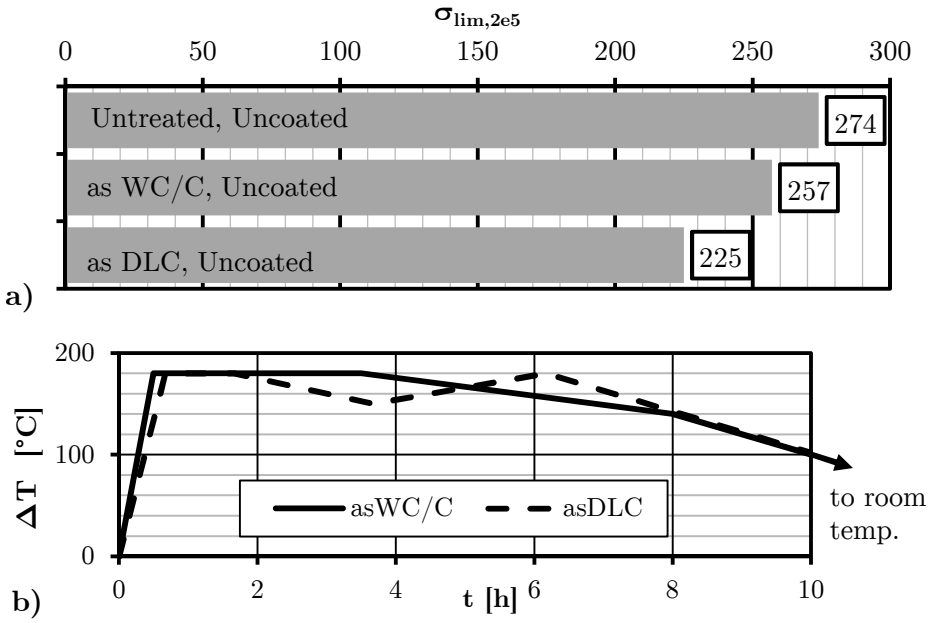

Figure 4.4: Effects of the low temperature PVD WC/C and DLC heat cycle on 7075-T6 fatigue strength at *2e5* cycles on uncoated, mirror polished 7075-T6 specimens: (a) $\sigma_{lim,2e5}$ on uncoated specimens subjected to PVD heat loads; (b) WC/C and DLC processes heat loads as reproduced on specimens, adapted from [21].

aggressive environment of -9 and -10 % respectively. The confirmation runs are reported, for several tested configurations, in Table 4.2. The confirmation runs for the specimens tested in air are of the same order of magnitude of the number of cycles selected for the step-loading procedure - i.e. *2e5* - while, if considering specimens tested in methanol, confirmation runs are significantly longer. This aspect is surely linked to the different immersion time under loading experienced by the confirmation specimens: while the step-loading tested specimens sustained repeated load blocks from σ_0 to the specimen failure, the confirmation specimens were in contact with the environment only during their single run. According to *Genel* [91], the loss of fatigue strength in an aggressive media is linked not only to the applied load, but also to the immersion times, as accounted for in Figure 4.1. The longer run times of the confirmations specimens in methanol are indeed to be linked to the reduced exposure to the aggressive environment: indeed, a single confirmation run to *2e5* cycles would imply only 100 mins. at 2000 rpm.

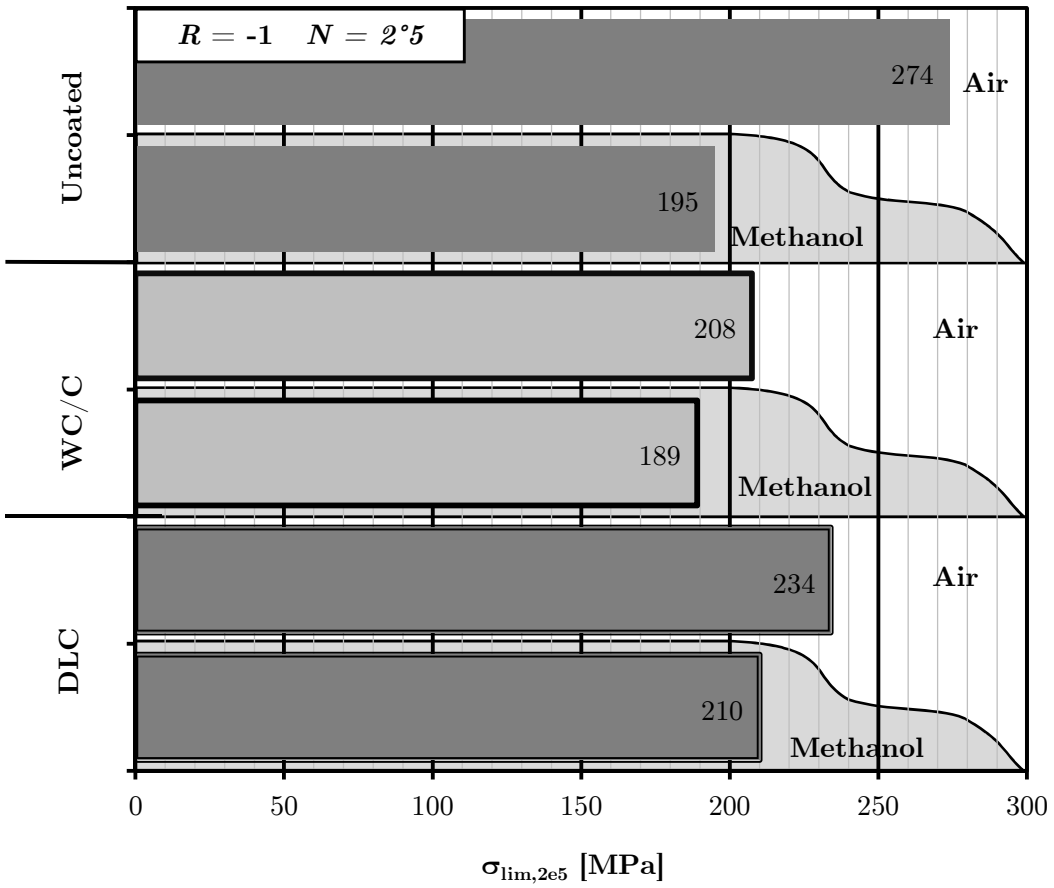

Figure 4.5: Effects of the PVD WC/C and DLC deposition on the $\sigma_{lim,2e5}$ fatigue strength at *2e5* cycles on uncoated, mirror polished 7075-T6 specimens tested in air, adapted from [25].

Environment	Specimen	$\sigma_{lim,2e5}$ [MPa]	N_{conf}
Air	Untreated	274	123276
	As WC/C	257	217566
	As DLC	225	130516
	WC/C	208	N/A
	DLC	234	223429
Methanol	Untreated	195	2.5e6
	WC/C	189	1.2e6
	DLC	210	879863

Table 4.2: Confirmation runs for several step-loading tested specimens object of the present campaign.

4.5 SEM Analysis

From the fracture surface of the uncoated specimen tested in methanol, presented in Figure 4.6, multiple nucleation is observed on the external surface. After a region profoundly modified by the methanol environment, in which the crack propagation direction is hardly recognizable, multiple crack propagating on different planes are present, separated by finite steps, as found also by *Puchi-Cabrera* et al. [18]. The different initiation sites are identified by the presence of surface corrosion pits, as can be seen in the highlighted region of Figure 4.6. The different propagations fronts then coalesce prior to the final fracture of the specimen. The identified limiting stress at *2e5* cycles identified with this figure is 195 *MPa*, with a reduction of -29% with respect to the specimen tested in air. The following fracture surface, presented in Figure 4.7, is related to the WC/C coated specimen tested in methanol for *2e5* cycles, with a limiting stress of 189 MPa. In this case, multiple initiation spots are present, but if compared to Figure 4.6 they appear to be concentrated, near to a region where coating delamination and cracking was observed, as pointed out in Figure 4.7. Only a couple of wide propagation fronts are recognizable, and they coalesce homogeneously into a final fracture region. The final SEM micrograph, presented in Figure 4.8, is related to the fracture surface of the DLC coated specimen. In this latter case, the fracture is nucleated from a single point near the coating-substrate interface. The coating appears as cracked near the initiation region, but no delamination as in the WC/C case is observed. The crack propagates following a more regular path, if compared to the previous specimens. The details of the crack region near the nucleation point show signs of the methanol environment, as the fracture edges appear to be blunted by the medium. However, the fracture surface is more regular with respect to what observed in Figure 4.6 and 4.7. A transition from environmental affected fracture surface to classical fatigue fracture shape is observed at the bottom of Figure 4.8. The regular crack propagation front then propagates towards the final fracture. Considering WC/C and DLC coated specimens tested

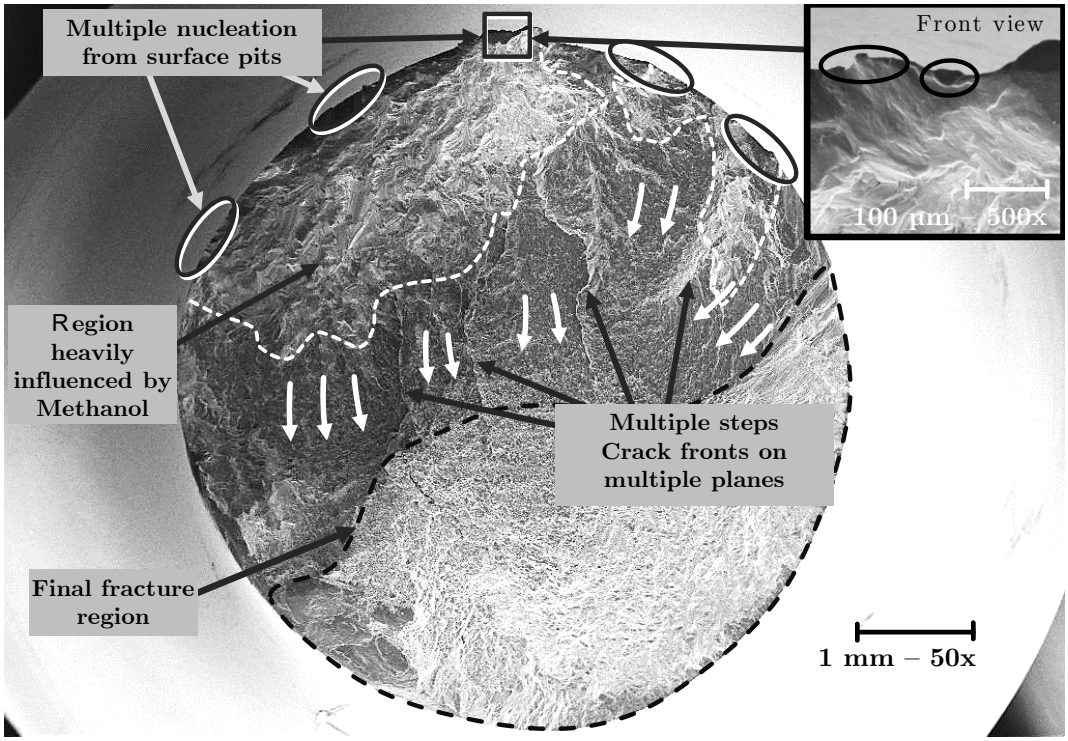

Figure 4.6: Uncoated 7075-T6 mirror polished specimen, tested with step-loading in methanol at *2e5* cycles - $\sigma_{lim,2e5} = 195\ MPa$. Adapted from [25].

in air, and presented in Figure 4.9, it can be seen that the same coating behaviour of the specimens tested in methanol is found. In particular, the WC/C coating shows an extended cracked delaminated region near the nucleation zone, while only coating cracking is found on the DLC coated specimen. The environmental effect is obviously not present in Figure 4.9, resulting in a classical fatigue crack propagation pattern.

4.6 Discussion

Thin hard coatings are supposed to provide beneficial effects due to the compressive stresses generated in the deposition process, as indicated by *Oskouei, Ibrahim* et al. [19, 20, 94] and *Puchi-Cabrera* et al. [18]. Indeed, beneficial effects on case-hardened steel was found, especially for low stressed components - i.e. high fatigue lives - in the works by *Baragetti* et al. on coated spur gears [47, 83], and by *Saini*

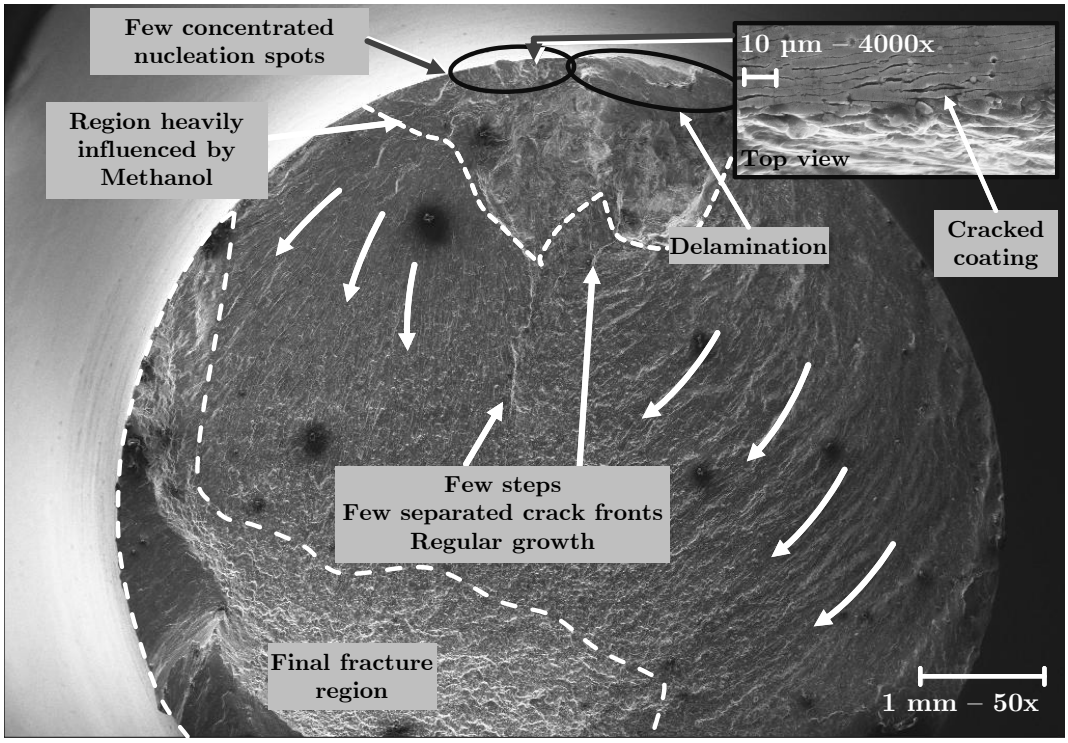

Figure 4.7: WC/C coated 7075-T6 mirror polished specimen, tested with step-loading in methanol at *2e5* cycles - $\sigma_{lim,2e5} = 189\ MPa$. Adapted from [25].

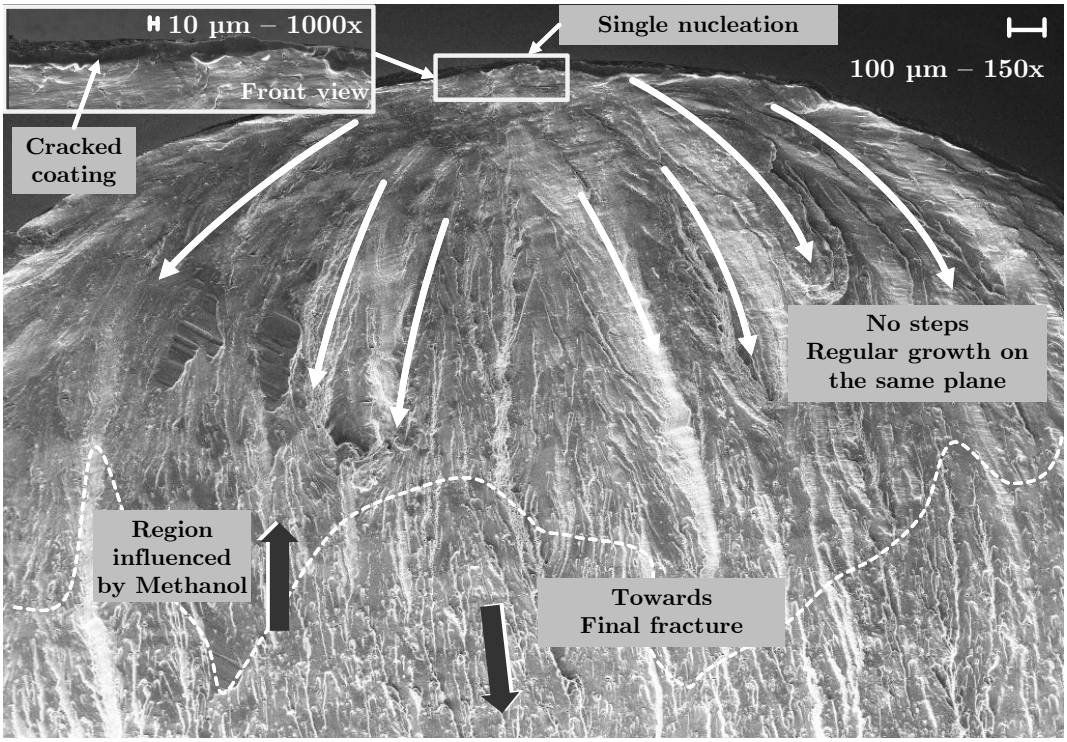

Figure 4.8: DLC coated 7075-T6 mirror polished specimen, tested with step-loading in methanol at *2e5* cycles - $\sigma_{lim,2e5} = 210\ MPa$. Adapted from [25].

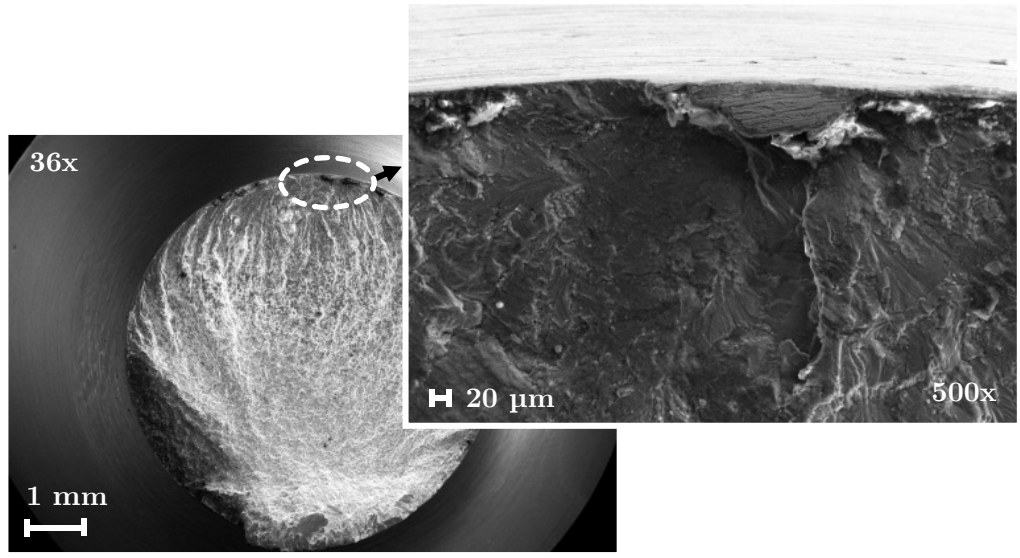

a)

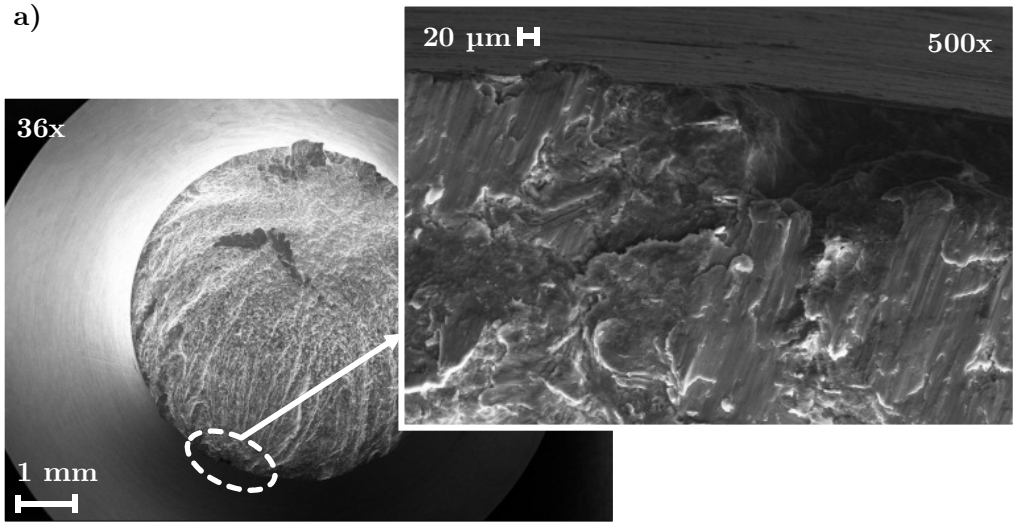

b)

Figure 4.9: 7075-T6 coated specimens tested in air: (a) WC/C coated 7075-T6 specimen and (b) DLC coated 7075-T6 specimen, tested at *2e5* cycles, from [21].

and Gupta in [102]. However, concerning the effects of thin hard coatings on a light alloy 7075-T6 substrate, as presented in Figure 4.5, the contribution of several factors must be considered. At first, the PVD processes selected, although being the lowest temperature alternative on the market, presented a non-negligible effect on the microstructure of the material, as reported in Figure 4.4. The detrimental contribution caused by the heat load of the PVD processes is indeed the main cause of fatigue strength loss for most of the higher temperature processes adopted in literature, as ZrN and TiN, as reported in [18–20,94]. Indeed, in [20] a post heat treatment is proposed to restore the microstructural properties of the substrate providing, as a favourable side effect, an increase in the compressive stresses generated by the coating. In the present case, although the temperatures in play are not elevated, with a maximum of 180 °C as can be assessed in Figure 4.4, they are above the 7075-T6 ageing temperature of 121 °C [18], thus resulting in overaging and loss of mechanical properties.

In addition to the effects of the PVD process on the material microstructure, the mechanical interaction between the thin hard coating and the substrate have to be considered, when light alloys are involved. Observations on fractured rotating bending specimens of 7075-T6 aluminium, coated with a PVD ZrN layer, have highlighted cracking and delamination of the ZrN coating for applied cyclic stresses above 220 MPa [18]. The phenomenon is not only related to the very high hardness of the applied coatings, which tend to fracture when ductility is reached, but also on the shear interaction that takes place during elastic deformation. Indeed, the marked difference between the elastic modulus of the aluminium substrate and the thin hard coating is indicated as responsible of the coating delamination by the authors of [18]. Another possible factor in the lack of adhesion of the coating is the likely presence of an oxidation film, formed before and during the PVD process on the target surface. The same coating behaviour has been found by *Oskouei, Ibrahim* et al. in [95], where delamination was present on axial $R = 0.1$ fatigue tested TiN

coated 7075-T6 specimens, at alternated stress levels above 200 MPa. According to the authors of [95], the main driving force of the delamination is the same found in [18], i.e. the different elasticity between the substrate and the coating.

Considering the work exposed in the present chapter, result of a global study conducted on several published articles [21,23,25,27], all the described factors found in literature come into play at different levels, when considering the results presented in sections 4.4 and 4.5. A thermal degradation is indeed caused in the substrate by the exposure to the temperatures of the PVD cycle, as indicated in Figure 4.4, although it is not responsible of the whole degradation of the fatigue strength, but only of a fraction of 26% for the WC/C and of 82 % for the DLC. Thus, the mechanical effects of the coatings are to be considered responsible of the further decrease of the fatigue strength of the specimens. However, by looking at the DLC coated specimen, it is evident that the mechanical interaction between the substrate and the thin hard coating is less critical than in the WC/C case, since the fatigue strength identified at *2e5* is remarkably higher than the results on the WC/C coated sample tested in air. The latter behaviour may be related with the extended delaminations found in the WC/C specimens, tested both in air and in methanol, as can be seen in Figures 4.7 and 4.9, considering also the fact that a delaminated coating may interfere with the substrate and contribute to crack nucleation. Concerning DLC coatings, no delamination was found in Figures 4.8 and 4.9, but only limited cracking, which may have been caused by the final failure of the specimen. Indeed, when comparing the fatigue strengths in methanol, the DLC coating produces a significant protection effect, with a +8% increase in fatigue limit with respect to the uncoated specimen in methanol, against a limited protective effect of the WC/C coated specimen with a -3 % fatigue strength loss in methanol at *2e5* cycles against the uncoated specimen.

4.7 Remarks

The present chapter reported a complete overview on the problems of fatigue in aggressive environments concerning the 7075-T6 alloy. The main influence of the corrosive environment concerns the crack nucleation, as confirmed by most of the literature sources [15, 89, 91], which causes an anticipation of the threshold value ΔK_{th}. Since the alloy is also susceptible to SCC [14], the effects of cyclic SCC in the propagation stages may indeed be relevant in the propagation stage. However, the majority of the studies [15, 18, 89] does not take into account this effect, by testing at higher frequencies with respect to the typical corrosion fatigue tests, i.e. above 10 Hz.

In order to increase the corrosion fatigue resistance of the 7075-T6 alloy, some authors have proposed to adopt surface coatings to protect the surface from the aggressive medium [18,98,100]. *Genel* [98] adopted 25 μm oxide coating, with some protection effects but a very detrimental effect on fatigue, and *Villaloboz-Gutiérrez* et al. [100], which proposed a 250 μm thick HVOF spray, with good results on fatigue on coated specimens in air and aggressive environment. Restricting the interest to PVD thin hard coatings, the most remarkable work has been performed by *Puchi-Cabrera* et al. [18]. In [18], 3 μm thick ZrN PVD coating was deposited on 7075-T6 surface, and fatigue tested by means of rotating bending tests in air and 3.5 wt.% NaCl solution. The results indicated that a certain protection effect of the coating was granted at higher fatigue lives, whilst a non-negligible detrimental effect of the coating on fatigue was present. The effect of the thermal loads of the PVD cycle, above 400 °C for the ZrN process, and the mechanical interaction between the coating and the substrate at high applied stresses are involved. Similar effects are found in the work by *Oskouei, Ibrahim* et al. [18–20, 94], concerning axial fatigue of TiN coated 7075-T6 specimens at 450 °C, where a post deposition heat treatment is proposed. The PHT restores almost completely the fatigue performances of the 7075-T6 alloy.

In the present work, the effect on fatigue in air and aggressive methanolic environment of low temperatures PVD coatings has been analysed by means of rotating bending, step loading fatigue tests of uncoated, WC/C and DLC coated specimens. The results show that both coatings have a detrimental effect on the limiting fatigue strength at *2e5* cycles $\sigma_{lim,2e5}$, partly caused by the deposition process temperature of 180 °C, and partly due to the mechanical interaction between the coating and the substrate. The microstructural modification of the substrate accounts for the 26% of the WC/C fatigue strength loss, and for the 82% of the DLC loss in fatigue strength at *2e5* cycles. The effects of the mechanical interaction between the thin hard coating and the substrate are, as investigated in [18, 95], the delamination of the coating under elastic deformation, due to the difference in the elastic moduli of the substrate and the coating, and the cracking of the coating for high, mainly plastic deformations. In the present work, extended delamination and cracking has been identified on the WC/C coated specimens, while DLC coated specimens showed only limited cracking, most likely limited to the final fracture phases. This aspect is related also with the good behaviour found for the DLC specimens in methanol. Despite of the loss of -15% in fatigue strength at *2e5* cycles in air indeed, the DLC coated specimen tested in methanol showed a +8 % increase in fatigue strength at *2e5* cycles, with respect to its counterpart in air. Such a positive behaviour, considering the high applied stresses and their effects on the coating-substrate interface, show that the DLC coating has an interesting protection capability even starting from fatigue lives of *2e5* cycles. Despite of its detrimental effects on fatigue in air, the application of a DLC layer may be beneficial for 7075-T6 specimens exposed to dynamic loading in aggressive environment. The same results are not obvious for the WC/C coating, which has showed extended delamination and limited protection capabilities.

Chapter 5

Conclusions and Future Developments

5.1 Conclusions

By summarizing the research performed during the writing of the present dissertation, a wide literature and experimental investigation over the static and corrosion fatigue of structural materials with high strength-to-mass ratio is presented. The research has focused in particular on two high-strength light alloys, i.e. the Ti-6Al-4V titanium alloy and the 7075-T6 alloy. Both materials are fundamental in new applications for structural components, due to the current necessity for energy efficient solutions in most engineering fields. However, the experience of the past decades has shown that their application can be limited by the operating environment, which can be critical only under certain circumstances, concerning for example of Ti-6Al-4V in methanol, or in a wider application range, as in the 7075-T6 case. Moreover, new technical challenges in advanced sectors, such as biomedical, oil&gas and fuel cells, require new applications in potential aggressive environments. The proposed study aims to address the research towards possible solutions to the critical issues which can be encountered in present and future engineering applications.

In Chapter 2, the effects of SCC of the Ti-6Al-4V titanium alloys are addressed. A complete literature study is performed, highlighting the critical environments and the SCC mechanisms for the considered alloy. The well-established research framework is delineated, including industrial standards. The experimental work, carried out on SCC tests in methanol solution at different concentration, highlighted the fundamental role of the metallurgical condition of the Ti-6Al-4V surface, particularly concerning the amount of water needed to passivate the SCC mechanism, resulted higher in comparison with the literature. The reason of such behaviour was identified in the presence of an α-layer, probably generated by the stress-relieving heat treatment, which changed the surface interaction between the medium and the material, including cracks in the harder surface layer which promoted the SCC process. The experiments highlighted the possibility of critical situations, which may arise from the use of the alloy in not sufficiently passivated environments, with surface conditions which are not intended or foreseen by the mechanical designer, resulting in possible catastrophic situations in applications in direct contact with the medium. Another aspect which may affect the identified behaviour could be identified in the low oxygenation of the aggressive environment. Remembering the present application fields of Ti-6Al-4V for structural applications in the presence of methanol, they include at present days the aeronautic sector, the oil&gas applications and the fuel cells research.

Chapter 3 investigates deeper into the fatigue and corrosion fatigue behaviour of the Ti-6Al-4V. The effects of methanol concerning corrosion fatigue are analysed by presenting literature data which confirm the effect of the methanol concentration on the reduction of the Ti-6Al-4V fatigue strength, which is directly related to the methanol content. The methanol effect is active even from low concentrations, in contrast with the SCC behaviour. Studies of the previous research indicated that no passivation is found near the crack tip once the corrosion fatigue process takes place and cyclic SCC sets on, resulting in a constant acceleration of FCGR in the whole

ΔK rate, and in a likely anticipation of crack nucleation by reduction of ΔK_{th}. The effects of corrosion fatigue are not limited to the environments in which the Ti-6Al-4V alloy is sensible to SCC. Indeed, once the fatigue crack is initiated, the typical passivation to most aggressive environments granted by the TiO_2 protective oxide layer decays, and sensitivity to common aggressive media, such as NaCl chloride solutions is encountered. Axial fatigue tests in air, paraffin oil and 3.5 wt. % NaCl have highlighted a substantial acceleration of the FCGR in the NaCl environment, as confirmed by literature. The numerical reconstruction of $\mathrm{d}a/\mathrm{d}N$ vs. ΔK FCGR curves from the experimental data of step loading axial fatigue tests on smooth specimens showed some differences in the FCGR rate at low and high ΔK values, with respect to classic FCGR data obtained by thick SEN specimens from literature. The results on the predicted number of cycles confirmed that the numerically obtained FCGR curves resulted in better failure prediction, with respect to literature data. This assumption highlights the necessity to develop proper numerical models for the FCGR data, depending on the specimen or component shape, in order to obtain accurate fatigue life predictions. Simply relying on the literature data for FCGR prediction may not be sufficient when different geometries with respect to the standard plane strain propagation considered in FCGR literature are adopted.

Chapter 4 is related to the fatigue and corrosion fatigue of the 7075-T6 alloy. A detailed literature review and experimental analysis is dedicated to the study of the effects of thin hard PVD coatings on the fatigue and corrosion fatigue behaviour of the considered aluminium alloy. Concerning fatigue behaviour, three main aspects come into play when considering the effects of PVD coatings on a light alloy substrate. The first effect of a PVD deposition concerns the beneficial effects that the generation of compressive residual stresses has on the fatigue behaviour of the metallic substrate. This aspect is commonly found in steel substrates, but research data highlight that the effects are also present on light alloys. The other two contributes, which are more critical on light alloys substrates, if compared to case-hardened steel,

are the thermal microstructural modifications of the substrate, induced by the PVD process, and the mechanical interaction under dynamic load of the soft aluminium substrate coupled with thin hard coating. Concerning the thermal effect, a highly detrimental contribution to the fatigue strength of the substrate has been found for high temperature PVD depositions, such as the processes for generating TiN and ZrN layers, which are typically above 400 °C. The degradation of the mechanical characteristics of the substrate results in a dramatic reduction of fatigue strength in the whole interval of fatigue life. For this reason, post processing with heat treatments has been proposed in literature. The second critical aspect when considering PVD deposition of thin hard coatings on light alloys is the marked difference, in terms of hardness and of elastic modulus, between the substrate and the coating. Due to the difference of elastic modulus, high shear stresses may be present between the coating and the substrate, resulting in coating delamination for dynamic loading in the elastic regime. Moreover, the high hardness of the coating results in coating cracking when high deformations, correlated with substrate plasticity, are reached. These aspects, and in particular the delamination in the elastic field, affect the fatigue strength of the material, and are critical also concerning fatigue in aggressive environments, since the protection of the substrate surface is directly linked to the integrity of the external coating.

In Chapter 4, experimental results concerning step loading rotating bending fatigue tests at *2e5* cycles on low temperature (180 °C) WC/C and DLC coatings in air and aggressive methanol environment are presented. The aim of the work is to assess the influence of the discussed factors on the fatigue behaviour of the 7075-T6 alloy in air and aggressive environment, in order to find viable procedures to improve the fatigue strength of the proposed alloy in critical environments, by the adoption of thin hard coatings. In order to minimize the thermal effects of the coating process, low temperature PVD depositions have been selected. Although the temperature of 180 °C was the lowest in commercial PVD applications, the WC/C and DLC

thermal loads resulted responsible of 26 % and of 82 % of the loss in fatigue strength, respectively. The microstructural modification is indeed inevitable, since the ageing temperature of the T6 temper is of 121 °C. Concerning the mechanical behaviour of the coating-substrate system, the application of a WC/C coating resulted in significant delamination and in a wide reduction of fatigue strength, with the lowest result of the experimental campaign, i.e. -24 % of fatigue strenght at *2e5* cycles, including the thermal effect. The DLC coating showed indeed a better mechanical interaction, with an overall reduction of fatigue strength of only -15 %, of which the 82 % is imputable to the thermal process. Concerning the coating performances in aggressive environment, the WC/C coating resulted in limited protection, with a -3% drop with respect to uncoated specimen in methanol, while the DLC produced a +8 % gain in fatigue strength at *2e5* cycles. The reason of this discrepancy is to be found in the coating delamination, identified by SEM analysis on the WC/C samples, but not found on the DLC coated specimens. The good behaviour of the DLC in aggressive environment is remarkable, considering the fact that the high applied stresses at *2e5* cycles have created sensible coating delamination in most of the research works on thin hard coated 7075-T6 fatigue. The adoption of a DLC coating for aggressive environment protection on dynamically loaded 7075-T6 substrate is hence a viable solution, although further testing at different fatigue lives is recommended.

5.2 Future Developments

When considering the SCC characterization on Ti-6Al-4V, new research activities should involve the consideration of further effects which may clarify the SCC behaviour of this particular alloy in methanol and other aggressive environments. Particularly, the presence of sharp notches, oxide removal or other influencing factors affecting the interaction between the surface and the aggressive environment must

be considered. Furthermore, the effects of oxygenation of methanol-water solution are to be considered, to assess their influence in the SCC passivation mechanism, in particular concerning the effect of the solution oxygenation on the maximum water concentration required for SCC passivation. In the presented work indeed, oxygenation was limited, so future tests with increased oxygenation may shed light on this aspect.

Concerning corrosion fatigue behaviour of the Ti-6Al-4V alloy in methanol, further fatigue tests are recommended, in particular to obtain proper, test specific FCGR data, to be used for the generation of numerical models and predictions of fatigue life in aggressive environments. Indeed, in the presented work and literature sources, FCGR experimental data was missing, mainly due to the difficulty of measurement in methanol, where propagation was so fast to avoid detection during test stops. Constant acquisition of fatigue crack advancement is recommended, for example by using crack gages. The effects of crack gages application on test results, particularly concerning the removal of the TiO_2 layer, have to be properly addressed. The sensor application after an amount of time suitable for a sufficient reforming of the passivating layer is hence recommended. A correct identification of the nucleation and propagation process is fundamental to identify the environmental driving forces in the two different stages, and their contribution to fatigue life in aggressive environments. With this aim, the monitoring of the cracking process, via crack gages for axial fatigue, or via digital control of the applied load concerning rotating bending fatigue tests is desirable for future considerations on FCGR in methanol.

Other research paths concerning fatigue of the Ti-6Al-4V alloy in air and aggressive environments involve the analysis of the effects of PVD coatings for SCC and corrosion fatigue protection, as already performed in the present study on 7075-T6 aluminium alloy. The identification of proper coatings, suitable for the substrate in terms of fatigue behaviour and adhesion should be followed by fatigue tests in air and corrosive methanol environment. Particular care should be taken in the

identification of the effects of the methanol environment at different concentrations on nucleation and propagation.

The research on 7075-T6 PVD coated specimens is indeed still in its starting point. The present work highlights the potential beneficial effects of the DLC, and other research indicates the potentiality of post heat treatments and multi-layered coatings to improve the fatigue behaviour of the PVD coatings. In order to investigate the ability of DLC and other coatings to provide a satisfactory fatigue behaviour, some critical question marks have to be answered. The present work involves testing at *2e5* cyles, with rather high applied stresses, which might generate severe shear stresses at the interface between the surface and the coating. Although no delamination was found on the 7075-T6 specimens, a contribution in the mechanical reduction of fatigue life, although limited, could be still present. A method to assess this fact is to carefully observe the specimens during calibrated test interruptions, to assess if the cracking of the DLC susbtrate is caused in the context of the final fracture, or if previous cracking with possible effects on the crack nucleation are detected. Moreover, the investigation of the coated specimen fatigue behaviour at higher fatigue lives, i.e. with lower applied stresses, is indispensable to shed light on the mechanical contribution of the coating. Regarding the not negligible loss in fatigue strength of the coated specimens, evidence on post heat treatments should be deeply investigated, in order to identify a viable procedure to remove the detrimental effects on the microstructure of the PVD coatings. Another significant contribution to the advancement of PVD coatings adoption on light alloys is the development of specific coating strategies for light alloys. In particular, literature results show that the development of ductile layers can significantly improve the fatigue behaviour of coated 7075-T6 alloys. Moreover, a promising development of PVD techniques should involve the dedicated design of multi-layered coatings for aluminium alloys, consisting of properly chosen PVD layers of different nature, with increasing hardness and elastic modulus from the substrate to the outer layer. The

generation of an hardness gradient could indeed smooth the abrupt elastic modulus and hardness discontinuity found on the direct application of industrial PVD treatments, developed for hard substrates such as steel, resulting in an improved fatigue behaviour on light aluminium alloys from the mechanical standpoint.

Bibliography

[1] W. S. Miller, L. Zhuang, J. Bottema, A. J. Wittebrood, P. De Smet, A. Haszler, and A. Vieregge. Recent development in aluminium alloys for the automotive industry. *Materials Science and Engineering: A*, 280(1):37–49, 2000.

[2] S. Baragetti and G. D'Urso. Aluminum 6060-T6 friction stir welded butt joints: Fatigue resistance with different tools and feed rates. *Journal of Mechanical Science and Technology*, 28(3):867–877, 2014.

[3] A. S. Franchim, F. F. Fernandez, and D. N. Travessa. Microstructural aspects and mechanical properties of friction stir welded AA2024-T3 aluminium alloy sheet. *Materials and Design*, 32(10):4684–4688, 2011.

[4] R. Nandan, T. DebRoy, and H. K. D. H. Bhadeshia. Recent advances in friction-stir welding – Process, weldment structure and properties. *Progress in Materials Science*, 53(6):980–1023, 2008.

[5] P. M. G. P. Moreira, M. A. V. de Figueiredo, and P. M. S. T. de Castro. Fatigue behaviour of FSW and MIG weldments for two aluminium alloys. *Theoretical and Applied Fracture Mechanics*, 48(2):169–177, 2007.

[6] P. M. G. P. Moreira, F. M. F. de Oliveira, and P. M. S. T. de Castro. Fatigue behaviour of notched specimens of friction stir welded aluminium alloy 6063-T6. *Journal of Materials Processing Technology*, 207(1-3):283–292, 2008.

[7] N. Hägele and C. M. Sonsino. Structural durability of forged automotive aluminium chassis components submitted to spectrum loading and salt-corrosion by the example of a tension strut. *Procedia Engineering*, 10:330–339, 2011.

[8] M. Kumar, N. Sotirov, and C. M. Chimani. Investigations on warm forming of AW-7020-T6 alloy sheet. *Journal of Materials Processing Technology*, 214(8):1769–1776, 2014.

[9] Z. Yu, Z. Lin, and Y. Zhao. Evaluation of fracture limit in automotive aluminium alloy sheet forming. *Materials & Design*, 28:203–207, 2007.

[10] S. Lomolino, R. Tovo, and J. dos Santos. On the fatigue behaviour and design curves of friction stir butt-welded Al alloys. *International Journal of Fatigue*, 27(3):305–316, 2005.

[11] J. Hirsch. Aluminium in Innovative Light-Weight Car Design. *Materials Transactions*, 52(5):818–824, 2011.

[12] L. Ceschini, I. Boromei, G. Minak, A. Morri, and F. Tarterini. Effect of friction stir welding on microstructure, tensile and fatigue properties of the AA7005/10 vol.%Al2O3p composite. *Composites Science and Technology*, 67(3-4):605–615, 2007.

[13] S. Di, X. Yang, D. Fang, and G. Luan. The influence of zigzag-curve defect on the fatigue properties of friction stir welds in 7075-T6 Al alloy. *Materials Chemistry and Physics*, 104(2-3):244–248, 2007.

[14] G. Silva, B. Rivolta, R. Gerosa, and U. Derudi. Study of the SCC Behavior of 7075 Aluminum Alloy After One-Step Aging at 163 °C. *Journal of Materials Engineering and Performance*, 22(1):210–214, 2013.

[15] K. K. Sankaran, R. Perez, and K. V. Jata. Effects of pitting corrosion on the fatigue behavior of aluminum alloy 7075-T6: modeling and experimental studies. *Materials Science and Engineering: A*, 297(1-2):223–229, 2001.

[16] B. F. Brown. *Stress-Corrosion Cracking in High Strength Steels and in Titanium and Aluminum Alloys*. Naval Research Laboratory, Washington, D.C., 1972.

[17] S. Baragetti, L. Lusvarghi, G. Bolelli, and F. Tordini. Fatigue behaviour of 2011-T6 aluminium alloy coated with PVD WC/C, PA-CVD DLC and PE-CVD SiOx coatings. *Surface and Coatings Technology*, 203(20-21):3078–3087, 2009.

[18] E. S. Puchi-Cabrera, M. H. Staia, J. Lesage, L. Gil, C. Villalobos-Gutiérrez, J. La Barbera-Sosa, E. a. Ochoa-Pérez, and E. Le Bourhis. Fatigue behavior of AA7075-T6 aluminum alloy coated with ZrN by PVD. *International Journal of Fatigue*, 30:1220–1230, 2008.

[19] R. H. Oskouei and R. N. Ibrahim. An investigation on the fatigue behaviour of Al 7075-T6 coated with titanium nitride using physical vapour deposition process. *Materials and Design*, 39:294–302, 2012.

[20] R. H. Oskouei and R. N. Ibrahim. Restoring the tensile properties of PVD-TiN coated Al 7075-T6 using a post heat treatment. *Surface and Coatings Technology*, 205(15):3967–3973, 2011.

[21] S. Baragetti, R. Gerosa, and F. Villa. Fatigue Behaviour of Thin Coated Al 7075 Alloy with Low Temperature PVD Coatings. *Key Engineering Materials*, 577-578:221–224, 2013.

[22] S. Baragetti and F. Villa. An Updated Review of the Fatigue Behavior of Components Coated with Thin Hard Corrosion-Resistant Coatings. *The Open Materials Science Journal*, 8:87–98, 2014.

[23] S. Baragetti, R. Gerosa, and F. Villa. WC/C Coating Protection Effects on 7075-T6 Fatigue Strength in an Aggressive Environment. *Procedia Engineering*, 74:33–36, 2014.

[24] S. Baragetti, R. Gerosa, and F. Villa. Analisi degli effetti di rivestimenti PVD sul comportamento a fatica di provini in lega 7075-T6 in ambiente aggressivo. In *AIAS – Associazione Italiana per l'Analisi delle Sollecitazioni - 43° Convegno Nazionale*, pages 9–12, Rimini, 2014.

[25] S. Baragetti, R. Gerosa, and F. Villa. Light Alloys Structural Behaviour in Severe Environmental Conditions. *Key Engineering Materials*, 665:37–40, 2016.

[26] S. Baragetti and F. Villa. Mechanical Behavior Due to Innovative Processes on Light Alloys – A Review. *World of Mechanics*, 2(2):1–17, 2015.

[27] S. Baragetti, R. Gerosa, and F. Villa. Fatigue behaviour of DLC coated Al 7075-T6 alloy in an aggressive mixture. *Key Engineering Materials*, 627:81–84, 2015.

[28] R. R. Boyer. An overview on the use of titanium in the aerospace industry. *Materials Science and Engineering A*, 213(1-2):103–114, 1996.

[29] J. C. Williams and G. Lütjering. *Titanium*. 2007.

[30] C. Soares. *Gas Turbines*. Elsevier, Amsterdam, 2008.

[31] M. Niinomi. Mechanical properties of biomedical titanium alloys. *Materials Science and Engineering: A*, 243(1-2):231–236, 1998.

[32] S. P. Trasatti and E. Sivieri. Corrosion behaviour of titanium in non-aqueous solvents. *Materials Chemistry and Physics*, 92(2-3):475–479, 2005.

[33] A. Aladjem. Review Anodic oxidation of titanium and its alloys. *Journal of materials science*, 8:688–704, 1973.

[34] I. Gurrappa. Characterization of titanium alloy Ti-6Al-4V for chemical, marine and industrial applications. *Materials Characterization*, 51(2-3):131–139, 2003.

[35] R. W. Schutz and H. B. Watkins. Recent developments in titanium alloy application in the energy industry. *Materials Science and Engineering: A*, 243(1-2):305–315, 1998.

[36] R. W. Schutz. Guidelines for successful integration of Titanium alloy components into subsea production systems. In *Corrosion*, number 01023. NACE International, 2001.

[37] M. K. Dimah, F. Devesa Albeza, V. Amigó Borrás, and A. Igual Muñoz. Study of the biotribocorrosion behaviour of titanium biomedical alloys in simulated body fluids by electrochemical techniques. *Wear*, 294-295:409–418, 2012.

[38] E. N. Codaro, R. Z. Nakazato, A. L. Horovistiz, and R. B. Ribeiro. An image analysis study of pit formation on Ti-6Al-4V. *Materials Science*, 341:202–210, 2002.

[39] C. M. Chen, H. B. Kirkpatrick, and H.L. Gegel. Stress Corrosion Cracking of Titanium alloys in methanolic and other media. Technical report, AD-751 528, Air Force Materials Laboratory, Wright-Patterson AFB, Ohio, 1972.

[40] R. E. Johnson. NASA Experiences with Ti-6A1-4V in Methanol. Technical report, DMIC Memorandum 228, Battelle Memorial Institute, Columbus, Ohio, 1967.

[41] R. L. Johnston, R. E. Johnson, G. M Ecord, and L. C. Willard. Stress-corrosion cracking of Ti-6Al-4V alloy in methanol. Technical report, TN D-3868, Nasa, Manned Spacecraft Center, Houston, Texas, 1967.

[42] K. Bordji, J. Y. Jouzeau, D. Mainard, E. Payan, P. Netter, K. T. Ries, T. Stucky, and Hage-Ali M. Cytocompatibility of Ti-6Al4V and Ti-5Al-2.5Fe alloys according to three surface treatments , using human fibroblasts and osteoblasts. *Biomaterials*, 17(9):929–940, 1996.

[43] C. A. Love, R. B. Cook, T. J. Harvey, P. A. Dearnley, and R. J. K. Wood. Diamond like carbon coatings for potential application in biological implants—a review. *Tribology International*, 63:141–150, 2013.

[44] R. A. Zavanelli, G. E. Pessanha Henriques, I. Ferreira, and J. M. D. de Almeida Rollo. Corrosion-fatigue life of commercially pure titanium and Ti-6Al-4V alloys in different storage environments. *The Journal of prosthetic dentistry*, 84(3):274–9, 2000.

[45] A. L. Pilchak, A. H. Young, and J. C. Williams. Stress corrosion cracking facet crystallography of Ti-8Al-1Mo-1V. *Corrosion Science*, 52(10):3287–3296, 2010.

[46] S. Baragetti and F. Villa. Recent Patents on Physical and Chemical Vapour Deposition for Static and Fatigue Corrosion Protection of Thin Coated Components. *Recent Patents on Corrosion Science*, 3:148–155, 2013.

[47] S. Baragetti, S. Cavalleri, and F. Tordini. A Numerical Method to Predict the RCF Behaviour of PVD-coated Transmission Gears and Experimental Results. *Procedia Engineering*, 10:1485–1490, 2011.

[48] S. Baragetti and F. Tordini. A numerical study on the fatigue and rolling contact fatigue behaviour of PVD-coated steel and titanium spur gears. *Engineering with Computers*, 27(2):127–137, 2011.

[49] Y.-C. Park, S.-H. Lee, S.-K. Kim, S. Lim, D.-H. Jung, S.-Y. Choi, J.-H. Kim, and D.-H. Peck. Effects of CrN/Cr coating layer on durability of metal bi-

polar plates under a fuel recirculation system of direct methanol fuel cells. *International Journal of Hydrogen Energy*, 38(25):10567–10576, 2013.

[50] A. D. Wilson, A. Leyland, and A. Matthews. A comparative study of the influence of plasma treatments, PVD coatings and ion implantation on the tribological performance of Ti–6Al–4V. *Surface and Coatings Technology*, 114:70–80, 1999.

[51] S. Baragetti, L. Lusvarghi, F. Pighetti Mantini, and F. Tordini. Fatigue Behaviour of Notched PVD-coated Titanium Components. *Key Engineering Materials*, 348-349:313–316, 2007.

[52] G. Cassar, J. C. Avelar-Batista Wilson, S. Banfield, J. Housden, M. Fenech, A. Matthews, and A. Leyland. Evaluating the effects of plasma diffusion processing and duplex diffusion/PVD-coating on the fatigue performance of Ti–6Al–4V alloy. *International Journal of Fatigue*, 33(9):1313–1323, 2011.

[53] J. A. Hall. Fatigue crack initiation in alpha-beta titanium alloys. *International Journal of Fatigue*, 19(1):23–37, 1998.

[54] G. Sanderson and J. C. Scully. The stress corrosion of Ti alloys in methanolic solutions. *Corrosion Science*, 8(7):541–548, 1968.

[55] S. Baragetti, R. Gerosa, and F. Villa. Quasi-static behavior of notched Ti-6Al-4V specimens in water-methanol solution. *Corrosion Reviews*, 33(6), 2015.

[56] D. B. Dawson and R. M. Pelloux. Corrosion Fatigue Crack Growth of Titanium Alloys in Aqueous Environments. *Metallurgical Transactions*, 5(March), 1974.

[57] D. B. Dawson. Fatigue Crack Growth Behavior of Ti-6AI-6V-2Sn in Methanol and Methanol-Water Solutions. *Metallurgical Transactions A*, 12(May):791–800, 1981.

[58] S. Baragetti. Notch corrosion fatigue behavior of Ti-6Al-4V. *Materials*, 7(6):4349–4366, 2014.

[59] S. Baragetti and F. Villa. SCC and Corrosion Fatigue characterization of a Ti-6Al-4V alloy in a corrosive environment – experiments and numerical models. *Frattura ed Integrità Strutturale*, 8(30):84–94, 2014.

[60] S. Baragetti and F. Villa. Corrosion Fatigue of High-Strength Titanium Alloys Under Different Stress Gradients. *Jom*, 67(5):1154–1161, 2015.

[61] Y. Zhang, Y. S. Sato, H. Kokawa, S. H. C Park, and S. Hirano. Microstructural characteristics and mechanical properties of Ti-6Al-4V friction stir welds. *Materials Science and Engineering A*, 485(1-2):448–455, 2008.

[62] D. G. Sanders, M. Ramulu, P. D. Edwards, and a. Cantrell. Effects on the surface texture, superplastic forming, and fatigue performance of titanium 6Al-4V friction stir welds. *Journal of Materials Engineering and Performance*, 19(June):503–509, 2010.

[63] P. Edwards and M. Ramulu. Identification of Process Parameters for Friction Stir Welding Ti–6Al–4V. *Journal of Engineering Materials and Technology*, 132(3):031006, 2010.

[64] P. Edwards and M. Ramulu. Fatigue performance of Friction Stir Welded titanium structural joints. *International Journal of Fatigue*, 70:171–177, 2015.

[65] Y. Uematsu, K. Tokaji, Y. Tozaki, and H. Shibata. Fatigue behaviour of friction stir welded A7075-T6 aluminium alloy in air and 3% NaCl solution. *Welding International*, 27(6):441–449, 2013.

[66] S. Baragetti, R. Gerosa, and F. Villa. Comportamento quasi-statico di provini intagliati in lega Ti-6Al-4V in metanolo. In *AIAS – Associazione Italiana per l'Analisi delle Sollecitazioni - 42° convegno nazionale*, pages 11–14, 2013.

[67] G. Sanderson, D.T. Powell, and J.C. Scully. The stress-corrosion cracking of Ti alloys in aqueous chloride solutions at room temperature. *Corrosion Science*, 8(7):473–481, 1968.

[68] W.-T. Tsai, C.-L. Lin, and S.-J. Pan. Susceptibility of Ti–6Al–4V alloy to stress corrosion cracking in a Lewis-neutral aluminium chloride–1-ethyl-3-methylimidazolium chloride ionic liquid. *Corrosion Science*, 76:494–497, 2013.

[69] ASTM International. Standard Pratice for Statistical Analysis of Linear or Linearized Stress-Life (S-N) and Strain-Life (ϵ-N) Fatigue Data, 1991.

[70] J. Dong, F. Li, and C. Wang. Micromechanical behavior study of α phase with different morphologies of Ti-6Al-4V alloy by microindentation. *Materials Science and Engineering A*, 580:105–113, 2013.

[71] I. J. Polmear. *Light Alloys - From Traditional Alloys to Nanocrystals*. Butterworth-Heinemann, Oxford, iv edition, 2006.

[72] E. U. Lee, A. K. Vasudevan, and K. Sadananda. Effects of various environments on fatigue crack growth in Laser formed and im Ti-6Al-4V alloys. *Fatigue Damage of Structural Materials V*, 27(10-12):1597–1607, 2005.

[73] S. Baragetti. Corrosion fatigue behaviour of Ti-6Al-4V in methanol environment. *Surface and Interface Analysis*, 45(10):1654–1658, 2013.

[74] S. Baragetti, S. Cavalleri, and F. Tordini. Fatigue behavior of notched Ti-6Al-4V in air and corrosive environment. *Procedia Engineering*, 10:2435–2440, 2011.

[75] R. S. Bellows, S. Muju, and T. Nicholas. Validation of the step test method for generating Haigh diagrams for Ti – 6Al – 4V. *International Journal of Fatigue*, 21(8):687–697, 1999.

[76] D. B. Lanning, G. K. Haritos, and T. Nicholas. Influence of stress state on high cycle fatigue of notched Ti-6Al-4V specimens. *International Journal of Fatigue*, 21:S87–S95, 1999.

[77] K. Sadananda, S. Sarkar, D. Kujawski, and A. K. Vasudevan. A two-parameter analysis of S-N fatigue life using $\Delta\sigma$ and σmax. *International Journal of Fatigue*, 31(11-12):1648–1659, 2009.

[78] J. O. Peters, B. L. Boyce, X. Chen, J. M. McNaney, J. W. Hutchinson, and R. O. Ritchie. On the application of the Kitagawa-Takahashi diagram to foreign-object damage and high-cycle fatigue. *Engineering Fracture Mechanics*, 69(13):1425–1446, 2002.

[79] D. B. Lanning, T. Nicholas, and A. Palazotto. HCF notch predictions based on weakest-link failure models. *International Journal of Fatigue*, 25(9-11):835–841, 2003.

[80] P. P. Milella. *Fatigue and Corrosion in Metals*. 2013.

[81] T. L. Anderson. *Fracture Mechanics: fundamentals and application*. Taylor & Francis, Boca Raton, Fl., 3rd edition, 2005.

[82] S. Baragetti and A. Terranova. Fatigue Resistance of Thin Hard Coated Spur Gears. *Structural Integrity and Durability*, 1(4):267–276, 2005.

[83] S. Baragetti. Fatigue resistance of steel and titanium PVD coated spur gears. *International Journal of Fatigue*, 29:1893–1903, 2007.

[84] S. M. Beden, S. Abdullah, and A. K. Ariffin. *Review of Crack Propagation Models for Metallic Components*, volume 28. 2009.

[85] M. Kato, G. Deng, K. Inoue, and N. Takatsu. Evaluation of the Strength of Carburized Spur Gear Teeth Based on Fracture Mechanics. *JSME International Journal Series C*, 36(2):233–240, 1993.

[86] A. Carpinteri and M. Paggi. Self-similarity and crack growth instability in the correlation between the Paris' constants. *Engineering Fracture Mechanics*, 74(7):1041–1053, 2007.

[87] S. Pitt and R. Jones and B. Farahmand. Crack Growth in Mil Annealed Ti-6Al-4V Structural Components. *Biomolecular Engineering*, pages 10142–10142, 2008.

[88] S. Baragetti and F. Villa. Crack propagation models: numerical and experimental results on Ti-6Al-4V notched specimens. In *International Workshop on Stress Assisted Environmental Damage in Structural Materials - Invited Speech*, 2015.

[89] U. Zupanc and J. Grum. Effect of pitting corrosion on fatigue performance of shot-peened aluminium alloy 7075-T651. *Journal of Materials Processing Technology*, 210(9):1197–1202, 2010.

[90] K. Jones and D. W. Hoeppner. The interaction between pitting corrosion, grain boundaries, and constituent particles during corrosion fatigue of 7075-T6 aluminum alloy. *International Journal of Fatigue*, 31(4):686–692, 2009.

[91] K. Genel. The effect of pitting on the bending fatigue performance of high-strength aluminum alloy. *Scripta Materialia*, 57(4):297–300, 2007.

[92] R. Messier and S. Trolier-McKinstry. Thin-film Processes, 2001.

[93] E. Lugscheider, G. Krämer, C. Barimani, and H. Zimmermann. PVD coatings on aluminium substrates. *Surface and Coatings Technology*, 74-75:497–502, 1995.

[94] R. H. Oskouei and R. N. Ibrahim. The effect of a heat treatment on improving the fatigue properties of aluminium alloy 7075-T6 coated with TiN by PVD. *Procedia Engineering*, 10:1936–1942, 2011.

[95] R. H. Oskouei, R. N. Ibrahim, and M. R. Barati. An experimental study on the characteristics and delamination of TiN coatings deposited on Al 7075-T6 under fatigue cycling. *Thin Solid Films*, 526:155–162, 2012.

[96] Y. Z. Chang, P. H. Tsai, J. B. Li, H. C. Lin, J. S. C. Jang, C. Li, G. J. Chen, Y. C. Chen, J. P. Chu, and P. K. Liaw. Zr-based metallic glass thin film coating for fatigue-properties improvement of 7075-T6 aluminum alloy. *Thin Solid Films*, 544:331–334, 2013.

[97] S. Baragetti, L. Lusvarghi, G. Bolelli, and F. Tordini. Fatigue behaviour of 2011-T6 aluminium alloy coated with PVD WC/C, PA-CVD DLC and PE-CVD SiOx coatings. *Surface and Coatings Technology*, 203(20-21):3078–3087, 2009.

[98] K. Genel. Environmental effect on the fatigue performance of bare and oxide coated 7075-T6 alloy. *Engineering Failure Analysis*, 32:248–260, 2013.

[99] E. S. Puchi-Cabrera, C. Villalobos-Gutiérrez, I. Irausquín, J. La Barbera-Sosa, and G. Mesmacque. Fatigue behavior of a 7075-T6 aluminum alloy coated with an electroless Ni-P deposit. *International Journal of Fatigue*, 28(12):1854–1866, 2006.

[100] C. J. Villalobos-Gutiérrez, G. E. Gedler-Chacón, J. G. La Barbera-Sosa, A. Piñeiro, M. H. Staia, J. Lesage, D. Chicot, G. Mesmacque, and E. S. Puchi-Cabrera. Fatigue and corrosion fatigue behavior of an AA6063-T6 aluminum alloy coated with a WC-10Co-4Cr alloy deposited by HVOF thermal spraying. *Surface and Coatings Technology*, 202(18):4572–4577, 2008.

[101] Lafer S.p.A. www.lafer.eu - last accessed Jan. 2016.

[102] B. S. Saini and V. K. Gupta. Effect of WC / C PVD coating on fatigue behaviour of case carburized SAE8620 steel. *Surface & Coatings Technology*, 205(2):511–518, 2010.

[103] L. P. Pook, N. E. Frost, and K. J. Marsh. *Metal Fatigue*, volume 1. Oxford University Press, 1975.

Appendix A: The Step Loading Method

The Step Loading Method is employed to determine the limiting fatigue strength $\sigma_{lim,N}$ of a material at a given number of cycles N, with a limited number of specimens. The method has been adopted in most of the axial and rotating bending fatigue testing presented in the experimental works correlated to the present dissertation [21,25,27,58,60,73,74] to obtain the fatigue limits at *2e5* cycles for Ti-6Al-4V and 7075-T6 coated and uncoated specimens. The Step Loading method uses a single specimen to determine the limiting fatigue strength at a constant life N, and for this reason is extremely recommended where a limited number of specimens or a particular specimen specific treatment or damaged configuration, difficult to replicate on a huge set of other specimens, is present. Moreover, the method is very useful for experimental campaigns with a high number of tests involving different loading conditions, such as the generation of Haigh diagrams [75], or when very long testing is expected for high cycle fatigue analyses [76].

The fatigue endurance at a certain number of cycles N is calculated by testing a single specimen starting from an initial alternated stress level σ_0, which is typically a fraction of the expected fatigue strength. From this starting level, the specimen is tested until failure or run-out at N cycles. In the event of a run-out, which is extremely likely in the first steps of the method, the load is raised by a small $\Delta\sigma$ amount, typically a fraction of 5% of the applied stress. The procedure is hence

repeated for several blocks of N cycles, until the specimen fails. After the failure, occurred at a number of cycles $N_f < N$, the limiting strength at N cycles $\sigma_{lim,N}$ is calculated by linear interpolation, weighted on the number of cycles, between the stress applied within the failed block σ_f and the stress applied in the previous, not failed block σ_{pf}. The limit $\sigma_{lim,N}$ is hence obtained as:

$$\sigma_{lim,N} = \sigma_{pf} + \frac{N_f}{N}(\sigma_f - \sigma_{pf})$$

Concerning the statistical validity of the Step-Loading method, a detailed statistical study, performed by *Bellows* et al. [75] to validate the method for generating Haigh diagrams for Ti-6Al-4V fatigue testing at different R values has been conducted. The results showed that the Step Loading Method is a statistically sound alternative to other commonly employed methods, i.e. the Staircase method, concerning the evaluation of endurance limit of the Ti-6Al-4V alloy. In [75], it is pointed out that the results of the Step Loading Method are satisfactory from as statistical point of view, if the stress increase $\Delta\sigma$ is maintained limited, i.e. within 3-5% of the applied stress. A discussion on the possible effects of coaxing, i.e. the artificial increase of fatigue limit due to prior fatigue testing, on the validity of the results is also reported. Coaxing is related to the strain-aging of materials, and some indications of this effect have been found for steel materials [103], but evidence of its effects on titanium and aluminium light alloys has not been detected [75, 103], and the same relevancy of the coaxing effect has been questioned based on statistical argumentations [75].

In the recent works of *Baragetti* et al. [21,25,27,58,60,73,74], a further validation of the method has been introduced, by assigning to each step-loading tested specimen a second confirmation specimen. The confirmation run, executed at the identified $\sigma_{lim,N}$ limiting strength, must produce a number of cycles to failure of the same order of magnitude of N, to confirm the soundness of the identified fatigue strength $\sigma_{lim,N}$. By looking at Table 4.2, confirmation runs performed during the study of uncoated

and PVD coated 7075-T6 specimens in air have shown a good correspondence with the nominal *2e5* number of cycles. A final remark and warning has to be raised however regarding the use of the Step Loading Method in aggressive environments. By looking at the data presented in Table 4.2, it can be seen that confirmation runs in methanol aggressive environment showed a number of cycles to failure which is significantly higher with respect to the nominal value. The reason of this behaviour is in the fact that the step-loading tested specimens sustained longer immersion times in the aggressive environment, due to the repeated tests at increasing load, while the confirmation runs were subjected to a single load level, and hence to reduced test (and immersion) times, as discussed in section 4.4. Step-loading results in aggressive environments may hence lead to an over-conservative fatigue strength prediction. The adoption of the method in corrosive media testing is however not to be discouraged, whenever the higher exposition to the aggressive environment may account for environmental effects on crack nucleation which may be found in operative situations. For example, actual components in aggressive environments may be subjected to continuous exposition to the medium, even when limiting fatigue stresses are not present, resulting in potential critical situations.

Nomenclature

ΔK_C $[MPa\sqrt{m}]$ Kato model applied Stress Intensity Factor range intermediate threshold

ΔK_{SCC} $[MPa\sqrt{m}]$ Applied Stress Intensity Factor range threshold for Stress Corrosion Cracking

ΔK $[MPa\sqrt{m}]$ Applied Stress Intensity Factor range

ΔK_{th} $[MPa\sqrt{m}]$ Applied Stress Intensity Factor range threshold for nucleation

C Paris law constant

ν Poisson's ratio

ρ $[mm]$ Distance from the crack tip

θ $[rad]$ Crack tip angle

a $[mm]$ Crack length

u $[mm]$ half of the Crack Tip Opening Displacement (CTOD)

E $[MPa]$ Young's modulus

γ Walker trimming parameter

K_I $[MPa\sqrt{m}]$ First opening mode stress intensity factor

K_{IC} $[MPa\sqrt{m}]$ Fracture toughness of the material

K_{max} $[MPa\sqrt{m}]$ Maximum stress intensity factor

da/dN [mm/cycle] Fatigue Crack Growth Rate (FCGR) - i.e. rate of increase of the crack length a over cycles N

UTS $[MPa]$ Ultimate Tensile Strength

YS $[MPa]$ Yielding Strength

ρ_s $[mm]$ Axial fatigue specimens notch radius

σ_{nom} $[MPa]$ Nominal applied stress, neglecting notch effect

σ_{prop} $[MPa]$ Stress driving crack propagation away from the tip of a specimen notch

σ_{tip} $[MPa]$ Stress driving crack nucleation at the tip of a specimen notch

N_f Number of cycles to failure

$R = \frac{\sigma_{min}}{\sigma_{max}}$ Fatigue tests load ratio

R^2 Coefficient of determination

f $[Hz]$ Fatigue test load frequency

K_t $[MPa]$ Stress concentration factor on notched specimens

N Number of cycles for the indicated fatigue strength

$\Delta\sigma$ $[MPa]$ Step loading stress increment

σ_0 $[MPa]$ Step loading initial stress

σ_f $[MPa]$ Step loading failure stress

$\sigma_{lim,N}$ $[MPa]$ Limiting strength found by step loading at N cycles

σ_{pf} $[MPa]$ Step loading applied stress prior to failure - i.e. in the last not failed block